




Review

Recent Advances in Electrochemical Sensing of Hydrogen Peroxide (H₂O₂) Released from Cancer Cells

Touqeer Ahmad¹, Ayesha Iqbal², Sobia Ahsan Halim¹, Jalal Uddin³ , Ajmal Khan^{1,*}, Sami El Deeb^{1,4,*} 
and Ahmed Al-Harrasi^{1,*} 

¹ Natural and Medical Sciences Research Center, University of Nizwa, P.O. Box 33, Birkat Al Mauz, Nizwa 616, Oman; touqeer.nano@hotmail.com (T.A.); sobia_halim@unizwa.edu.om (S.A.H.)

² Division of Pharmacy Practice and Policy, School of Pharmacy, University of Nottingham, Nottingham NG7 2RD, UK; ayesharph@hotmail.com

³ Department of Pharmaceutical Chemistry, College of Pharmacy, King Khalid University, Abha 62529, Saudi Arabia; jalaluddinamin@gmail.com

⁴ Institute of Medicinal and Pharmaceutical Chemistry, Technische Universitaet Braunschweig, 38106 Braunschweig, Germany

* Correspondence: ajmalkhan@unizwa.edu.om (A.K.); s.eldeeb@tu-bs.de (S.E.D.); aharrasi@unizwa.edu.om (A.A.-H.)

Abstract: Cancer is by far the most common cause of death worldwide. There are more than 200 types of cancer known hitherto depending upon the origin and type. Early diagnosis of cancer provides better disease prognosis and the best chance for a cure. This fact prompts world-leading scientists and clinicians to develop techniques for the early detection of cancer. Thus, less morbidity and lower mortality rates are envisioned. The latest advancements in the diagnosis of cancer utilizing nanotechnology have manifested encouraging results. Cancerous cells are well known for their substantial amounts of hydrogen peroxide (H₂O₂). The common methods for the detection of H₂O₂ include colorimetry, titration, chromatography, spectrophotometry, fluorimetry, and chemiluminescence. These methods commonly lack selectivity, sensitivity, and reproducibility and have prolonged analytical time. New biosensors are reported to circumvent these obstacles. The production of detectable amounts of H₂O₂ by cancerous cells has promoted the use of bio- and electrochemical sensors because of their high sensitivity, selectivity, robustness, and miniaturized point-of-care cancer diagnostics. Thus, this review will emphasize the principles, analytical parameters, advantages, and disadvantages of the latest electrochemical biosensors in the detection of H₂O₂. It will provide a summary of the latest technological advancements of biosensors based on potentiometric, impedimetric, amperometric, and voltammetric H₂O₂ detection. Moreover, it will critically describe the classification of biosensors based on the material, nature, conjugation, and carbon-nanocomposite electrodes for rapid and effective detection of H₂O₂, which can be useful in the early detection of cancerous cells.

Keywords: analytical methods; biosensors; carbon materials; electrochemical sensing; H₂O₂; nanomaterial



Citation: Ahmad, T.; Iqbal, A.; Halim, S.A.; Uddin, J.; Khan, A.; El Deeb, S.; Al-Harrasi, A. Recent Advances in Electrochemical Sensing of Hydrogen Peroxide (H₂O₂) Released from Cancer Cells. *Nanomaterials* **2022**, *12*, 1475. <https://doi.org/10.3390/nano12091475>

Academic Editors: Dong Liu and Baiqing Yuan

Received: 16 February 2022

Accepted: 23 March 2022

Published: 26 April 2022

Publisher's Note: MDPI stays neutral with regard to jurisdictional claims in published maps and institutional affiliations.



Copyright: © 2022 by the authors. Licensee MDPI, Basel, Switzerland. This article is an open access article distributed under the terms and conditions of the Creative Commons Attribution (CC BY) license (<https://creativecommons.org/licenses/by/4.0/>).

1. Introduction

Biosensors are simple devices that are small and are generally used in the field of medicine, pharmaceutical industries, environmental technology, and food industry. They are used for the measurement of many biological and chemical substances [1]. Owing to the advancement of science and technology, the research involved in biosensors has successfully made the biosensing devices small and efficient [2]. The use of the latest novel techniques and availability of a new biomaterial have made the biosensors efficient and have extended their use in multiple industries such as pharmaceutical, environmental, agriculture, and industrial laboratories [3]. Biosensors are of many types, and electrochemical biosensors have been commonly used for over 20 years in the field of diagnostics

to detect biochemicals like glucose, lactate, cholesterol, urea, creatinine, DNA, antigens, antibodies, and cancer markers [4]. Electrochemical biosensors are also useful in the analysis of food materials and drinks and are extensively utilized in environmental and pharmaceutical laboratories [5,6]. Cancer is one of the most fatal diseases, and every year, more than 10 million new cases and 6 million deaths are reported worldwide [7,8]. Cancer is linked with high rates of morbidities and mortalities and more than 8.7 million deaths worldwide in 2015 [9]. The cancer incidence in high- and low-income countries is similar to the trend of increase in lower-middle-income countries because of the increase in risk factors associated with cancer [10]. In the United States of America (USA), cancer is the second leading cause of mortality, with heart disease being the first, and in a study published in 2017, it was estimated that more than 0.6 million people will die annually from cancer [8]. The survival rate of cancer patients drastically increases if the cancer is detected in earlier stages. The appearance of alarming systems in cancer patients is usually after cancer has spread in the body to multiple locations or has metastasized in different locations and organs, which characterizes an advanced stage of cancer. Most of the people are diagnosed with cancer at an advanced stage, which causes a high risk for mortality. To have a better disease prognosis, it is imperative that new research should focus on the early detection of cancerous cells in the body.

The use of biosensing devices, which have been designed to detect biochemicals, holds vast potential in the early diagnosis of cancers. Biosensors work by detecting a biological moiety or analyte and then converting it into an electrical signal, which can be detected and analyzed by the biosensor device. Many cancerous cells release specific chemicals called biomarkers, which can be detected using a biosensor device. The specific biomarker levels can also help in analyzing the effectiveness of anticancer therapy. The use of biosensor devices is a promising technique, which can help in early and accurate detection, imaging of cancerous cells, monitoring of angiogenesis, detection of proliferation, and tracking of metastatic changes and the efficacy of anticancer therapeutic regimens [11]. The latest research in biosensor devices using the latest techniques, such as nanotechnology-empowered diagnostics, can help in the identification of specific cancer biomarkers, which can help in the detection of cancer, disease progression, disease remission, and further proliferation. The biomarkers of cancer can be overexpressed proteins, surface antigens, active or inactive metabolites, miRNA, or the cancerous cells themselves. Many biosensors are excellent for use as an effective analytical device because of their capability to detect specific cancer biomarkers due to their highly sensitive, selective, robust, and miniaturized point-of-care cancer diagnostic capability [12]. Hydrogen peroxide (H_2O_2) is normally present inside the body and is vital in initiating and performing many important physiological processes. H_2O_2 is a by-product of respiratory chain and enzymes oxidases (glucose oxidase, cholesterol oxidase, glutamate oxidase, etc.) [13–17]. Hydrogen peroxide is a reactive oxygen species (ROS), which helps in regulating normal body functions such as cell growth, activation of the immune system, and programmed apoptotic changes [13–17]. The body system normally functions in homeostasis, and an increased level of H_2O_2 due to increased production can cause harm to the body. Increased levels of H_2O_2 can cause damage to normal cells [18], increase inflammatory responses [19], and cause cancer [20]. H_2O_2 regulates cancer cell characteristics, including invasion, proliferation, migration, apoptosis, and angiogenesis. Oxidative stress is associated with high levels of ROS, common in many types of cancerous cells. H_2O_2 has a specific role as a second messenger in pro-tumorigenic signaling pathways of cancerous cells [21,22]. GPX2 regulates cancer progression by regulating the hydrogen peroxide level in the cells, so when the level of H_2O_2 is downregulated to a normal level and the oxidative stress is relieved, it can help in dysregulating cancer cell homeostasis [23]. H_2O_2 has recently been a prime focus of research because of its high biological significance. When studied within living systems, it is noteworthy to check the concentration of H_2O_2 in mammals. The cellular compartment concentration has to be in the physiological range of 1 nM to 0.5 μ M [24,25]. The latest research in the field of cancer diagnosis via biomarker-based techniques has been evaluated

as successful because the process ensures high-precision, reliable, and sensitive data. The processes of biomarker-based cancer diagnostic are simple, which makes it a popular choice. Recent studies are focusing on profiling the cell functions with the efflux of endogenous H_2O_2 as potential biomarkers for diagnosing various cancers by measuring them using conventional biological assays [26]. However, before moving to the practical implications of using H_2O_2 as a potential biomarker for cancer diagnostics in living systems, detection of increased oxidative stress, prediction of neurodegenerative diseases, and detection of tumor growth inside living organisms, it is imperative to develop methods and techniques that can precisely detect and measure the level of H_2O_2 inside the cellular compartments [27].

The current problem with detecting H_2O_2 in cellular compartments is its low concentration in the body, as well as reactivity, which makes it difficult to separate its normal physiological concentration in a healthy organism from the concentration in a diseased or high-risk state. Therefore, scientists and researchers are focusing on developing sensors that can detect and quantify H_2O_2 in different systems and physiological conditions. Currently, many analytical techniques such as titrimetry, spectrophotometry, chemiluminescence, chromatography, fluorescence, and phosphorescence are measuring and determining the concentration of H_2O_2 in cellular compartments to develop consistent, precise, sensitive, fast, efficient, and low-cost methods. Currently, many methods investigated based on these analytical techniques have methodological disadvantages such as small sensitivity and selectivity, time-consuming and complex process, susceptibility to interference, and high-cost running instruments [28]. Alternatively, the advantages of “electrochemical sensors” are that they are highly sensitive and selective, reliable, quick, less costly, simple, and practical, and therefore, they are an optimum solution for exact and sensitive H_2O_2 detection [29]. The advancements of science and the latest research are looking for potential solutions to detect cancer at early stages and provide individualized therapeutic regimens. However, these techniques and methods still have many restrictions and limitations in the context of clinical examinations, histopathological analysis, imaging mammography, and chemotherapeutic adverse drug effects, as well as their high running costs [30,31]. In the detection of breast cancer, the patients are first exposed to a high amount of radiation in mammography because of its inadequate test sensitivity. Detection and disease progression are usually confirmed using a biopsy, an invasive procedure used to conduct histopathology of the disease [32]. These commonly used procedures are highly risky, uncomfortable, invasive, and costly. Therefore, the latest research is currently focused on developing noninvasive, inexpensive, highly selective screening, diagnostic, and therapeutic approaches to improve the disease prognosis. Several reviews regarding the importance of the carbon nanomaterial in the electrochemical sensing of H_2O_2 have been published. Out of those reviews, Yang et al. and Wang et al. conducted their reviews by comparing different nanomaterials for the creation of electrochemical biosensors and their applications for the detection of biomolecules [33,34]. Other materials have also been used in creating biosensors such as graphene electrochemical biosensors [35–37] and chemical sensors [38,39], which have been reviewed by Kuila and coworkers. Depending on the aim of the existing reviews, they provide an overview of biosensors that have been used to detect biological analytes. Similarly, Ping and coworkers [40] reviewed the strengths, advantages, and existing applications of 2D graphene-based aptasensors, whereas Chen and coworkers [13] focused their review on the carbon nanomaterial and transition metals in the electrocatalytic reduction of H_2O_2 in different samples. Similarly, Zhang et al. aimed to review the role of carbon materials in improving the sensitivity of H_2O_2 biosensors [41]. Regardless of these existing review articles, a comprehensive overview on the carbon-based nanomaterials and their composite with metal NPs, metal oxides, and biomolecules for the electrochemical detection of H_2O_2 secreted from cancerous cells is still missing in the literature.

This review highlights the recent development in the application of carbon nanomaterials and metal nanoparticles for H_2O_2 detection. A subdivision of the sensors has been made depending on the nanomaterial used: (i) metal nanoparticles, (ii) graphene modified with metal or metal oxide nanoparticles to form “graphene nanocomposites,” (iii) enzyme-

loaded graphene-like 2D nanomaterials, and (iv) carbon nanotubes modified with metal or metal oxide nanoparticles. Finally, the current potential and challenges of using carbon nanomaterials for H_2O_2 detection are outlined. Relative electrochemical properties such as limit of detection (LOD), sensitivity, and stability are reported for each sensor, and a critical comparison between the results has been carried out by summarizing the strengths and weaknesses of the various sensors found in the review.

2. Classical Methods for H_2O_2 Detection

2.1. Electrochemical Systems

Electrochemical biosensors are built on the principle that they have a biorecognition component providing an electroactive constituent after reacting with an analyte that is transformed into an electrical signal that is measured using a physiochemical transducer as shown in Figure 1. The electrochemical transducers help in the detection and monitoring of the changes in the electrical current and potential. The commonly used easily detected biorecognition elements are enzymes. Antibodies, complete cells, and DNA can also be conventionally used for the construction of electrochemical biosensors as biorecognizable elements [1,42] by loading on a metal surface or carbon electrodes [43]. The most used electrochemical transducers are amperometric, potentiometric, conductometric, and impedimetric. The advantage of using electrochemical biosensors in analytical techniques is that they can be effectively used to reduce the size of the device. Additional advantages are that these sensors are low cost, highly sensitive, stable, and reproducible; show a linear response; can detect turbid samples; and are efficient due to using low sample volumes and chemical consumption [5,6,44,45].

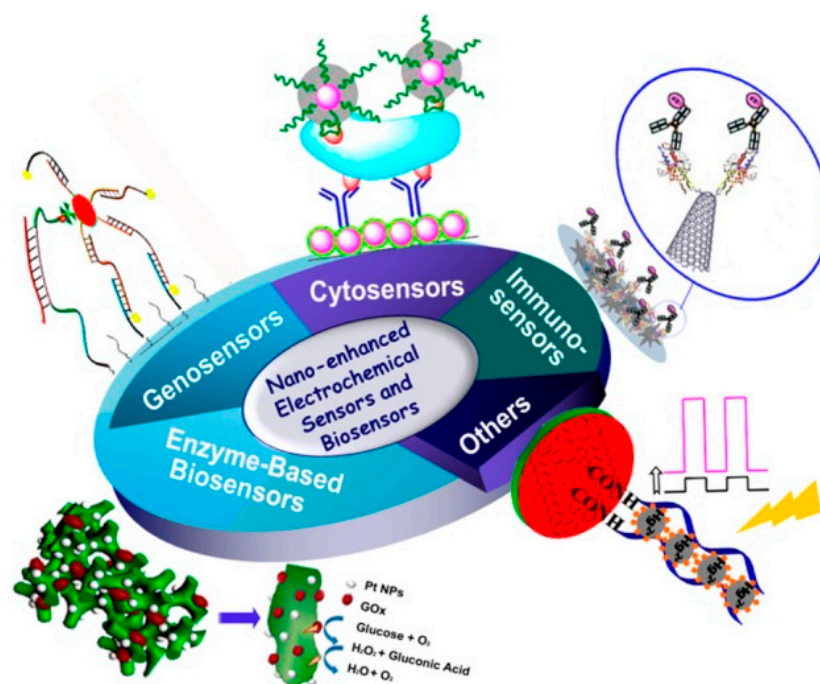


Figure 1. Distinct strategies for the electrochemical detection of H_2O_2 including Cyto-biosensors, Immuno-biosensors, Enzymatic and non-enzymatic biosensors. Figure reproduced with permission from [46]. Copyright 2014. American Chemical Society (Washington, DC, USA).

2.2. Potentiometric

Biosensors act on the principle of measuring the electric potential generated by an electrode in the absence of a substantial amount of current via a reference and functional electrode that has been adjusted to sense selective analytes, with membranes that cover the electrode surface. When a target analyte interacts with the membrane covering the electrode surface, a subsequent change in electric potential is detected and measured by

the electrode [47]. Potentiometric biosensors work by measuring the electric potential at zero current, which helps in differentiating the reference and functional electrodes. Potentiometric sensors measure the generated electric potential of ion-selective electrodes during biological reactions with target-specific ions. In potentiometric biosensors, the enzyme is attached on the surface of the electrode by glutaraldehyde crosslinking or an adsorption process. The probe of pH meter is covered by the membrane, where biological reaction either produces or absorbs hydrogen ions. The alteration in hydrogen ions causes a change in pH, which is a measure of the concentration of the analyte [48]. For instance, two examples of potentiometric biosensors depending upon the type of electrode used are as follows: (a) Potentiometric biosensors use a Nafion membrane/Pt electrode for H_2O_2 determination, with an additional advantage of a perm-selective barrier [49]. Ascorbate and redox-active species reduce the overall electrode response, which further potentiates coupling between the redox potential on the Pt electrode and Donnan potential and increases sensitivity in detecting H_2O_2 . The present potentiometric biosensor has a sensitivity of 125.1 ± 5.9 mV/decade, linear range of 10–1000 μM , and LOD of 10 μM [49]. (b) Zheng et al. used an MnO_2/CPE to detect H_2O_2 [50]. The biosensor shows sensitivity of 19.4–121 mV/decade, with a wide linear range of 0.3–363 μM and LOD of 0.12 μM . The analytical parameters of the MnO_2 doped/CPE biosensor were superior to those of the up-to-date potentiometric biosensors, i.e., Nafion membrane/Pt electrode [49], because of the enhanced electrode surface area, linear range, and LOD, except for the sensitivity. The coupling between the redox potential on the Pt electrode and Donnan potential made the Nafion membrane/Pt electrode superior to the MnO_2 doped/CPE in terms of sensitivity [50].

2.3. Amperometric Biosensor

Zhao et al. developed an amperometric biosensor by immobilizing HRP on a silica sol-gel matrix on CPE for the determination of extracellular H_2O_2 excreted from breast cancer cells. The amperometric biosensor detected H_2O_2 via a sequence-specific peptide immobilized on the electrode surface and explicitly bound with horseradish peroxidase (HRP) in an auspicious orientation. The composed biosensors showed a linear range from 1.0×10^{-7} to 1.0×10^{-4} M, with a detection limit (LOD) of 3.0×10^{-8} M [51]. Zhao et al. showed a linear calibration of H_2O_2 , i.e., 2×10^{-5} to 2.6×10^{-3} M, under optimum conditions [52]. In another strategy, a hydrogen peroxide biosensor was fabricated by coating a sol-gel-horseradish peroxidase LSPR layer onto a Nafion-methylene green modified electrode to develop a probe for H_2O_2 detection. The developed electrode exhibited sensitivity of $13.5 \mu\text{A mM}^{-1}$, with a detection limit of 1.0×10^{-7} M and response to 95% of the steady-state current in <20 s [53]. To detect H_2O_2 , Tripathi et al. developed a novel biosensor by entrapping HRP in a new Ormosil composite doped with ferrocene monocarboxylic acid-bovine serum albumin conjugate and multiwalled carbon nanotubes (MWNs). The developed biosensor showed a linear range of 0.02–4.0 mM, with a LOD of 5.0 μM ($S/N = 3$) [54]. In another study, a titania sol-gel matrix entrapping hemoglobin (Hb) was used as a peroxidase mimetic to sense H_2O_2 with a linear range from 5.0×10^{-7} to 5.4×10^{-5} M and a detection limit of 1.2×10^{-7} M [55]. Povedano et al. used His-Tag-Zinc finger commercial (His-Tag-ZFP) protein. The His-Tag-ZFP prefers to bind with RNA hybrids over ssRNAs, ssDNAs, and dsDNAs. These were further conjugated with streptavidin-HRP (Strep-HRP) in order to detect H_2O_2 with a LOD of 0.91 nM [56]. Reduced graphene oxide wrapped ZnMn_2O_4 microspheres ($\text{ZnMn}_2\text{O}_4/\text{rGO}$)-modified glassy carbon electrode (GCE) ($\text{ZnMn}_2\text{O}_4/\text{rGO}/\text{GCE}$) was used to make amperometric biosensors to detect H_2O_2 . The resultant electrode showed a linear detection with a wide concentration range of 0.03–6000 μM and was used to detect H_2O_2 released from human breast carcinoma cells (MCF-7) as low as 0.012 μM [57]. Dong et al. reported a high-performance sensor using high-index facets of Au-Pd nanocubes loaded on large surface reduced graphene oxide (rGO), and GCEs were modified by physical adsorption of both nanocomposites. The synthesized biosensor with three-dimensional nanocomposites possessed high sensitivity

toward H_2O_2 , with a minimum LOD of 4 nM, wide linear range from 0.005 μM to 3.5 mM, and swift response time [58]. Later, Jia and his coworker developed a nonenzymatic biosensor composed of poly(diallyldimethylammonium chloride) (PDDA)-capped rGO nanosheets loaded with a trimetallic AuPtAg nanoalloy. This biosensor detects H_2O_2 released from carcinoma cells with a LOD of 1.2 nM and a wide linear range from 0.05 μM to 5.5 mM [59]. In another study, hierarchical $\text{Mo}_2\text{C}@\text{MoS}_2$ consisting of interlayer-expanded MoS_2 nanosheets wrapped on Mo_2C nanorods was built as a highly sensitive, bifunctional electrochemical biosensor to detect H_2O_2 produced by cancerous cells, with sensitivity of $1080 \mu\text{A mM}^{-1} \text{cm}^{-2}$ and LOD of 0.2 μM [60]. Thirupatthi et al. reported a simple stimulus responding aminophenol, pre-anodized screen-printed carbon electrode (SPCE*/AP) that could detect NADH and H_2O_2 . The electrode was built by adsorbing aminophenol on the surface of the electrode, prepared from aminophenylboronic acid via boronic acid deprotection with H_2O_2 . The resulting biosensor displayed linear ranges from 50 to 500 μM and from 200 μM to 2 mM, with detection limits ($S/N = 3$) of 4.2 and 28.9 μM for NADH and H_2O_2 , respectively [61]. Maji et al. used cetyltrimethylammonium bromide-loaded gold nanorods (AuNRs) immobilized on a GC electrode to construct an amperometric biosensor (AuNRs/GC) for the electrocatalytic detection of H_2O_2 under localized surface Plasmon resonance (LSPR) excitation (808 nm, 2 W cm^{-2}). This biosensor showed an exaggerated improvement in its biosensing properties ($\sim 2\text{--}4$ -fold), with a wide linear range from 5.0 μM to 5.0 mM, LOD of 1.8 μM , and sensitivity of $1.6 \mu\text{A mM}^{-1} \text{cm}^{-2}$ [62]. In another study, self-supported MoS_2 nanosheet arrays were built, and they showed highly potent electrocatalytic performance, with a LOD of 1.0 μM ($S/N = 3$) and high sensitivity of $5.3 \text{ mA mM}^{-1} \text{cm}^{-2}$. This biosensor with self-supported MoS_2 nanosheet arrays successfully detected trace amounts of H_2O_2 released from live A549 cancer cells [63].

2.4. Calorimetric Biosensors

A new area of nanotechnology and its integration with biosensors has introduced the concept of calorimetric biosensors for cancerous cell diagnosis and detection. Li et al. used a microfluidic paper-based analytical device (μ -PAD) for the synchronous sensitive and visual detection of H_2O_2 released from cancer cells. μ -PAD construction was done using a layer-by-layer modification of concanavalin A, graphene quantum dots (GQDs)-labeled flower-like Au@Pd alloy nanoparticles (NPs) probe, and vertical alignment of cancerous cells on the surface of ZnO [64]. In the study by Zhang et al. porous platinum NPs on graphene oxide (Pt-NPs/GO) were used in building a calorimetric biosensor. The resultant nanocomposite functioned as a peroxidase mimetic, which could catalyze peroxidase substrate reaction in the presence of H_2O_2 . Building on this phenomenon, Pt-NPs/GO acts as a signal transducer in developing a colorimetric assay for cancerous cell detection [65]. Additionally, porous, alloy-structured PtPd nanorods (PtPd PNRs) were used as a peroxidase mimetic for H_2O_2 detection. The PtPd PNRs were found to have a detection limit of 8.6 nM and a linear range from 20 nM to 50 mM and were used as a signal transducer to develop an innovative detection method for studying the flux of H_2O_2 released from cells [66]. Folate and iron-substituted polyoxometalate [$(\text{FeOH}_2)_2\text{SiW}_{10}\text{O}_{36}$] provided a novel method for the detection of H_2O_2 with good sensitivity, with a linear range of 1.34×10^{-7} to $6.7 \times 10^{-5} \text{ mol L}^{-1}$, and low detection limit ($1 \times 10^{-7} \text{ mol L}^{-1}$) and swift response toward H_2O_2 . Ye et al. showed a new analysis method based on calorimetric analysis. The colorimetric biosensing strategy was based on iodide-responsive Cu–Au nanoparticles (Cu–Au NPs) combined with the iodide-catalyzed H_2O_2 –3,3,5,5-tetramethylbenzidine (TMB) reaction system. The bimetallic Cu–Au NPs absorbed iodide, thus indirectly inducing the colorimetric signal variation of the H_2O_2 –TMB system. The results demonstrated economically effective, simple, label-free visualization of H_2O_2 from cancerous cells with high selectivity and sensitivity. The resultant calorimetric biosensor operates with a linear range from 50 to 500 cells/mL and a LOD of 5 cells in 100 μL [67]. Calorimetric biosensors can be designed using single wall nano tube (SWNT), which is subsequently embedded within a collagen matrix. When there is an angiogenic stimulation

of human umbilical vein endothelial cells (HUVECs), H_2O_2 molecules are released, which can be detected using this SWNT sensor. The constructed calorimetric biosensor shows calibration from 12.5 to 400 nM and can measure H_2O_2 at a nanomolar concentration in HUVEC from humans, with 1 s temporal and 300 nm spatial resolutions [68]. Other biosensors based on the principle of calorimetry include a biosensor with an electrode made of a 2D hybrid material (RGO-PMS@AuNPs). This biosensor displayed remarkable electrochemical performance and possessed high sensitivity and high selectivity in detecting H_2O_2 in 0.1 M phosphate-buffered saline as compared to enzymatic biosensors. The developed biosensor has an additional advantage over other sensors because it is nontoxic and can detect H_2O_2 without any intrusion by common interfering agents, with high sensitivity of $39.2 \mu A mM^{-1} cm^{-2}$, broad detection ranges from 0.5 μM to 50 mM, and a LOD of 60 nM. The sensor has high efficiency and can detect H_2O_2 in trace amounts, i.e., as low as nanomolar, secreted from living HeLa and HepG2 tumor cells [69].

2.5. Chemiluminescence Material for the Detection of H_2O_2

For the early diagnosis and detection of cancerous cells, it is important that molecules that indicate changes or biomarkers should be efficiently imaged and sensed. These parameters are important especially in studies that are evaluating the clinical mechanisms and designing effective chemotherapeutic agents [70,71]. The diagnostic and therapeutic methods for multiple detections are slow and need repetitive sampling, which results in low sensitivity and accuracy, because of heterogeneous sampling for separate detections [72]. The multiple fluorescence (FL) technique has promising results when used in in situ concurrent detection of multiple biomolecules. This technique has certain limitations such as weak compatibility with different biological systems, toxicity to living cells, and necessity for specialized synthesis and preparation [70]. Additionally, the FL signals generated using this technique faced interference, changes from background effects, and photobleaching while operating. Thus, it is highly desirable that in situ sequential detection of multiple biomolecules using within a complex biological sample is greatly desirable, the FL technique should be researched in cancer diagnostics without the current limitations [73]. The chemiluminescence (CL) technique is based on the principle that light is generated because of the energy released during a chemical reaction due to the de-excitation of the high energy moieties to the ground state or through energy transfer to luminophore molecules as shown in Figure 2 [74–76]. CL methods have gained popularity because these techniques are highly sensitive, are free of interference, phototoxicity, and photobleaching, and show no changes from background effects. The combination of CL methods with enzymes and analytes such as firefly luciferase (FFLuc) for 5'-triphosphate disodium salt (ATP) [77,78] and HRP [79,80] may result in a highly sensitive and competent method for H_2O_2 detection. In the recent advancement in the field of NPs, the multifunctional NPs with shell-like structures in their core have promising results in simultaneous diagnosis and treatment in living systems [81–84]. These multifunctional NPs were synthesized in the study by Ren et al. where dual functioning NPs were developed by combining HRPSiO₂@FFLuc NPs with the enzyme-based core-shell structures, where the enzymes HRP and FFLuc were the main components of the core and shell of the NPs. They used the dual functioning NPs for the simultaneous in situ sequential detections and imaging of two biomolecules, namely, ATP and H_2O_2 , in the same biological system. The surroundings of tumor cells or tissues are slightly acidic, and SiO₂ is sensitive to an acidic environment, which causes the breakage of the SiO₂ layer/component and exposes FFLuc and HRP (outside) and the SiO₂ core (inside) to catalytic reactions. This results in the emission of two separate but simultaneous chemiluminescence signals for the sequential detection of ATP and H_2O_2 , which avoids the signal interference between each other [73]. In another study by Lee et al., a novel contrasting agent was successfully synthesized, which was highly sensitive and specific and could image H_2O_2 in living systems [85]. The authors used peroxalate NPs to image H_2O_2 by inducing a chemiluminescent reaction using three components: H_2O_2 , peroxalate esters, and fluorescent dyes. The peroxalate NPs were coated with peroxalate esters (hydrophobic polymer in its matrix). These NPs image H_2O_2 via a dual step process. Firstly, H_2O_2 diffusion occurs in the NPs, which then causes a reaction

with the peroxalate ester groups and generates dioxetanedione, creating high energy inside the NPs [86,87], which subsequently then chemically excites the encapsulated fluorescent dyes, via a chemically initiated electron-exchange luminescence mechanism [88,89], leading to CL from the NPs and allows imaging of H_2O_2 . Additionally, Lee et al. developed a method to synthesize peroxalate micelles, with a composition of amphiphilic peroxalate-based copolymers, rubrene (fluorescent dye), and a “stealth” polyethylene glycol (PEG) molecule to evade macrophage phagocytosis, which could successfully detect H_2O_2 through CL. These peroxalate-loaded micelles detected H_2O_2 within nanomolar concentrations (>50 nM) and were highly sensitive in detecting H_2O_2 in low physiological concentrations inside living systems [90].

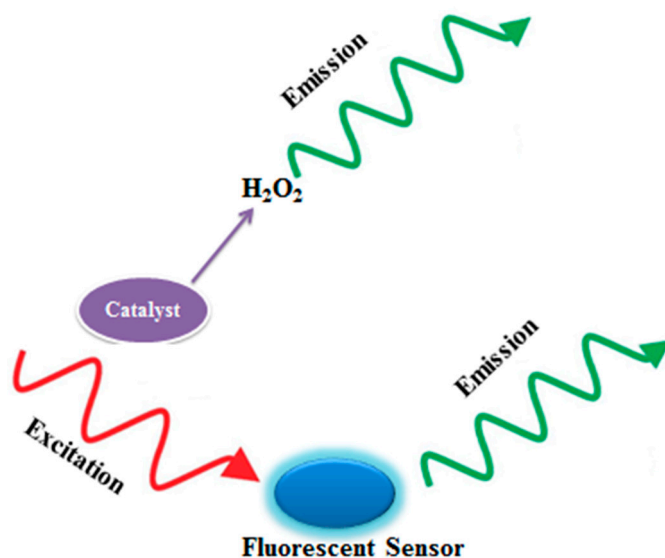


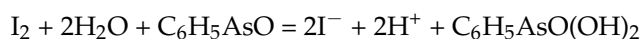
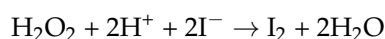
Figure 2. Mechanism of the chemiluminescent material for the detection of H_2O_2 released in cancer cells. Excitation and de-excitation of chemiluminescence materials can be seen during chemical reaction.

Another study found that using peroxyoxalate chemiluminescent (POCL) NPs, H_2O_2 could be detected in trace amounts within living systems (in vivo) using optimized CL techniques in the near-infrared (NIR) wavelength. The detection of H_2O_2 using NIR is efficient in living systems because the penetration power of these NIR rays is higher because of the reduced photon-limiting interferences (scattering and absorption) happening within biological mediums [91–93]. CL using luminol was synthesized using o-benzyl alcohol-decorated block poly(carbonate)s copolymer, viz., PMPC–ONA, giving the resultant micelles a high H_2O_2 detection ability. In these micelles, luminol, fluorophore, and hemin were wrapped, forming an L/H/S@PMPC–ONA nanoprobe. These micelles work based on the principle that in the presence of H_2O_2 in the system, H_2O_2 diffuses within NPs, reacts with the hemin, and generates high energy reactive oxygen. The high energy reactive oxygen then chemically excites the luminol, activating the CL to expose nitrosobenzaldehyde recognition sites. This process destabilizes the micelles and releases the fluorescent indicator (fluorophore), which helps in imaging H_2O_2 [94]. Lee et al. additionally synthesized a nanoprobe using multiple molecule integration, i.e., dye/peroxalate NPs, which exhibited more enhanced and controlled CL, and hence displayed widespread applications in biomedical imaging of H_2O_2 . This new enhanced nanoprobe was synthesized using nanoscopic coaggregation of a dye, which exhibited the aggregation-enhanced fluorescence phenomenon with a peroxalate, which had a high response to H_2O_2 , which converted the energy generated from the chemical reaction to electronic excitation [95]. Additionally, Lee et al. successfully detected and imaged H_2O_2 via CL resonance energy transfer in the NIR wavelength using quantum dots functionalized with a luminol derivative [96]. Geng et al. devised a method to detect H_2O_2 via aggregation-induced emission fluorogen using 2,3-bis(4-(phenyl(4-(1,2,2-triphenylvinyl)-phenyl)amino)phenyl)-fumarionitrile

(TPETPAFN), resulting in dye-encapsulated NPs [97]. A polyoxometalate (POM), vanadomolybdophosphoric heteropoly acid ($H_5PMo_{10}V_2O_{40}$, PMoV2), shows similar activity like peroxidases and functions by catalyzing the luminol/ H_2O_2 reaction to generate CL. This phenomenon was shown in the study by Jia et al. where the study results showed an enzyme-free luminol/ H_2O_2 /PMoV₂ CL system, which could be utilized for its high sensitivity in detecting H_2O_2 . This enzyme-free luminol/ H_2O_2 /PMoV₂ CL system exhibited good linear dependence with respect to H_2O_2 concentration within a wide range of up to 5 to 5000 nM (LOD) [98].

2.6. Titrimetry

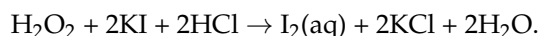
The titrimetry technique can be used to analyze an unknown amount of H_2O_2 in a known sample concentration. The titrimetric technique uses iodometry, permanganate, and cerium (IV) in an acidic medium. In the study by Klassen et al., the concentration of H_2O_2 was assessed at 300 μ M using the I_3^- method after the calibration with permanganate. ϵ max measurement was made at 351 nm as 25,800 $M^{-1} cm^{-1}$ using the calibration plot of the I_3^- method titrated against potassium dichromate ($KMnO_4$) [99]. In the study by Murty et al., the concentration of H_2O_2 was measured potentiometrically in an acidic medium using 8–11 M phosphoric acid [47]. Kieber and Helz synthesized a method for the detection of H_2O_2 by modifying the iodometric titration method using water matrices, where iodine was liberated as follows:



The I_2 produced was consumed by adding an excess of phenylarsine oxide. The end result was declared by titrating the remaining amount of phenylarsine oxide with iodine [100] when the intense blue color of the starch–iodine complex disappeared. The LOD was 0.02 μ M. In another study, a two-step absorbance, microtiter plate method was developed by titrating an acidified H_2O_2 solution with standard cerium (IV) sulfate. In the second step, cerium (IV) sulfate was converted into cerium (III) sulfate, and potassium iodide was converted into iodine [101]. This process is commonly used and possesses additional advantages over the other methods because of its simplicity and low running costs, but its limitation is its inaccuracy at lower concentrations. Additionally, the other limitations of the method are that it consumes more time and requires skilled personnel to perform the calibration of the instrument.

2.7. Spectroscopy

One of the most common, convenient, and extensively used methods for determining and measuring H_2O_2 is spectroscopy. This method is based on the principle that colored compounds are formed with respect to absorbance measurements comparative method of methyl blue and toluidine. A method comparing the reaction of methyl blue and toluidine blue with iodine solution was introduced for determination of H_2O_2 based on the following reaction:

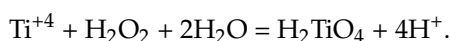


In the comparison, methyl blue when reacted with iodine gave a single-peak visible spectrum with a higher extinction coefficient ($=49,100 M^{-1} cm^{-1}$) [102]. In another study by Matsubara et al., a method using a mixture of titanium IV and 2,4((5-bromopyridyl)azo)5-(*N*-propyl-*N*-sulfopropyl amino) phenol disodium for determining H_2O_2 [103] was demonstrated. Molar absorptivity was found to be 5.7104 $M^{-1} cm^{-1}$ at 539 nm. In the study by Clapp et al., the measurement of H_2O_2 was done using an aqueous solution with titanium (IV) sulfate. This method yielded a yellow peroxotitanium species at a wavelength of 407 nm [104]. An in vitro method for the detection of H_2O_2 was developed using the

1,10-phenanthroline method. The advantages of this method are its short processing time, increased sensitivity, and high reproducibility [105]. In another study, catalytic decomposition of H_2O_2 was demonstrated by monomeric molybdenum (VI) by mixing hydroquinone, ammonium molybdate, and anilinium sulfate with varying H_2O_2 concentrations and determining the absorbance at 550 nm [106]. Zhang and Wong demonstrated a method for the estimation of the concentration of H_2O_2 in marine water at acidic pH of 4 in the presence of HRP at 592 nm using leuco crystal violet oxidation. The LOD for H_2O_2 was found to be 20 nM with $\pm 1\%$ accuracy [107]. In the study by Huang et al., a fast, reproducible, and reliable method for the detection and measurement of H_2O_2 was demonstrated. This method used 4AAP-DEA- β CD-hemin, and the LOD was 8.4×10^{-5} , with a molar absorption coefficient of 1.65×10^4 mol/L/cm [108]. Zhang et al. showed the determination of H_2O_2 in pulp bleaching effluents. The study shows that H_2O_2 , in the presence of sulfuric acid solution, chemically reacted with vanadium pentoxide and formed a peroxovanadate complex that is reddish-brown [109].

2.8. Colorimetry

The method of determining H_2O_2 using iodide and starch was first developed in 1943 by Eisenberg. The H_2O_2 samples were treated with a titanium sulfate reagent, and the changes in color were quantified with the presence of H_2O_2 . The chemical reaction of H_2O_2 with the titanium sulfate reagent is shown as follows:



The formation of a yellow compound called pertitanic acid determined the H_2O_2 concentration within a range of 0.2–3.0 mg/100 mL [110]. Another study showed a more sensitive method using colorimetry. The study showed that the oxidation of iodide takes place in the presence of $(\text{NH}_4)_2\text{MoO}_4$ (ammonium molybdate), which helps in determining the concentration of H_2O_2 even in micromolar quantities. The study determined the molar absorptivity of the starch–iodine complex (intense blue) at a value of $39.45 \text{ mmol}^{-1} \text{ cm}$ per liter at a wavelength of 570 nm [111]. The colorimetric method based on enzymes using plant extracts was developed by Fernando et al., where a sharp pink quinoneimine dye was formed. The pink dye formation took place when H_2O_2 reacted with phenol, 4-aminoantipyrine, and HRP in 0.4 M phosphate buffer with pH of 7.0 [112]. The assay results were considered optimum when the assay conditions were maintained at pH 7.0, temperature of 37°C , 0.7 mM H_2O_2 concentration, and 1 U/mL enzyme concentration within 30 min. The optimum assay resulted in a limit of quantitation and LOD of 411 and 136 mM, respectively. Another simple method to detect the H_2O_2 released by cells within a tissue culture was based on the principle that phenol red oxidizes in the presence of H_2O_2 . The study results showed a direct linear relationship between the concentration of H_2O_2 and absorbance, which had a range of 1 to 60 nmol/mL. The absorbance was measured at 520 nm [113]. Another fast and reliable method for determining H_2O_2 was developed using a colorimetry technique. In the method, 4-nitrophenylboronic acid was utilized for determining the concentration of H_2O_2 in an aqueous medium, where nitrophenylboronic acid reacted with H_2O_2 and produced 4-nitrophenol. The LOD was found to be $\sim 1.0 \mu\text{M}$ [114]. Nitinaivinij et al. used the principle of colorimetry and demonstrated the determination of H_2O_2 in a very low concentration. The method utilized the technique of chromatography analysis of silver nanoprisms (AgNPrs). The AgNPrs decomposed in the presence of H_2O_2 , producing yellow color, and showed the H_2O_2 concentration at 1.57 mM with high accuracy and sensitivity [115]. The advantage of this method is that the determination of H_2O_2 can be carried out using a simple apparatus, but this method could give false-positive readings, and the results were not applicable to determine H_2O_2 within turbid samples.

2.9. Chromatography

Chromatographic techniques are commonly used for separation. High-performance liquid chromatography (HPLC) is an analytical technique used for the detection and separa-

tion of different moieties. In the study by Takahashi, separation of H_2O_2 was achieved using an electrochemical detector and a cation-exchange resin gel column of sulfonated styrene-divinylbenzene copolymer. This method was found to have a linearity of 0.9984. The LOD was measured at 0.2 pmol [116]. In another method by Wada et al., H_2O_2 separation was achieved using an octadecylsilyl column, and the LOD was measured at 1.1 μM [117]. In another study, H_2O_2 was determined using gas chromatography in the presence of oxidized butyric acid, and its absorbance was found at a wavelength of 517 nm [118]. Another method in a study used a ligand exchange-type column for the separation of H_2O_2 . The column was packed using a sulfonated polystyrene/divinylbenzene cation-exchange [119]. Steinberg et al. used the principle of reverse-phase chromatographic techniques in HPLC to determine H_2O_2 . Iodovanillic acid was formed and was detected using UV absorption at 280 nm with a LOD of $\sim 0.1 \mu\text{M}$ [120]. The advantages of chromatographic techniques in H_2O_2 determination are that these methods are relatively simple, have low operational costs, and use a wide range of stationary phases and columns. The limitations of this technique are its costly overall equipment, its long operational time, interferences, and the necessity for a specialized operator to run the machine.

2.10. Fluorescence

Another common method to detect H_2O_2 that has wide applications is based on the principle of fluorescent signal detection. In fluorescence sensors, the excitation of electrons is achieved from an external photon source, in contrast to CL, where light is generated via a chemical reaction [121]. Many fluorescent probes have been constructed using different materials. The probes include naphthofluorescein disulfonate [122], homovanillic acid [123], peroxyfluor-1 [124], peroxyresorufin-1 [124], single-walled carbon nanotubes [125], peroxyxanthone-1 [124], and phosphine-based fluorescent reagents [126]. In one study, the fluorescent biosensors helped in the detection of intracellular H_2O_2 in mice peritoneal macrophages [122]. In the study by Miller et al., three fluorescent probes that were detectable via confocal and two-photon spectroscopic methods from the peroxysensor family were successfully developed. Each fluorescent probe emitted at a different wavelength from the other, which allowed these probes to be used in various applications with respect to specific emitting wavelengths [124]. Recently, intracellular H_2O_2 concentration can be measured using HyPer, a genetically encoded H_2O_2 biosensor (Figure 3) [127]. HyPer is a chimeric protein [128] composed from the permuted yellow fluorescent protein (cpYFP) and H_2O_2 -sensitive domain of the bacterial transcription factor OxyR, which is responsible for sensing H_2O_2 [129]. In the study by Belousov et al., an H_2O_2 sensor named HyPer was developed and studied. The HyPer sensor was successful in detecting an increase in H_2O_2 levels in HeLa cells during Apo2L/TRAIL protein-induced apoptosis (programmed cell death). This sensor also detected increased levels of H_2O_2 in cells taken from rat adrenal medulla (PC-12) that had been previously exposed to nerve growth factor [128]. The HyPer family includes five probes: HyPer [128], HyPer2 [130], HyPer3 [131], HyPer7 [132], and HyPerRed [133]. GEFls of this family consist of a circularly permuted fluorescent protein (cpYFP for the numbered HyPers or cpmApple for HyPerRed) integrated via short peptide linkers into the bacterial transcription factor OxyR lacking a DNA-binding domain. Upon oxidation by H_2O_2 , OxyR forms an intramolecular disulfide bond [134] that elicits conformational rearrangements. These rearrangements are then transmitted into the chromophore center of a fluorescent moiety of a GEFl, causing fluorescence alterations that can be subsequently detected. HyPer and its improved derivatives, HyPer2 and HyPer3, contain cpYFP. cpYFP has two excitation peaks at 420 and 500 nm and a single emission peak at 516 nm. When the OxyR domain is oxidized by H_2O_2 , the intensity of fluorescence excited at approximately 420 nm (F_{420}) decreases, whereas the intensity of fluorescence excited at approximately 500 nm (F_{500}) increases proportionally. A sensor readout is generated as a F_{500}/F_{420} ratio [128].

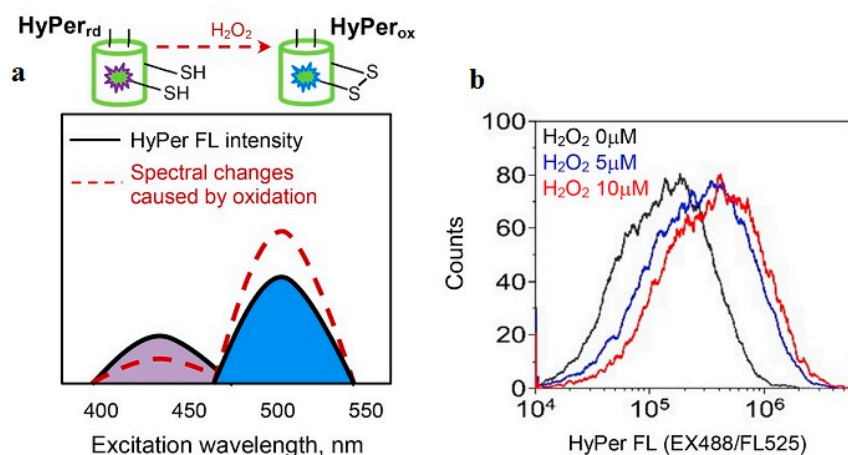


Figure 3. Analysis of HyPer fluorescence in K562 cells exposed to extracellular H_2O_2 . (a) Scheme demonstrating the changes in the excitation spectrum of HyPer upon oxidation. (b) Flow cytometry histograms of K562 cells measured after two-minute exposure to different concentrations of H_2O_2 . Reproduced with permission from [127]. Copyright 2019, Science Direct (Amsterdam, The Netherlands).

Another study by Xu et al. showed a specific probe called Mito- H_2O_2 , which is used to detect mitochondrial-associated H_2O_2 levels in HeLa cells. The study further showed that Mito- H_2O_2 was an effective, sensitive, and quick mitochondrial-targeted sensor [135]. Xiao et al. also developed another fluorescent probe called ER- H_2O_2 specifically for targeting the endoplasmic reticulum, which was equally effective, sensitive, and quick in the detection of H_2O_2 . Xiao et al. induced apoptosis in both the organelles using L-buthionine sulfoximine, and both of these probes were tested for H_2O_2 specificity and selectivity [136]. Shen et al. developed a microfluidic method, which had droplets in combination with gold nanoclusters. This method was demonstrated to have high sensitivity for the detection of H_2O_2 secreted by a single cell. When a single cell was isolated using a microdroplet (with a volume of 4.2 nL), it can secrete H_2O_2 , which causes fluorescent changes in HRP-gold nanoclusters with high specificity and high sensitivity of 200–400 attomole. The high throughput performance (~103 single-cell encapsulated microdroplets per minute) of the resultant microfluidic device makes it a powerful tool to investigate cell-to-cell heterogeneity in releasing H_2O_2 at the large scale, promising revelation of new knowledge to understand the biological role of H_2O_2 in tumor cells [137]. Moreover, Wang et al. fabricated a Ce6@Lum-AuNPs nanoprobe using green syntheses methods. They successfully loaded luminol-gold NPs with the fluorescent receptor Chlorin e6 (Ce6). The resultant fluorescent Ce6@Lum-AuNPs proved successful towards fluorescent bioimaging of cancerous cells [138].

3. Recent Advances

3.1. Current Approaches in the Construction of Biosensors

Over the past 200 years, the use of enzymes was common because of specific substrate sensitivity. However, enzymes are highly unstable and sensitive and are prone to denaturation caused by environmental changes such as pH and temperature. Therefore, recent studies have focused on using an artificial pseudo-catalyst instead of enzymes to overcome the drawbacks [139–141]. Denaturation of enzymes is common in enzyme groups such as peroxidases, catalases, monoamine oxidase, choline oxidase, uricase, and ascorbate oxidase. Peroxidases, also known as heme proteins, constitute the prosthetic group, i.e., ferriprotoporphyrin, and are usually found to have a molecular weight of 30 to 150 kDa [142,143]. Peroxidases are oxidoreductases and are produced by many animals, plants, and microorganisms. Peroxidases reduce H_2O_2 and help in the oxidation of aromatic amines, phenols, and organic and inorganic substrates [144] and are extensively utilized in biochemistry, enzyme immunoassays, wastewater treatment plants containing phenol compounds, synthesis of aromatic compounds, and removing H_2O_2 from food

materials [143]. The application of peroxidase enzymes is extensive, and they are commonly used in analytical techniques for the detection of glucose [145], cholesterol [146], uric acid [147], H_2O_2 [148], alcohols [149], and phenols [144]. Peroxidase enzymes are also used in the pharmaceutical industry for the construction of biosensors for the detection of different drugs in the body. As previously mentioned, enzymes are prone to degradation; hence, the latest research involves the replacement of enzymes with pseudo-catalysts, i.e., inorganic/organic. These materials are chosen because of their low cost, stability, and convenience [150–152].

3.2. Electrochemical Sensing of H_2O_2 via Metal Nanoparticles

Nanotechnology has advanced, and there are many types of NPs available nowadays. NPs can be classified based on the nanomaterial used to synthesize them. Commonly available nanomaterials include metal NPs [153,154], carbon nanomaterials [155,156], and metallic oxide nanostructures [157]. Nowadays, NPs are used in manufacturing H_2O_2 electrochemical sensors, exhibiting distinctive electrical and catalytic properties toward the reduction or oxidization of H_2O_2 and having a broad range of stability based on the nanomaterial used in them. However, until now, most of the studies reporting cost-effective H_2O_2 detecting electrochemical sensors have a detection limit of the sub-micromolar level [38,158]. To detect H_2O_2 in cellular matrices, the electrobiochemical sensors should be sensitive enough to sense H_2O_2 concentration in nanomoles. Currently, those biosensors that are highly sensitive and have optimum H_2O_2 detection limits have been developed using HRP and metal nanoparticles [159,160], which decreases the long-term operational stability and increases the operational costs. In the study by Wang et al., real-time electrochemical detection of H_2O_2 via small MoS_2 NPs in Raw 264.7 cancerous cells was performed. The resulting device had a detection limit lower than 2.5 nM and a wide linear range of up to five orders of magnitude [161]. In vivo monitoring of H_2O_2 secreted from living cells is essential in understanding cellular signaling pathways. The release of H_2O_2 from living cells is very low because the selective detection of H_2O_2 at a low level is challenging. To overcome this difficulty of detecting endogenous H_2O_2 from live cells, Dou et al. synthesized three hybrid metal nanoflower sensors for the detection and monitoring of H_2O_2 concealed from living MCF-7 cancerous cells. The three-hybrid metal Au–Pd–Pt nanoflower-decorated MoS_2 nanosheet-modified sensors were developed using simple wet chemistry. The three-hybrid metal nanoflower sensors (Au–Pd–Pt/ MoS_2) show a synergistic increase in the electrocatalytic reduction of H_2O_2 with an ultrasensitive detection limit as low as the sub-nanomolar level. Immobilization of aminin glycoproteins on the nanocomposite surface will result in an increase of its biocompatibility, which, in turn, enhances composite adherence to cells. This property of nanocomposites can be effectively used in future applications directed toward monitoring the secretion of H_2O_2 from living cells and cellular apparatus and may be utilized in developing highly efficient and sensitive cancer diagnostics sensors [162]. Sun et al. synthesized a dumbbell-shaped $Pt_xPd_{100-x}-Fe_3O_4$ NP composite, which could effectively determine the secretion of H_2O_2 from Raw 264.7 cells with a detection limit of 5 nM [160]. Chang et al. developed a sensitive fluorescent assay to determine H_2O_2 with a wide linear range of 1 to 100 μ M and detection limit of 0.8 μ M. A fluorescent biosensor based on the inner filter effect (IFE) was manufactured using poly (vinyl pyrrolidone)-protected gold nanoparticles (PVP–AuNPs) and fluorescent BSA-protected gold nanoclusters (BSA–AuNCs). The BSA–AuNCs acted as an IFE fluorophore pair. The high extinction coefficient of PVP–AuNPs served as a dominant absorber and influenced the emission of the fluorophore in the BSA–AuNCs assay. The surface Plasmon resonance (SPR) of PVP–AuNPs was significantly enhanced with an increase in H_2O_2 concentration. The increased H_2O_2 then caused the significant induction of the fluorescent quenching effect of BSA–AuNCs [163]. Cui et al. showed a fast, simple, and reagent-free method for H_2O_2 detection. The study used luminol-reduced Au NPs for the determination of H_2O_2 . The resulting biosensor had the electrochemiluminescence application in effectively

determining the concentration of H_2O_2 within limits of 3×10^{-7} – $1.0 \times 10^{-3} \text{ mol L}^{-1}$ with a low detection limit of $1.0 \times 10^{-7} \text{ mol L}^{-1}$ ($S/N = 3$) [164].

Liu et al. synthesized porphyrin functionalized ceria (Por-Ceria) uniform nanoparticles as a calorimetric probe for H_2O_2 detection [165]. A nickel phosphide nanosheet array on a titanium mesh ($\text{Ni}_2\text{P NA/TM}$) possesses superior analytical performance with a rapid retort time of $<5 \text{ s}$. Manufactured biosensors showed high selectivity and stability, with a wide linear range of 0.001–20 mM, ultrasmall LOD of 0.2 μM ($S/N = 3$), and high sensitivity of $690.7 \mu\text{A mM}^{-1} \text{ cm}^{-2}$ [166]. Small (10–30 nm) platinum nanoparticles (Pt-NPs) were prepared via protein-directed one-pot reduction. The resultant BSA/Pt-NPs composite shows colorimetric determination of H_2O_2 with a linear range from 50 μM to 3.0 mM, LOD of 7.9 μM , and visually detected lowest concentration of 200 μM [167].

Ultrathin silver nanosheets that can detect H_2O_2 with a LOD of 0.17 μM , linear range of 5–6000 μM , and fast response time $<2 \text{ s}$ were synthesized by Ma et al. The synthesized biosensors showed real-time determination of H_2O_2 released from living HeLa and SH-SY5Y cells, with high sensitivity of $320.3 \mu\text{A mM}^{-1} \text{ cm}^{-2}$ [168].

The synergistic combination of p-type semiconductive channels of layered double hydroxides (LDHs) exhibited multifunctional properties, a distinctive morphology, and abundant surface active sites. The $\text{Fe}_3\text{O}_4@\text{CuAl NSs}$ modified electrode exhibited excellent electrocatalytic activity toward H_2O_2 reduction. The projected biosensor revealed prominent electrochemical sensing of H_2O_2 with an extensive linear range of eight orders of magnitude and a low detection limit of 1 nM ($S/N = 3$) [169]. Copper(I) phosphide nanowires on 3D porous copper foam ($\text{Cu}_3\text{P NWs/CF}$) were fabricated via electrochemical anodized $\text{Cu}(\text{OH})_2$ NWs to manufacture noble metal-free electrocatalysts. The $\text{Cu}_3\text{P NWs/CF}$ -based sensor exhibited first-rate electrocatalytic reduction of H_2O_2 with a detection limit as low as that achieved by noble metal-free electrocatalysts, i.e., 2 nM. The developed sensor assured sensitive and consistent determination of H_2O_2 excretion from living tumorigenic cells [170]. Xiong et al. developed a nickel phosphide nanosheet array on a titanium mesh ($\text{Ni}_2\text{P NA/TM}$) using an economical and effective metal toward electrocatalytic H_2O_2 reduction. $\text{Ni}_2\text{P NA/TM}$, being a nonenzymatic H_2O_2 sensor, presented superior analytical performance, with a swift response time $<5 \text{ s}$ and wide linear range of 0.001–20 mM. The resultant electrode exhibited high sensitivity of $690.7 \mu\text{A mM}^{-1} \text{ cm}^{-2}$ and ultrasmall detection limit of 0.2 μM ($S/N = 3$) [166]. A Prussian blue nanocube-decorated molybdenum disulfide ($\text{MoS}_2\text{-PBNCs}$) nanocomposite was designed for the electrochemical sensing of H_2O_2 . Interestingly, a sensor for label-free sensing of carcinoembryonic antigen (CEA) can be constructed by using $\text{MoS}_2\text{-PBNCs}$ nanocomposites. The electrochemical response of the MoS_2 -based immunosensor was linear, with a CEA concentration range from 0.005 to 10 ng mL^{-1} and minimum recognition limit of 0.54 pg mL^{-1} [171].

3.3. H_2O_2 Detection Using Enzymatic Biosensors

Various analytical techniques, i.e., chemiluminescence [95], fluorescence [172], and electrochemistry [80,160], have been employed for the analysis of H_2O_2 at the cellular level. Among them, electrochemical sensors are an area of high interest and provide fast, economically effective, and real-time determination via a simple mechanism with ultrahigh sensitivity and selectivity. Electrochemical detection is considered a powerful tool for the determination of other electroactive metabolites such as glucose [173], dopamine [174], and O_2 [175] secreted from live cells. The high selectivity and sensitivity of enzymes made them valuable for the electrochemical biosensing of H_2O_2 . Horseradish peroxidase (HRP) enzymes draw considerable attention for the construction of electrochemical biosensors because of their efficient catalysis of H_2O_2 [176,177]. Wang et al. reported a highly sensitive sequence-selective DNA sensor composed of an HRP-labeled probe. The proposed biosensor successfully detected the K-ras gene, which is associated with colorectal cancer. Thiol ($-\text{SH}$) modified capture probe adsorbed chemically on the gold electrode via self-assembly and exhibiting a detection limit of $5.85 \times 10^{-12} \text{ mol L}^{-1}$, hybridization of nucleic acid (target DNA:K-ras gene), and a HRP labeled oligonucleotide detection probe can be

achieved using the sandwich way method. Wang et al. developed an extremely sensitive sequence-selective DNA sensor on an HRP-labeled probe to detect the specific K-ras gene which is associated with colorectal cancer. At first, the capture probe modified with $-SH$ was chemically adsorbed on the gold electrode by self assembly. Then, a complementary nucleic acid (target DNA:K-ras gene) was hybridized with an HRP labeled oligonucleotide detection probe in a sandwich way with a detection limit of $5.85 \times 10^{-12} \text{ mol L}^{-1}$ [178]. Bruno et al. developed horseradish peroxidase conjugated gold nano biosensors for detection of H_2O_2 released by prostate cancerous cells. The proposed biosensor can detect hydrogen peroxide (H_2O_2) in a wide linear range from 2 to 100 μM with a low detection limit of 0.01 μM [179]. A Cyt c loaded nanostructured TiO_2 film was successfully prepared by Luo, which exhibits natural enzymatic activity toward H_2O_2 , redox formal potential (E^0) of $108.0 \pm 1.9 \text{ mV}$ versus $Ag | AgCl$, and an heterogeneous electron transfer rate constant (k_s) of $13.8 \pm 2.1 \text{ s}^{-1}$ [157]. To stabilize the enzyme model, Zhou et al. used an enzyme cytochrome c (Cyt c), to facilitate the transfer of electrons between the redox enzyme and electrode. Cyt c was immobilized stably into the molecular hydrogel to maintain its innate bioactivity toward H_2O_2 . The use of Cyt c is a consistent methodology to regulate H_2O_2 at an optimized potential with high selectivity over other ROS, oxygen, metal ions, and ascorbic acid. The in vivo sensing of H_2O_2 from living cells, a small molecular hydrogel provides long-lasting stability and good reproducibility [180].

3.4. Carbon-Based Material for H_2O_2 Sensing

The success of graphene has boosted great research in the synthesis and characterization of graphene-like 2D materials, single and few-atom-thick layers of van der Waals materials, which show fascinating and useful properties. The single atom layer of C is the most transparent, strongest, and thinnest material and exhibits electrical conductance much better than Cu, with the ability to endure a current density that is six orders of magnitude [36,181,182]. The structure of some of the carbon-based material is shown in Figure 4. Recently, graphene has attracted great interest in the development of biosensors, i.e., optical and electrochemical, with improved performance owing to its integration with different nanomaterials (metals and metal oxides) and quantum dots [183–185]. Researchers have developed great interest in the emerging class of carbon-based 2D materials (graphene) because of their distinctive properties with applications in sensing and biosensing, electronics, catalysis, composites, and coatings. The excellent optical and electrical properties of carbon-based 2D materials made their use emergent in sensing and biosensing and showed real-time application in the field of biochemistry and nanomedicines [186,187]. Graphene-like 2D layered nanomaterials boron nitride (BN), transition metal dichalcogenides, graphite-carbon nitride (gC_3N_4), graphenes, and transition metal oxides have been investigated broadly [188,189]. Boron nitride nanosheets contain alternate nitrogen and boron atoms in a honeycomb lattice structure with extensive band gap, and BN is an insulator [190]. Instead of various transduction techniques, electrochemical methods are well known for analytical biomarker detection via graphene 2D-based sensors [191].

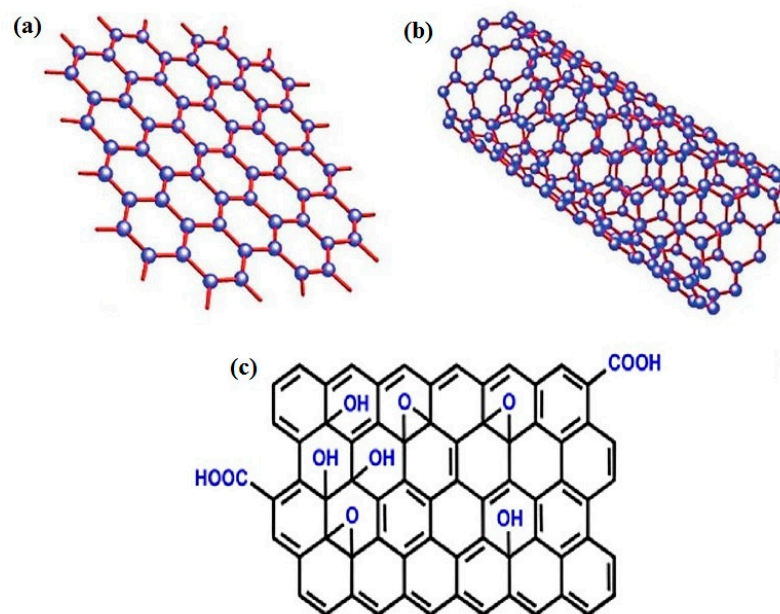


Figure 4. Different types of carbon-based materials, i.e., (a) Graphene, (b) Carbon nanotube, and (c) reduced graphene oxide, used in electrochemical sensing of H_2O_2 .

3.4.1. Graphene-Based Metal-Free Electrocatalysts

The application of carbon materials in analytical and industrial electrochemistry is well known owing to their low cost and electrocatalytic potential in a number of redox reactions [192]. Recently, groups of researchers showed that surface functionalization of graphene materials results in diverse behavior, which made them benevolent in sensing in contrast to intrinsic graphene. Zhou et al. showed the chemical reduction of graphene oxide into chemically reduced graphene oxide (CR-GO) via hydrazine, and the resultant GCE constructed from the obtained CR-GO showed excellent sensing capability for H_2O_2 detection. The synthesized electrochemical biosensor exhibited a lower detection limit of $0.05 \mu\text{M}$ and wide linear range from 0.05 to $1500 \mu\text{M}$, which precedes the use of functionalized carbon materials in electrochemical sensing [155].

In another work, Takahashi et al. reported rGO modified GCE via electrodeposition. The electrochemical studies showed an enhancement in the sensing performance of the rGO modified electrode that was considerably better than the original electrode for hydrogen peroxide detection. Some studies showed a high electron density on the defective sites (edges) of modified graphene oxide, which made it a potential candidate for the electrocatalytic reduction of H_2O_2 [193]. The synthesis of novel quality graphene is important in exploiting graphene application for electrochemical sensing. Chemical and physical (thermal method) reduction of GO (hydrophilic GO to hydrophobic graphene) is the most effective method to manufacture graphene on a large scale. During chemical and physical reduction, exfoliated graphene becomes disorderly aggregated, which results in the decrease in their disperse behavior in water and limits their practical applications [194]. Later on, some researchers fixed this problem using various dispersants, i.e., sodium dodecyl sulfate, cetyltrimethyl ammonium bromide (CTAB), and DNA. These dispersants enhanced the disperse behavior and stability of graphene in an aqueous environment. Lv et al. simply introduced DNA molecules on the graphene surface using the self-assembly method and formed graphene–DNA hybrids (GN/DNA). DNA–graphene was found to show a physical interaction, i.e., π – π stacking via aromatic rings of graphene and *N*-containing functional moiety in DNA, which results in a strong interaction between graphene and DNA. Stacking DNA on the graphene surface not only enhanced graphene dispersion in aqueous media but also imparted an electron-rich character to graphene by forming a GN/DNA composite. Comparative studies showed that the GN/DNA modified electrode

exhibited higher sensitivity, wide detection range, and swift response time in contrast to the GN-modified electrode for the electrochemical sensing of H_2O_2 [195]. Woo et al. fabricated a multiwalled carbon nanotube–graphene composite (MWCNT–graphene) via a direct in situ chemical reduction of graphene oxide and pre-treated MWCNT mixture. The prepared component showed a uniform network of ultrathin graphene sheets stuck between nanotube bundles. Structural analysis showed that the morphology of graphene present between nanotube bundles was comparatively higher than pure graphene, which showed wrinkled and aggregated morphology. The electrochemical sensor constructed from the resultant MWCNT–graphene exhibited a wide detection range from 20 μM to 2.1 mM and low detection limit of 9.4 μM . Synergic increase in the electrochemical performance of the MWCNT–graphene composite is attributed to high electrical conductivity of MWCNTs [196]. Recently, metal-free electrocatalysts, heteroatom-doped graphene, play a crucial role in H_2O_2 detection. The electronic properties of graphene can be altered drastically by doping graphene with N, S, and B, which play a crucial role in operating the electronic properties. Wang and coworkers used the nitrogen plasma treatment strategy to produce N-doped graphene from reduced graphene oxide as a starting material. Spectral studies of N-graphene showed that the nitrogen atom was substituted into graphene sheets with three different nitrogens, including graphitic N, pyridinic N, and pyrrolic N. The concentration of nitrogen in graphene sheets was optimized by monitoring the plasma exposure time, and the resultant N-doped graphene showed improved electrocatalytic performance as compared to pristine graphene in electrochemical sensing [197].

Wu et al. reported the synthesis of N-doped graphene using hydrazine as a nitrogen source, with a 4.5% N/C atomic ratio, and reducing agent. Structural studies of N-doped graphene were made via XPS measurements. Structural analyses showed 28% pyridinic N, 49% pyrrolic N, 19% graphitic N, and 4% oxidized N [198]. Increased sensitivity, a wide linear range, and a low detection limit were achieved using N-doped graphene as compared to pristine graphene. In addition to N, Yeh et al. successfully synthesized boron-doped graphene nanosheets (BGNs) using B_2O_3 and graphene nanosheets through an atmospheric-pressure carbothermal reaction. Boron doping on the graphene surface created defects in nearby sites and uneven charge separation, which, in turn, facilitated the charge transfer to neighbor atoms. The resultant BGN-doped graphene showed a wide linearity range from 1.0 to 20.0 mM, detection limit of 3.8 μM , and much higher sensitivity ($266.7 \mu\text{A mM}^{-1} \text{cm}^{-2}$) compared with undoped GNs [199]. Recently, the electrochemical performance of the detection of H_2O_2 was further improved using co-doped graphene with two elements. Yang et al. synthesized N and B co-doped graphene (NB-G) using a microwave-activated chemical–thermal treatment strategy. In this strategy, they first developed N-graphene using GO and cyanamide as a precursor, followed by microwave treatment. The boron atom was doped on N-modified graphene via the pyrolysis of the N-G and B_2O_3 mixture at 900 °C for 0.5 h in an Ar atmosphere to obtain BN-G [200]. Electrochemical studies of NB-G were made using ferric/ferrous coupling of $\text{K}_3[\text{Fe}(\text{CN})_6]/\text{K}_4[\text{Fe}(\text{CN})_6]$. The prepared electrode exhibited outstanding electrocatalytic reduction of H_2O_2 and a rapid response time, with a linear range from 0.5 μM to 5 mM and detection limit as low as 0.05 μM . The excellent electrochemical performance of the NB-G electrode is attributed to the novel structural network, with high charge transfer and large surface area, and the synergistic effect between the two heteroatoms of B and N [200]. Table 1 shows electrochemical performance of non-enzymatic metal free H_2O_2 sensors based on graphene.

Table 1. Non-enzymatic metal free H₂O₂ electrochemical sensors based on graphene.

Carbon Material	Sensitivity $\mu\text{A mM}^{-1} \text{cm}^{-2}$	Linear Range (μM)	Detection Limit (μM)	Ref.
CR-GO	-	0.05–1500	0.05	[155]
Graphene-MWCNT	32.91	20–2100	9.4	[196]
rGO/nPPy	47.69	0.1–4	0.034	[201]
IL-GR-s-PANI	280.0	0.5–2000	0.06	[202]
rGO/Tyrosine	69.07	100–2100	80	[203]
Poly(o-Phenylenediamine)/GO	16.2	2.5–25	0.84	[204]
BGNs	266.7	1000–20,000	3.8	[199]
NB-G	-	0.5–5000	0.05	[200]
GSnano/CS	18.78	5.22–10,430	2.6	[205]
GN-HN-SWCNT	0.015	0.2–400	0.05	[206]
H-GNs/PEDOT	235	0.1–10	0.08	[207]
NS-GQD/G	-	0.4–33	0.026	[208]
Functionalized 3D Graphene	169.7	0.4–660	0.08	[209]
rGO/GO hybrid MEA	-	0.18–9.6	-	[210]
3D-G/GCE	-	0.2–41,200	0.17	[211]

3.4.2. Carbon Composite with Enzymes for H₂O₂ Detection

Noble metals, nonnoble metal oxide, and sulfide-modified graphene composites are used to immobilize HRP for the construction of enzymatic H₂O₂ biosensors [212,213]. Song et al. [214] reported MoS₂–graphene (MoS₂-Gr)-based biocompatible biosensors for the ultrasensitive detection of H₂O₂. MoS₂-Gr nanosheets were prepared using GO and NaMoO₄ as precursors using the solvothermal method, and a change in solution color from reddish-brown (GO) to black confirmed the dispersion of dark flower-like MoS₂ nanoparticles on the Gr surface. Structural analyses were made using XRD results, which confirmed the formation of MoS₂-Gr composites. Electrostatic interaction arose between negatively charged MoS₂-Gr nanosheets and positively charged HRP and resulted in the formation of the HRP-MoS₂-Gr composite. The appearance of the peak in the UV–Vis spectra at 402 nm confirmed the immobilization of HRP on MoS₂-Gr, whereas no peak was noticed in case of MoS₂-Gr nanosheets. The HRP-MoS₂-Gr fabricated biosensor showed excellent stability and enhanced electrocatalytic performance for H₂O₂ detection. The resultant biosensors exhibited a low detection limit of 0.049 μM and broad linear range from 0.2 μM to 1.103 mM.

Later, Yu et al. immobilized horseradish peroxidase (HRP) on Au-decorated graphene oxide. The fabricated biosensors showed a fast response with remarkable performance, such as low detection limit (7.5×10^{-9} M) and real-time measurement of cellular H₂O₂ in living cells [27]. Liu et al. used horseradish peroxidase (HRP) immobilized on 3D porous graphene (PGN) to develop a real-time biosensor for the detection of H₂O₂ from living cells. Nanoporous graphene plays a significant role in the excess absorption of HRP, accelerates the diffusion rate, and shows excellent electrochemical performance toward H₂O₂ with a LOD of 0.0267 nM and wide linear range of seven orders of magnitude [215]. Enzymatic biosensors suffer from two major problems, namely, enzymatic loss and inactivation, which greatly affect biosensor performance. Fan and his coworker overcame this problem by encapsulating horseradish peroxidase on biomimetic graphene capsules (GRCAPS) using CaCO₃ as a porous sacrificial template to mimic the existence form of bioenzymes in organisms as shown in Figure 5. As a result, the synthesized biosensor showed a low detection limit of 3.3 mmol L⁻¹ and wide linear range of 0.01–12 mmol L⁻¹ [216]. Wu et al. used another strategy to construct horseradish peroxidase–attapulgitite nanohybrids on glassy carbon to fabricate biosensors. The prepared biosensor showed a rapid response, high sensitivity, and a low detection limit with a wide linear range for the detection of hydrogen peroxide released from RAW 264.7 macrophage cells [217]. Table 2 shows electrochemical performance of enzymatic H₂O₂ biosensor loaded on graphene.

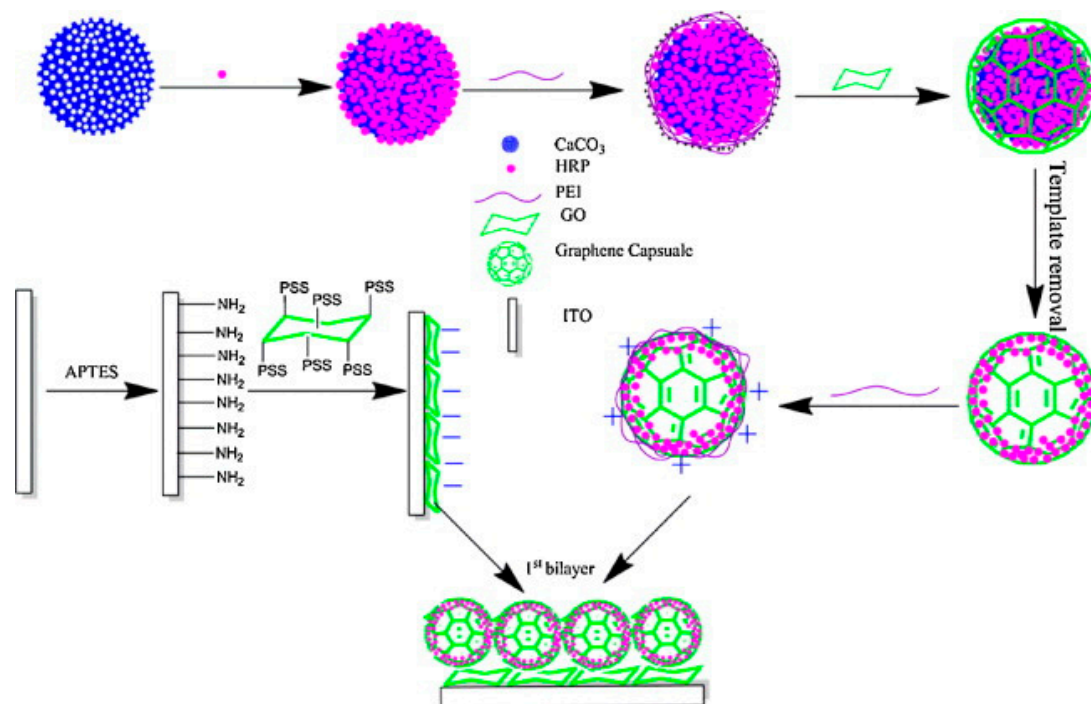


Figure 5. Mechanism of the synthesis of the graphene enzyme composite for the electrochemical sensing of H_2O_2 . Reproduced with permission from [216]. Copyright 2015, Science Direct.

Table 2. Graphene-based enzymatic biosensors for H_2O_2 detection in Cancerous cells.

Graphene-Based Materials	Sensitivity $\mu\text{A mM}^{-1} \text{cm}^{-2}$	Linear Range (μM)	Detection Limit (μM)	Ref.
GE/ Fe_3O_4 /Hb GCE	0.3837	100–1700	6.00	[218]
rGO-CMC/Hb	-	0.083–13.94	0.08	[219]
Hb/AuNPs/ZnO/Gr	-	6.0–1130	0.8	[220]
HRP/graphene	-	0.33–14.0	0.11	[221]
Hb/Au/GR-CS	3.47×10^5	2.0–935	0.35	[222]
Hb/Au NPs-Gr	-	0.1–70	0.03	[223]
HRP/P-L-His-rGO	2.6×10^5	0.2–5000	0.05	[224]
GS-PSS/GRCAPS	-	10–12,000	3.3	[216]
HRP/AuNP/ThGP	0.086	0.5–1800	0.01	[225]
PANI/HRP/GE-CNT/AuPt NPs	370	0.5–100	0.17	[226]
Au/graphene/HRP/CS	-	5.0–5130	1.7	[227]
MP11/DMPG-AuNPs/PDDA-G	243.7	20–280	2.6	[228]
(HRP-Pd)/f-graphene	92.82	25–3500	0.05	[229]
HRP-f-graphene-Ag	143.5	25–19,350	5.0	[230]
HRP/ CeO_2 -rGO	4.65	0.1–500	0.021	[212]
HRP- MoS_2 -Gr	679.7	0.2–1103	0.049	[214]
Catalase/AuNPs/graphene- NH_2	13.4	0.3–600	0.05	[231]
Cyt c/GO-MWCNT/Au NP	0.533	1×10^{-5} – 1.4×10^{-4}	27.7×10^{-6}	[232]
RGO-MWCNT-Pt/Mb	1.990	1×10^{-5} – 1.9×10^{-4}	16×10^{-6}	[233]
PPY-He-RGO	-	0.1–10	0.13	[41]
HRP/PGN/GCE	-	8.0×10^{-11} – 6.64×10^{-7}	2.6×10^{-5}	[215]
PGR/catalase/GCE	-	1.0×10^{-7} – 7.7×10^{-6}	1.5×10^{-3}	[234]
FeS_x /graphene	-	-	5×10^{-4}	[235]
F- MoS_2 -FePt NCs	-	8–300	2.24	[236]

3.4.3. Graphene Composite with Metal Nanoparticles for H_2O_2 Detection

Dai et al. prepared heterogeneous Co_3O_4 dodecahedrons that contain carbon, and encapsulated Au nanoparticles ($\text{Au@C-Co}_3\text{O}_4$) were proposed via the pyrolysis of Au nanoparticle-encapsulated zeolitic imidazolate framework-67 (Au@ZIF-67). A remarkable increase in electrocatalytic performance with ultrahigh sensitivity of $7553 \mu\text{A mM}^{-1} \text{cm}^{-2}$ and with a detection limit of 19 nM was observed using the electrode fabricated from the porous Au@C-

Co₃O₄ even with the 0.85% Au content in the composite. The synthesized biosensors were applicable for monitoring H₂O₂ concentration, which will be helpful in identifying cancerous cells [237]. A metal organic framework consisting of porphyrin and iron metal decorated on well-ordered mesoporous carbon (OMC) for hydrogen peroxide (H₂O₂) secreted from viable cells. Porphyrinic iron metal-organic framework (pFeMOF)-decorated ordered mesoporous carbon (OMC) was developed to detect hydrogen peroxide (H₂O₂) released from viable cells. Increased stability and electrical conduction were noticed with the introduction of OMC. Electrocatalytic reduction of H₂O₂ was observed at two different linear ranges, i.e., from 70.5 to 1830.5 μM and from 0.5 to 70.5 μM, with high sensitivity of 67.54 μA mM⁻¹ at a low concentration and 22.29 μA mM⁻¹ at a high concentration and with a detection limit (LOD) as low as 0.45 μM [238]. A nonenzymatic H₂O₂ electrochemical sensor was developed by immobilizing 2D ultrathin MnO₂ nanosheets onto glassy carbon electrodes (GCE) with a Nafion film. The amperometric study showed an excellent increase in electrocatalytic reduction of H₂O₂ with an extreme low detection limit (5 nM), wide linear range (25 nM⁻² μM and 10–454 μM), and high sensitivity of 3261 mA M⁻¹ cm⁻² via the immobilization of the MnO₂ nanosheets. The constructed biosensors were efficaciously employed for real-time monitoring of H₂O₂ released from SP2/0 cells in trace amounts [239].

The functionalized hollow-structured nanospheres (HNSs) centered on Pd nanoparticles (NPs) adorned double shell-structured N-doped graphene quantum dots (N-GQDs)@N-doped carbon (NC) HNSs, with ultrafine Pd NPs and “nanozyme” N-GQDs as dual signal-amplifying nanoprobe, act as an exceedingly effective electrochemical sensor for the detection of H₂O₂ released from cancer cells. The hybrid HNS material-based synthesized electrochemical biosensors demonstrate excellent performance, which involves an ultrasmall detection limit as low as nanomolar and a rapid response time. The extra sensitivity, selectivity, and reproducibility of the synthesized biosensors make them valuable for real-time tracking of H₂O₂ released from different living cancer cells in a normal state and treated with chemotherapy and radiotherapy [26]. Heteroatom-doped graphene (N and B) exhibits multidimensional electron transport pathways, which make their use valuable in electrocatalytic sensing of H₂O₂ with excellent stability and response time. Tables 3 and 4 show electrochemical performance of graphene-supported non-noble metal and noble metal nanoparticles.

Table 3. Graphene-supported non-Noble metal nanoparticles for electrochemical detection of H₂O₂.

Graphene-Based Materials	Sensitivity μA mM ⁻¹ cm ⁻²	Linear Range (μM)	Detection Limit (μM)	Ref.
Nafion/EGO/Co ₃ O ₄	560	1–100	0.3	[240]
CoHCFNPs/GR	0.0007	0.6–379.5	0.1	[41]
VS ₂ NPs/GCE	41.96	0.5–2.5	0.224	[241]
CoO _x NPs/ERGO	148.6	5–1000	0.2	[242]
CoTPP/RGO	0.0013	0.1–4600	0.02	[243]
rGO/CoPc-COOH	14.5	100–12,000	60	[244]
(PDDA-G/Fe ₃ O ₄) _n	61.2	20–6250	2.5	[245]
Fe ₃ O ₄ /GO-PAMAM	1.385	20–1000	2.0	[246]
CoS/RGO	2.519	0.1 to 2542.4	0.042	[247]
rGO-Fe ₂ O ₃	0.085	50–9000	6.0	[248]
Fe ₃ O ₄ /rGO	387.6	1–20,000	0.17	[249]
Ni ₂ P NA/TM	690.7	0.001–20	0.2	[166]
Fe ₃ O ₄ /RGO	22.27	0.5–3000	0.18	[41]
Fe ₃ O ₄ /RGO	0.0468	4.0–1000	2.0	[250]
PB/TiO ₂ -GR	480.97	0.04–2000	0.0086	[251]
RGO/Fe ₃ O ₄	688.0	100–6000	3.2	[252]
Cu-MOF-GN	57.73	10–11,180	2.0	[33]
PFECS/rGO	117.142	10–190	1.253	[253]
FeTSPc-GR-Nafion	36.93	0.2–5000	0.08	[254]
RGO/ZnO	13.49	0.02–22.48	0.02	[255]
Cu ₂ O/N-graphene	26.67	5.0–3570	0.8	[256]
Cu ₂ O-rGO	0.0207	30–12,800	21.7	[257]
CuS/RGO	0.035	5–1500	0.27	[80]
Cu ₂ O/GNs	-	300–7800	20.8	[258]
GO/MnO ₂	38.2	5.0–600	0.8	[259]
MnO ₂ -ERGO	59.0	100–45,400	10	[260]
MnO ₂ nanosheet/graphene	-	10–900	2.0	[261]
CoFe/NGR	435.7	-	0.28	[262]
Co@NCS	-	0.5–7500	0.08	[263]

The resultant N and B co-doped graphene (NB-G)-based electrochemical sensor showed a linear response from 0.5 μM to 5 mM with a LOD of 0.05 μM ($S/N = 3$). This increase in sensitivity with an ultralow detection limit to microlevel attributed to the NB-G constructive structure and special effects arose from the co-doping of N and boron in graphene [200]. CuFe_2O_4 nanoparticle-doped reduced graphene oxide based on a CPE was used as a voltammetric sensor for hydrogen peroxide (H_2O_2) sensing. The synthesized sensors showed a rapid amperometric response in less than 2 s and wide linear range of 2 to 200 μM with a low detection limit of 0.52 μM under optimum conditions (pH 5) [264]. Xi et al. synthesized N and S dual-doped graphene (NSG) co-doped carbocatalyst via one-pot syntheses. The NSG-modified electrode showed superior catalytic activity toward sensing, including a linear range up to 1.7 mM. ZnMn_2O_4 -wrapped reduced graphene oxide microspheres ($\text{ZnMn}_2\text{O}_4@\text{rGO}$) act as an excellent electrocatalyst for H_2O_2 reduction. The $\text{ZnMn}_2\text{O}_4@\text{rGO}$ -pasted glassy carbon electrode ($\text{ZnMn}_2\text{O}_4@\text{rGO}/\text{GCE}$) displayed a linear detection range of 0.03–6000 μM with a detection limit of 0.012 μM . The resultant biosensor showed promising results in physiology and diagnostics and was applicable in the determination of H_2O_2 secreted from human breast cancer cells (MCF-7) [57]. An AuNPs- NH_2 /Cu-MOF composite was prepared via ammoniation of Au NPs, anchored with a Cu-based metal organic framework (Cu-MOF). The synthesized AuNPs- NH_2 /Cu-MOF composite was further modified with a GCE to prepare an AuNPs- NH_2 /Cu-MOF/GCE electrode. The synthesized AuNPs- NH_2 /Cu-MOF/GCE composites possessed high sensitivity and selectivity, and they can be used as an electrochemical enzyme-free sensor for the quantitative detection of H_2O_2 . Instead of quantitative H_2O_2 detection, the synthesized electrochemical sensor showed a wide linear response toward H_2O_2 concentrations ranging 5–850 μM with a LOD down to 1.2 μM [265]. Wang et al. improved the sensitivity of the electrode using hemin-capped biomineralized gold nanoparticles (Hem@AuNPs)-doped reduced graphene oxide (rGO), followed by coating with chitosan (CS). The resultant electrode from the prepared nanohybrids showed excellent electrocatalytic reduction of H_2O_2 with superior sensitivity, stability, and response time of few seconds. The most important feature of the synthesized electrode from the resultant nanohybrid is its lower detection limit of 9.3 nM and linear range of five orders of magnitude. Such characteristics enable this biosensor to detect H_2O_2 releasing from living Hela cells accurately and make this biosensor valuable for ultrasmall detection of H_2O_2 from living HeLa cells precisely [266]. Sun and his coworkers designed a novel nonenzymatic hydrogen peroxide sensor using intermetallic PtPb nanoplates (PtPb/G) supported on graphene with enhanced electrochemical performance for H_2O_2 detection in neutral solution and H_2O_2 released from the cells. The nanocomposite exhibited excellent electrocatalytic activity for the electrochemical reduction of H_2O_2 in half-cell test and with wide linear detection range of 2 nM to 2.5 mM and ultralow detection limit of 2 nM. An experiment further showed that the sensitivity of intermetallic PtPb nanoplates is 12.7 times higher than that of a commercial Pt/C electrode for the detection of H_2O_2 released from Raw 264.7 cells [267]. A graphene/Nafion/azure/I/Au nanoparticle composites modified glass carbon electrode (graphene/Nafion/AzI/AuNPs/GCE) was used for the construction of a nonenzymatic H_2O_2 sensor. The performance of the synthesized biosensors was recorded under optimum conditions, i.e., pH of 4.0 and potential of -0.2 V, upon the addition of H_2O_2 . A stable current was obtained in less than 3 s, with a detection limit of 10 μM ($S/N = 3$) and a linear range of 30 μM to 5 mM [268]. Ju et al. reported a green and simple strategy for the in situ growth of surfactant-free Au nanoparticles (Au NPs) on nitrogen-doped graphene quantum dots (Au NPs-N-GQDs). The reported strategy showed the in situ formation of the Au NPs-N-GQDs hybrid by simple mixing of N-GQDs and $\text{HAuCl}_4 \cdot 4\text{H}_2\text{O}$ without any reductant and surfactant. The prepared nanocomposite (Au NPs-N-GQDs) exhibited a low detection limit of 0.12 μM and sensitivity of 186.22 $\mu\text{A}/\text{mM cm}^2$ for the electrochemical detection of hydrogen peroxide (H_2O_2) [79]. Another research group developed a microelectrode with high sensitivity, a wide linear range, and good selectivity for the detection of H_2O_2 released from female cancer cells. The synthesized hierarchical nanohybrid microelectrode was

composed of 3D porous graphene enfolded activated carbon fiber (ACF). This technique, i.e., green ionic liquid (IL), plays a crucial role in the simultaneous superficial and effective electrodeposition and electrochemical reduction of GO nanosheets on ACF to form a 3D porous ionic liquid functionalized electrochemically reduced GO (ERGO)-wrapped ACF (IL-ERGO/ACF) [269].

Table 4. Graphene supported noble metal nanoparticles for electrochemical detection of H₂O₂.

Graphene Based Material	Sensitivity $\mu\text{A mM}^{-1} \text{cm}^{-2}$	Linear Range (μM)	Detection Limit (μM)	Ref.
Au-PEI/GO	460.0	0.5–1680	0.2	[270]
AgNPs-MWCNT-rGO	0.833	100–100,000	0.9	[271]
RGO-Au-PTBO	63.39	5.0–1077.1	0.2	[272]
Ag-MnOOH-GO	59.14	0.5–17,800	0.2	[273]
Au NPs@POM-G	58.87	5.0–18,000	1.54	[274]
AgNPs-TWEEN-GO	0.7459	20–23,100	8.7	[41]
GO-ATP-Pd	504.85	0.1–10,000	0.016	[275]
GN/Au-NPs	-	0.5–500	0.22	[276]
GN-Pt	0.01	2–710	0.5	[277]
Ag NWs-graphene	12.37	10.0–34,300	1.0	[278]
GR-AuNRs	389.2	30–5000	10	[279]
Au@C-Co ₃ O ₄	7553	-	0.019	[237]
Au NPs-N-GQDs	186.22	0.25–13,327	0.12	[79]
AuNPs-NH ₂ /Cu-MOF/GCE	1.71	5–850	1.2	[265]
GO/Au@Pt@Au	-	0.05–17,500	0.02	[280]
NG-hAuPd	5095.5	0.1–20	0.02	[281]
PDA-RGO/Ag NP	0.0111	0.5–8000	2.07	[282]
AgNPs/GN	-	100–100,000	0.5	[283]
Ag/SG	-	100–136,500	0.14	[284]
Pt/PG	341.14	1–1477	0.5	[285]
PDDA-RGO/MnO ₂ /AuNPs	1132.8	5.0–500	0.6	[286]
AgNP/rGO	-	100–80,000	7.1	[287]
AgNPs-GO	-	10–20,000	0.5	[288]
RGO-AuNP	5.3	250–22,500	6.2	[289]
GNPs/SGS	27.7	20–15,000	0.2	[290]
AgNPs-CNT-rGO	-	10–10,000	1.0	[291]
PpyNFs/AgNPs-rGO	0.7367	100–5000	1.099	[292]
polystyrene@RGO-Pt	0.0675	0.5–8000	0.1	[41]
Graphene/Nafion/Azl/AuNPs	-	30–5000	10	[268]
Pt/GN	0.0204	2.5–6650	0.8	[41]
RGO-AuNPs (B)	9.5	25–41,500	5.0	[273]
PtAu/G-CNTs	313.4	2.0–8561	0.6	[293]
PtAuNPs-CTAB-GR	0.1654	0.005–4.8	0.0017	[294]
PtAu/RGO	4.105	0.015–8.73	0.008	[295]
Pt/graphene-CNT paper	1.41	0–25.0	0.01	[296]
pFeMOF/OMC	67.54	70.5–1830.5	0.45	[238]
Pd-PEI/GO	-	0.5–459	0.2	[297]
Pd-NPs/GN	0.019	0.001–2000	0.0002	[298]
PdNPGNs	2.75	0.1–1000	0.05	[299]
RGO-PMS@AuNPs	39.2	0.5–50,000	0.06	[69]
2Au1Ag-PDA/CFME	12966	0–55	0.12	[300]
TiO ₂ NTs/r-GO/AgNPs	1152	15,500–50,000	2.2	[301]
PtPb/G	-	2–2.5	0.02	[267]
3DGA-AuNPs/cytc/GCE	351.57	-	-	[302]
PdPt NCs@SGN/GCE	-	1–300	0.3	[303]
AuNFs/Fe ₃ O ₄ @ZIF-8-MoS ₂	-	5–120	0.9	[304]

3.4.4. Graphene-Loaded Biomolecules for Selective Detection of H₂O₂

Recently, graphene-based heme protein electrodes have gained wide attention for H₂O₂ detection. These graphene-based materials offer an appropriate microenvironment to maintain the redox bioactivity of proteins and make the transfer of electrons feasible between redox proteins (active centers) and the principal electrode [232]. A mixture of a strong acid and an oxidizing agent is used for the synthesis of graphene oxide from graphite [289]. GO serves as a precursor of graphene and as a sensing element. Several proteins, including cytochrome c, horseradish peroxidase (HRP), and myoglobin (Mb), were incubated. Zuo et al. [227] fabricated a heme proteins-modified GO electrode from GO suspension. Immobilization of protein on a GO sheet is associated with strong hydrophobic and electrostatic interactions between proteins and GO. The innate characteristics of the proteins remain unaltered in the presence of GO, which offers an appropriate microenvironment for the immobilization of protein with an intact structure. Studies revealed that the protein-based GO modified electrodes have an advantage over the featureless voltammograms because of the emittance of redox peaks from proteins on these electrodes, which stipulate an efficient electrical wiring of the redox centers of proteins to the surface of the electrode in the presence of GO. Importantly, the proteins retained their intrinsic peroxidase activity upon forming mixtures with GO and the catalytic properties provide a high sensing performance for H₂O₂ detection with low detection limit and wide detection range. Furthermore, Mani and coworkers improved the performance of Mb-based H₂O₂ biosensors using an RGO-MWCNT-Pt/Mb electrode [233]. The RGO-MWCNT-Pt composite was prepared using the wet chemical method, which provides good affinity and a large surface area for the accumulation of excess Mb. The Pt nanoparticles in the RGO-MWCNT-Pt/Mb composite showed excellent electrocatalytic activity and efficiently prohibited the accumulation and restacking of graphene sheets and CNTs. The resultant electrode (RGO-MWCNT-Pt/Mb) showed an excellent wide linear range from 10 pM to 0.19 nM with a detection limit of 6 pM and much higher sensitivity (1.99 $\mu\text{A pM}^{-1} \text{cm}^{-2}$) compared to other biosensors.

Additionally, HRP-fabricated H₂O₂ electrochemical biosensors were prepared using nano-graphene for the direct electron transfer from HRP to the substrates (electrode) [305]. These HRP-anchored graphene-based materials determine H₂O₂ with higher selectivity and sensitivity [224,306]. Zhang et al. reported immobilization of HRP and lysozyme enzymes on graphene oxide sheets in phosphate buffer solution by incubating GO with enzymes at 4 °C. The immobilized enzyme molecules were studied in situ using AFM, which clearly disclosed HRP molecules (bright spots) on the surface of GO. Strong hydrogen bonding and electrostatic interaction play a key role in loading enzymes (HRP and lysozyme) on graphene oxide, which was much higher than that on previously reported studies and was found to be the optimum solid substrate for the immobilization of the enzyme [307]. Moreover, Fan and coworkers applied the same method to generate graphene-poly (sodium 4-styrenesulfonate)/biomimetic graphene capsules (GS-PSS/GRCAPS) nanocomposites for direct electrochemical sensing of H₂O₂. Initially, porous CaCO₃ was used as a support for HRP encapsulation in GRCAPS. Afterward, a GS-PSS/GRCAPS composite was synthesized via layer-by-layer electrostatic self-assembly, in which negatively charged GS-PSS electrostatically interact with positively charged PEI@GRCAPS [261]. GRCAPS was revealed to mimic the existing enzymes in living cells and provide a satisfactory microenvironment for HRP to realize direct electron transfer at the modified electrode. The resultant electrochemical biosensor exhibited long-term stability, low detection limit, extensive linear range, and an excellent anti-interference ability. A nonenzymatic and highly electrocatalytic H₂O₂ biosensor was proposed using a novel electrode composed of hemin-capped biomineralized gold nanoparticles (Hem@AuNPs), rGO, and chitosan (CS). The excellent rGO conductivity and outstanding electrocatalytic performance of Hem@AuNPs make them suitable for developing ultrasensitive biosensors for real-time determination of H₂O₂. Taking advantages of the peroxidase-like activities of nanohybrids, the resultant electrode demonstrated a highly selective and outstanding electrochemical

performance toward H_2O_2 with fast response, improved sensitivity, and stability. More significantly, the lower determination limit of 9.3 nM and wider linear ranges of five orders of magnitude enable this biosensor to accurately detect H_2O_2 released from living HeLa cells [266]. Jiao et al. reported nonenzymatic biosensors for dynamic, most significant ROS. Intracellular nonenzymatic monitoring of H_2O_2 was achieved via loading of AuPtAg nanoalloy on rGO capped with poly (diallyldimethylammonium chloride). The constructed biosensor showed rapid and precise measurement of H_2O_2 released from cancerous cells. The precise and accurate detection of H_2O_2 is due to the remarkable rGO and PDDA conductivity with outstanding synergistic electrocatalytic performance of ternary alloys. The remarkable electrochemical performance of the resultant biosensor, with a low detection limit (1.2 nM) and wide linear range (from 0.05 μM to 5.5 mM), is due to the peroxidase-like activity of the AuPtAg nanoalloy [59]. In another study, a cytochrome c (Cyt c)-immobilized Au nanoparticle-loaded 3D graphene aerogel (3DGA) was synthesized for the detection of H_2O_2 . Morphological and surface study of the 3DGA-AuNPs revealed efficacious formation of 3D-networked assembly, which helps in enhancing conductivity and effective enzyme immobilization. The large surface of 3DGA and biocompatibility of AuNPs help in enabling direct electron transfer between the electrode and Cyt c. The as-prepared 3DGA-AuNPs/Cyt c/GCE exhibited a pair of well-defined redox peaks of a $\text{Fe}^{\text{III/II}}$ redox couple of Cyt c and revealed excellent electrocatalytic potential toward H_2O_2 with high sensitivity of 351.57 $\mu\text{A mM}^{-1} \text{cm}^{-2}$ [302].

3.5. Carbon Nanotubes (CNTs)

CNTs, an allotropic form of carbon, are composed of a graphene sheet packed in a tube constituting a cylinder (single-walled CNTs (SWCNTs)) or concentric and closed tubules (multiwalled CNTs (MWCNTs)) [308–310]. The combination of CNTs in biosensors offers numerous advantages, including increased surface area, smooth charge transfer, stacking of various biomolecules, and improved conductivity of the resulting platform as shown in Table 5 [310–312].

3.5.1. H_2O_2 Electrochemical Sensors Based on the Association of CNTs and Hemoproteins

Direct electrochemical assignment of proteins in biosensors is an area of high interest. However, direct electron transfer between proteins and electrodes is faced with major problems, i.e., the distance between the redox center and electrode and protein denaturation. Different methods, including polymer adsorption, covalent binding, and layer-by-layer film assembly, are well known for the deposition of protein molecules on the electrode surface. The excellent electrocatalytic properties of CNTs make them valuable in loading biomolecules and for use as biosensors. CNTs function as nanowires and boost the electron transfer from the protein's redox center to the electrode. The heme-containing proteins (Hb, Mb, Cyt c, and HRP) are the most common analytes for protein detection [313]. Heme proteins are the center of several biological redox reactions. Therefore, several studies reported the efficacy of these proteins as a biosensor for H_2O_2 , nitrite, or hydrogen sulfide detection. Yang et al. have developed a method to directly bind hemoglobin to a vertically aligned CNT surface. They modified the nanotubes so they could use diazonium chemistry to directly bind hemoglobin. In amperometric detection of H_2O_2 , an Hb-ACNT electrode exhibits a wide concentration range (40 μM to 3 mM), LOD of 5.4 M, high sensitivity, and long-term stability [314]. This aligned NT forest shows accumulation of Hb on a large area rather than immobilization in unsystematic tangled webs of CNT. Furthermore, Esplandiu et al. immobilized Mb to detect H_2O_2 , studied direct electron transfer kinetic, and showed that vertically aligned NT forests possess better kinetics compared to the epoxy incorporated SWCNT/Mb sensor [315]. In addition, their LOD was 50 nM for H_2O_2 , superior to other random and aligned NT methods. The release of H_2O_2 from living HepG2 cancer cells was studied by Zhang and coworkers, who constructed an enzyme-based biosensor with a LOD of 0.23 μM using SWCNTs as a robust scaffold for Hb immobilization. The constructed biosensor was also used for the

quantification of H_2O_2 released from HepG2 cells via in situ biosynthesis of ZnO quantum dots, which was further confirmed by fluorescence staining [316]. Wang et al. applied a simple dispersion method to coat a GCEs with SWCNT and heme proteins in the presence of cetyltrimethylammonium bromide (CTAB) [317]. CTAB-suspended NTs facilitate the immobilization of Mb, Cyt c, and HRP on the electrode surface. Redox chemistry of heme was studied in the presence of SWCNTs. The developed electrode was precisely used for nitrite and H_2O_2 detection, which gave rise to a new-fangled peak in cyclic voltammograms with decreased in heme reduction peak. The results indicate that the electrode exhibited a response time of only 4 s, LOD of 3.6 M, and less sensitivity for H_2O_2 detection. Several researchers have also demonstrated the efficacy of the immobilization of heme proteins on polymers. For instance, Hb was immobilized on polyelectrolyte surfactant polymers [318], where Hb retained a secondary structure, thus reducing the effect of protein denaturation in polymers. Moreover, the addition of SWCNT to the nanocomposite enhanced the reaction kinetics, and H_2O_2 was sensed with a LOD of 0.8 M. Likewise, MWCNT and Mb were immobilized on the collagen polymers [319], where H_2O_2 was measured with a linear range from 0.6 to 39 M. Nagaraju et al. used self-assembled monolayers of 4-aminothiophenol on gold electrodes with immobilized Cyt c for H_2O_2 detection [320]. Three orders of magnitude of faster electron transfer kinetics were observed with SWCNT in these monolayers as compared to the non-SWCNT monolayer. The results confirmed that NTs increased the direct electron transfer. However, large step changes (3.8 mM) in H_2O_2 were used, and no LOD was calculated. Thus, the sensitivity was not very significant. A layer-by-layer approach was also implemented to immobilize proteins rather than simultaneous deposition of all components, e.g., chitosan-stabilized NTs were placed on GCE, followed by the accumulation of gold NPs on chitosan, and subsequently, Hb was bound to the gold surface [321]. This method is beneficial in retaining the bioactivity of Hb and increases the amount of enzyme activity. The method showed a LOD of 0.2 M for H_2O_2 detection. The heme-based biosensors showed rapid and fast detection of changes in H_2O_2 . In general, HRP is the most widely used in biosensing as compared to other heme-containing proteins, which shows the best results compared to others. The lowest limits of detection for H_2O_2 were achieved using an aligned NT geometry, which supports the accumulation of the heme protein and which, in turn, leads to fast electron transfer from proteins to electrodes. Future studies are required to address the reproducibility of electrode fabrication, practical geometries, and uses for real samples. SWCNTs, HRP, and 1-butyl-3-methylimidazolium tetrafluoroborate (BMIM·BF₄) were combined to construct a cellular H_2O_2 sensor. At a working potential of $-0.35V$, HRP-BMIM·BF₄/SWCNTs/CFUME showed a dynamic range of $\sim 10.2 \mu M$, with a low detection limit of $0.13 \mu M$ ($S/N = 3$) and high sensitivity of $4.25 A/M cm^2$. Due to its small dimension and low working potential, HRP-BMIM·BF₄/SWCNTs/CFUME allowed direct amperometric real-time monitoring of H_2O_2 in HeLa cells treated with camptothecin (an anticancer drug) without complex data processing and extra surface coatings to prevent interference. Thus, its testing evidently demonstrated a significantly high level of H_2O_2 in HeLa cells under camptothecin stress [322]. A schematic presentation of enzyme loaded CNTs for the detection of H_2O_2 in living cells is shown in Figure 6.

Table 5. CNTs-supported metal nanoparticles biosensors for electrochemical sensing of H_2O_2 secreted from cancerous cells.

CNTs H_2O_2 Biosensors	Sensitivity $\mu A mM^{-1} cm^{-2}$	Linear Range (μM)	Detection Limit (μM)	Ref.
ZnO/COOH-MWNTs	-	1–21	-	[323]
GCE/MWCNTs-CDs	0.039	3.5–300	0.25	[324]
((APy) ₆ [H ₂ W ₁₂ O ₄₀])/ (SWCNT-COOH)	-	-	0.4	[325]
GCE/CNTs-PAMAM DENs-PtNCs	987.5	3–400	0.8	[326]

Table 5. Cont.

CNTs H ₂ O ₂ Biosensors	Sensitivity $\mu\text{A mM}^{-1} \text{cm}^{-2}$	Linear Range (μM)	Detection Limit (μM)	Ref.
GCE/C ₆₀ -MWCNTs	0.0243	2–4	0.055	[327]
CS-IL/MB/CuNP				
3D PB NPs/G-CNTs	0.11343	1–3161	0.095	[328]
CF@N-CNTAs–AuNPs	142	1–4300	0.05	[329]
CDs/MWCNTs/GCE	–	–	–	[324]
OECT/PET/CE-CNTs/PtNPs	–	0.5–100	0.2	[330]
ZNBs/fMWCNTs	–	0.049–22	0.035	[331]
ZnONPs/MWCNTs	–	1000–200,000	–	[332]
N-CNTs	30	–	0.5	[333]
(GC) (BG-CNPs/GC)	–	–	–	[334]
GCE/rGONRs/MnO ₂	0.0142	0.25–2245	0.071	[335]

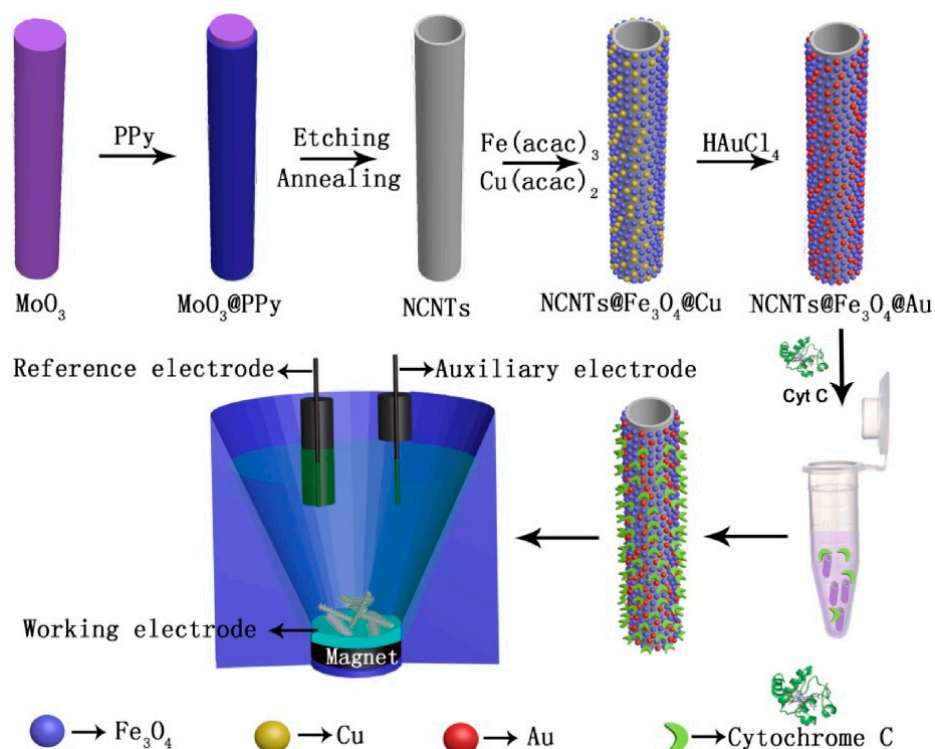


Figure 6. Enzyme-loaded CNTs for the detection of H₂O₂ in living cells. Reproduced with permission from [336]. Copyright 2019, Elsevier Ltd (Amsterdam, The Netherlands).

3.5.2. H₂O₂ Electrochemical Sensors Based on the Association of Metallic Nanoparticles and CNTs

In the last few years, the connotation of metal nanoparticles with CNTs has been considered a valuable alternate for the development of highly sensitive and selective sensors for H₂O₂ detection shown in Figure 7 [41,337,338]. Zhang et al. developed a remarkable stretchy nanohybrid microelectrode using carbon fibers [329]. The constructed microelectrode reproduced a remarkable analytical signal at 0.300 V, with an ultrasmall LOD as low as nanomolar. Rapid and ultrasmall sensing of H₂O₂ excreted from MCF-7 and MDA-MB-231 cells was achieved because of the synergistic catalytic activity of the N-CNTA-decorated AuNPs. Table 6 showed non-enzymatic CNTs biosensors for H₂O₂ sensing.

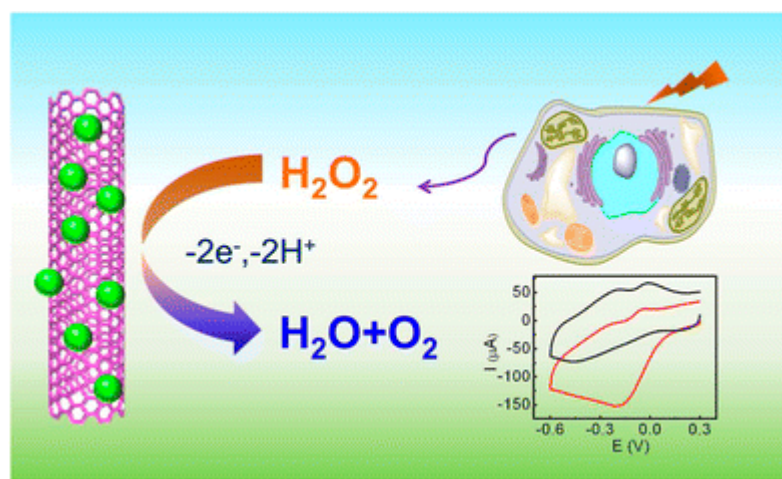


Figure 7. Mechanism of metal nanoparticle loaded CNTs for real-time analyses of H_2O_2 secreted from live cells. Reproduced with permission from [324], Copyright 2016 Springer Ltd (Berlin/Heidelberg, Germany).

Table 6. Ultra-sensitive electrochemical biosensors for detection of H_2O_2 .

H_2O_2 Biosensors	Sensitivity $\mu\text{A mM}^{-1} \text{cm}^{-2}$	Linear Range (μM)	Detection Limit (μM)	Ref.
GN-HN-SWCNT	0.015	0.2–400	0.05	[206]
Cyt c/GO-MWCNT/Au NP	0.533	1×10^{-5} – 1.4×10^{-4}	27.7×10^{-6}	[232]
HRP/P-L-His-rGO	2.6×10^5	0.2–5000	0.05	[224]
HRP/AuNP/ThGP	0.086	0.5–1800	0.01	[225]
RGO-MWCNT-Pt/Mb	1.990	1×10^{-5} – 1.9×10^{-4}	16×10^{-6}	[233]
CoTPP/RGO	0.0013	0.1–4600	0.02	[243]
GN-Pt	0.01	2–710	0.5	[277]
PDA-RGO/Ag NP	0.0111	0.5–8000	2.07	[282]
Pt/GN	0.0204	2.5–6650	0.8	[41]
PtAuNPs-CTAB-GR	0.1654	0.005–4.8	0.0017	[294]
Pd-NPs/GN	0.019	0.001–2000	0.0002	[298]
GCE/MWCNTs-CDs	0.039	3.5–300	0.25	[324]
GCE/ C_{60} -MWCNTs	0.0243	2–4	0.055	[327]
CS-IL/MB/CuNP	0.0142	0.25–2245	0.071	[335]

Bai et al. developed an electrode with high electrocatalytic activity using carbon dots (CDs) and oxidized MWCNTs modified GCEs [324]. The excellent biosensing capability of the MWCNT/CD/GCEs composite is associated with the large surface area and electron acceptor characteristics of MWCNTs and with the excellent donor capacity of the CDs. The analytical performance of the sensor is highly dependent on the MWCNT:CD ratio, so 10:1 was selected for electrode manufacturing. The developed biosensors successfully quantified the H_2O_2 secreted from HeLa cells with a linear range of 3.5×10^{-6} and 3×10^{-4} M and a LOD of 0.25 mM.

Liu and Ding used a Pt-encapsulated poly(amidoamine) dendrimer with amine terminations (G6- NH_2 PAMAM dendrimer) covalently attached to a carboxylated CNT composite [326]. Elaborated architectures showed a rapid, reproducible, and steady response at 0.150 V, with a linear range between 3 and 400 mM. The biosensor successfully detected H_2O_2 in MCF-7 cells with an LOD of 0.8 mM. Liu et al. modified GCEs by dendrimer-encapsulated Pt nanoclusters and carbon nanotubes (Pt-DENs/CNTs) to detect extracellular H_2O_2 excreted from live cells. Those Pt-DENs/CNTs nanocomposites were characterized by UV-Vis spectra, SEM, energy-dispersive X-ray spectroscopy, and TEM. The nonenzymatic sensor displayed exceptional catalytic activity in H_2O_2 reduction. The effective nonenzymatic sensing capability of H_2O_2 reduction revealed that the Pt-DENs/CNTs sensor has potential application in screening H_2O_2 in cellular processes [326].

Real-time monitoring of H_2O_2 secreted from living cells is important to understand the occurrence of diseases and searching of new therapeutic strategies. Zhao et al. successfully

synthesized three-dimensional carbon nanotubes spaced graphene aerogel decorated with Prussian blue nanoparticles (3D PB NPs/G-CNTs) by one-step mild temperature treatment, in which the PB NPs acquire intrinsic peroxidase-like activity. The 3D porous structure of G-CNTs with large surface and high electrical conductivity can efficiently enhance catalytic performance and help in real-time detection of H_2O_2 released from living cells. The composite exhibited good catalytic performance toward H_2O_2 reduction with sensitivity of $134.3 \mu\text{A mM}^{-1} \text{cm}^{-2}$, LOD of 95 nM, and wide linear range of 1–3161 μM [328].

Zhang et al. integrated Fe_3O_4 and Cu nanoparticles (NPs) into the NCNTs to produce N-doped carbon@ Fe_3O_4 -Cu nanotubes (NCNTs@ Fe_3O_4 @Cu) through a one-pot high-temperature decomposition. Then, Au NPs were assembled on the magnetic NCNTs to obtain an NCNTs@ Fe_3O_4 @Au composite by galvanic replacement with Cu NPs. The resultant composite provided a suitable platform for the immobilization of the enzyme to fabricate biosensors for H_2O_2 monitoring. After the cytochrome c (Cyt c) was accumulated by the NCNTs@ Fe_3O_4 @Au composite, the Cyt c/NCNTs@ Fe_3O_4 @Au gathered to the surface of the electrode with an external magnet [336]. Tabrizi et al. developed a flow injection amperometric sandwich-type aptasensor for the detection of human leukemic lymphoblasts (CCRF-CEM). An amperometric biosensor was synthesized by decorating nanogold on poly(3,4-ethylenedioxythiophene) (PEDOT- Au_{nano}). PEDOT- Au_{nano} acts as a nano-platform for immobilizing a thiolated sgc8c aptamer and MWCNTs loaded PdNPs/3,4,9,10-perylene tetracarboxylic acid (MWCNTs- Pd_{nano} /PTCA) to assemble a catalytic labeled aptamer. In this strategy, the CCRF-CEM cancer cells were sandwiched between the immobilized sgc8c aptamer on PEDOT- Au_{nano} (electrode) and sgc8c aptamer MWCNTs- Pd_{nano} /PTCA/aptamer (catalytic site). The resultant sandwich-type aptasensor determined the CCRF-CEM cancer cell concentration using 0.1 mM H_2O_2 (electroactive component). The MWCNTs- Pd_{nano} nanocomposites enhanced the electrocatalytic reduction of H_2O_2 , which further boost sensor sensitivity toward CCRF-CEM cancer cells. The proposed sandwich-type aptasensor displayed outstanding analytical performance for real-time determination of CCRF-CEM cancer cells with high selectivity, ranging from 1.0×10^1 to 5.0×10^5 cells mL^{-1} with an LOD of 8 cells mL^{-1} [339].

3.5.3. In Vivo Sensing of H_2O_2 Release from Carcinoma Cells

Considering the significance of cellular H_2O_2 in cell pharmacology and pathophysiology, accurate and reliable in vivo detection of cellular H_2O_2 is sorely needed. Sensing H_2O_2 at cellular level is constrained by several factors, including small cell size, low concentration of cellular H_2O_2 , and interferences in the culture medium [215,340]. Such in situ monitoring of the cellular release of H_2O_2 provides a new in vitro drug screening platform for personalized medicine and cancer therapy. Enzyme-based electrochemical sensing is efficient for continuous in situ monitoring of H_2O_2 because of its high sensitivity, rapid response, and selectivity [27,267]. In vivo monitoring of H_2O_2 secreted from living cells is essential in understanding cellular signaling pathways. The release of H_2O_2 from living cells is very low because the selective detection of H_2O_2 at a low level is challenging.

Chen et al. used a flow-through mode sensing strategy based on cell-in-lumen configuration for ultra-small detection of H_2O_2 secreted from the H1299 carcinoma cell. The current strategy involved the growth of cells on the inner surface of a porous hollow fiber (PHF), while a sensing layer comprised of multi-walled carbon nanotubes, gold nanoparticles (AuNPs), and enzymes accumulated on the outer surface of the PHF. The porous structure of the resultant electrode proved beneficial in the exchange of H_2O_2 from cell to sensing layer in a short time span. The resultant electrode exhibits ultra-small sensitivity to detect H_2O_2 at the nanomolar level having a detection limit of 6 nM with a wide linear range of 0.01–5 [341]. Ye et al. fabricated a PdPt NCs@SGN/GCE non enzymatic electrochemical biosensor comprised of Pd-Pt nanocages and SnO_2 /graphene nanosheets. The resultant electrode displayed excellent catalytic activity toward H_2O_2 in situ secreted from human cervical cancer cells (Hela cells) with high selectivity and sensitivity, a low detection limit of 0.3 mM, and a large linear range from 1 mM to 300 mM [303]. Fe_3O_4 quantum dot was

decorated on three-dimensional graphene nanocomposites ($\text{Fe}_3\text{O}_4/3\text{DG NCs}$) for real time in-situ monitoring of H_2O_2 released from living cancer cells. The fabricated electrochemical sensor mimics peroxidase-like activity with high sensitivity of $274.15 \text{ mA M}^{-1} \text{ cm}^{-2}$, a low detection limit (78 nM), fast response (2.8 s), and outstanding reproducibility [342].

A nonenzymatic electrochemical sensor was constructed by immobilizing 2D ultrathin MnO_2 nanosheets onto glassy carbon electrodes (GCE) with a Nafion film for real-time monitoring of H_2O_2 released from SP2/0 cells in trace amounts. The amperometric study showed an excellent increase in electrocatalytic reduction of H_2O_2 with an extreme low detection limit (5 nM), wide linear range ($25 \text{ nM}^{-2} \mu\text{M}$ and $10\text{--}454 \mu\text{M}$), and high sensitivity of $3261 \text{ mA M}^{-1} \text{ cm}^{-2}$ via the immobilization of the MnO_2 nanosheets [239]. Xi et al. synthesized N and S dual-doped graphene (NSG) co-doped carbocatalyst via one-pot syntheses. The NSG-modified electrode showed superior catalytic activity toward sensing, including a linear range up to 1.7 mM. The prepared electrode showed high sensitivity of $0.266 \text{ mA cm}^{-2} \text{ mM}^{-1}$ with a detection limit as low as $1 \mu\text{M}$ ($S/N = 3$), with good discernment, reproducibility, stability, and biocompatibility with real-time determination of H_2O_2 secreted from live cancerous cells [343]. Later on, Zhao et al. used a well-controlled strategy for the syntheses of the graphene fiber microelectrode via MnO_2 nanowire ($\text{MnO}_2\text{-NWs}$) assembly ($\text{MnO}_2\text{-NWs@Au-NPs}$). The prepared microelectrode showed proficient catalytic performance toward the redox reaction of H_2O_2 . The nanohybrid microelectrode showed in vivo real-time detection of H_2O_2 released from human breast cancer cells [344]. Recently, Chen and his co-worker established high-index facets of an Au-Pd nanocubes loaded rGO composite. The resultant electrode comprised of three-dimensional nanocomposites showed a detection limit of 4 nM, a wide linear range from $0.005 \mu\text{M}$ to 3.5 mM, and real time monitoring of endogenous H_2O_2 in human serum samples released from a living breast cancer cell [345].

3.6. MXenes Materials

So far, various nanomaterials have been reported and utilized for the development of incrementally efficient biosensors. Among the most recently reported nanomaterials available for biosensors, MXenes have attracted much attention for their huge potential in biosensor development because of their unique characteristics [346]. MXenes are two-dimensional inorganic compounds with a thickness of a few atomic layers and they are composed of transition metal carbides, nitrides, or carbonitrides such as titanium carbide (Ti_3C_2) and titanium carbonitride (Ti_2CN), which confers them with exceptional characteristics, including high conductivity and superior fluorescent, optical, and plasmonic properties [347,348]. Moreover, the biocompatible property of MXenes enables their biomedical application [349,350]. Since they were first reported in 2011, MXenes have been used to develop various types of advanced biosensors, including electrochemical, fluorescent/optical, and surface-enhanced Raman spectroscopy (SERS) biosensors, by augmenting MXene characteristics to make them suitable for specific types of biosensors or by combining them with other nanomaterials [351,352]. Recent studies on the development of highly effective MXene biosensors show that this novel nanomaterial is the most ideal candidate for biosensor development at present. So far, no considerable development was seen in MXenes-based biosensors for detection of H_2O_2 released from a cancer cell. However, we foresee MXenes as having outstanding potential for detection of H_2O_2 at an ultra-low level with durable stability and long working hours.

4. Conclusions and Future Perspectives

Carbon nanomaterials have gained prodigious attention over the last two decades because of their higher applicability in electrochemical sensors. This review shed light on the application of carbon nanomaterials and their composite with metal, metal oxides, and biomolecules for the fabrication of electrochemical sensors for real-time monitoring of hydrogen peroxide. Initially, we discussed the recent advancement in the development of heme protein biosensors with carbon nanomaterials as immobilization matrix and

their application in the detection of H₂O₂. Subsequently, the synthesis and application of graphene-supported nano-catalysts (metal-free, noble metals, and nonnoble metals) was discussed in detail for the construction of nonenzymatic H₂O₂ electrochemical sensors. Despite the extensive advancement in the design and application of carbon nanomaterials for the electrocatalytic determination of H₂O₂, it is crucially important to develop new techniques and methods for the synthesis of carbon-based electrocatalysts with a novel structure and extraordinary activity. Some of the most highly ultra-sensitive biosensors for detecting H₂O₂ at an ultra-low level are displayed in Table 6. Furthermore, the comprehensive understanding and exploration of the structure–property relationship of carbon nanomaterials and their extensive use in H₂O₂ sensors require more efforts and research. Particularly, its excellent electrical conductivity, electron mobility, small band gap, and ultrahigh surface area make it widely applicable in biosensors. These advantages of graphene would bestow good conductivity to the capsule film, further facilitate fast electron transfer between enzyme and basal electrode, and enhance the sensitivity and detection limit of biosensors. We prophesy excellent biosensing potential of new MXenes materials and carbon-based material for detection of H₂O₂ released from cancer cells at an ultra-low level with remarkable stability and selectivity.

Author Contributions: Conceptualization, A.K., A.A.-H. and S.E.D.; methodology, T.A. and A.I.; formal analysis, S.A.H. and A.K.; investigation, A.K. and S.E.D.; resources, A.K. and A.A.-H.; data curation, T.A., A.I. and S.A.H.; writing—original draft preparation, T.A., A.I. and A.K.; writing—review and editing, S.A.H., J.U., A.K. and A.A.-H.; supervision, A.K., A.A.-H. and S.E.D.; project administration, A.K., A.A.-H. and S.E.D.; funding acquisition, S.E.D. All authors have read and agreed to the published version of the manuscript.

Funding: The project was supported by grant from the Oman Research Council (TRC) through the funded project (BFP/RGP/HSS/19/198).

Informed Consent Statement: Not applicable.

Data Availability Statement: All data are available from the corresponding author upon request.

Acknowledgments: The authors would like to thank the University of Nizwa for the generous support of this project. The authors also extend their appreciation to the Deanship of scientific research at King Khalid University for funding this work through the research groups program under Grant No. RGP.1/259/42.

Conflicts of Interest: The authors declare no conflict of interest.

References

1. Martinkova, P.; Kostelnik, A.; Válek, T.; Pohanka, M. Main streams in the construction of biosensors and their applications. *Int. J. Electrochem. Sci.* **2017**, *12*, 7386–7403. [[CrossRef](#)]
2. Li, P.; Lee, G.-H.; Kim, S.Y.; Kwon, S.Y.; Kim, H.-R.; Park, S. From diagnosis to treatment: Recent advances in patient-friendly biosensors and implantable devices. *ACS Nano* **2021**, *15*, 1960–2004. [[CrossRef](#)] [[PubMed](#)]
3. Huang, Y.; Xu, J.; Liu, J.; Wang, X.; Chen, B. Disease-related detection with electrochemical biosensors: A review. *Sensors* **2017**, *17*, 2375. [[CrossRef](#)]
4. Monošík, R.; Stred'anský, M.; Šturdík, E. Application of electrochemical biosensors in clinical diagnosis. *J. Clin. Lab. Anal.* **2012**, *26*, 22–34. [[CrossRef](#)] [[PubMed](#)]
5. Monosik, R.; Stredansky, M.; Tkac, J.; Sturdik, E. Application of enzyme biosensors in analysis of food and beverages. *Food Anal. Methods* **2012**, *5*, 40–53. [[CrossRef](#)]
6. Faridbod, F.; Gupta, V.K.; Zamani, H.A. Electrochemical sensors and biosensors. *Int. J. Electrochem.* **2011**, *2011*. [[CrossRef](#)]
7. World Health Organization. *The World Health Report: 2004: Changing History*; World Health Organization: Geneva, Switzerland, 2004.
8. Siegel, R.L.; Miller, K.D.; Fedewa, S.A.; Ahnen, D.J.; Meester, R.G.; Barzi, A.; Jemal, A. Colorectal cancer statistics, 2017. *CA Cancer J. Clin.* **2017**, *67*, 177–193. [[CrossRef](#)] [[PubMed](#)]
9. Fitzmaurice, C.; Allen, C.; Barber, R.M.; Barregard, L.; Bhutta, Z.A.; Brenner, H.; Dicker, D.J.; Chimed-Orchir, O.; Dandona, R.; Dandona, L. Global, regional, and national cancer incidence, mortality, years of life lost, years lived with disability, and disability-adjusted life-years for 32 cancer groups, 1990 to 2015: A systematic analysis for the global burden of disease study. *JAMA Oncol.* **2017**, *3*, 524–548. [[PubMed](#)]
10. Steward, B.; Kleihues, P. *Colorectal Cancer*; World Cancer Report; IACR Press: Lyon, France, 2003.

11. Iannazzo, D.; Espro, C.; Celesti, C.; Ferlazzo, A.; Neri, G. Smart biosensors for cancer diagnosis based on graphene quantum dots. *Cancers* **2021**, *13*, 3194. [[CrossRef](#)]
12. Mahato, K.; Kumar, A.; Maurya, P.K.; Chandra, P. Shifting paradigm of cancer diagnoses in clinically relevant samples based on miniaturized electrochemical nanobiosensors and microfluidic devices. *Biosens. Bioelectron.* **2018**, *100*, 411–428. [[CrossRef](#)]
13. Chen, W.; Cai, S.; Ren, Q.-Q.; Wen, W.; Zhao, Y.-D. Recent advances in electrochemical sensing for hydrogen peroxide: A review. *Analyst* **2012**, *137*, 49–58. [[CrossRef](#)] [[PubMed](#)]
14. Wang, X.; Martindale, J.L.; Liu, Y.; Holbrook, N.J. The cellular response to oxidative stress: Influences of mitogen-activated protein kinase signalling pathways on cell survival. *Biochem. J.* **1998**, *333*, 291–300. [[CrossRef](#)] [[PubMed](#)]
15. Schreck, R.; Rieber, P.; Baeuerle, P.A. Reactive oxygen intermediates as apparently widely used messengers in the activation of the NF-kappa B transcription factor and HIV-1. *EMBO J.* **1991**, *10*, 2247–2258. [[CrossRef](#)] [[PubMed](#)]
16. Abe, J.-I.; Berk, B.C. Fyn and JAK2 mediate Ras activation by reactive oxygen species. *J. Biol. Chem.* **1999**, *274*, 21003–21010. [[CrossRef](#)] [[PubMed](#)]
17. Elias, H.; Vayssié, S. Reactive peroxy compounds generated in situ from hydrogen peroxide: Kinetics and catalytic application in oxidation processes. *Peroxide Chem. Mech. Prep. Asp. Oxyg. Transf.* **2000**, 128–138. [[CrossRef](#)]
18. Imlay, J.A.; Linn, S. Mutagenesis and stress responses induced in *Escherichia coli* by hydrogen peroxide. *J. Bacteriol.* **1987**, *169*, 2967–2976. [[CrossRef](#)] [[PubMed](#)]
19. Mittal, M.; Siddiqui, M.R.; Tran, K.; Reddy, S.P.; Malik, A.B. Reactive oxygen species in inflammation and tissue injury. *Antioxid. Redox Signal.* **2014**, *20*, 1126–1167. [[CrossRef](#)] [[PubMed](#)]
20. Sen, S.; Chakraborty, R.; Sridhar, C.; Reddy, Y.; De, B. Free radicals, antioxidants, diseases and phytomedicines: Current status and future prospect. *Int. J. Pharm. Sci. Rev. Res.* **2010**, *3*, 91–100.
21. Nogueira, V.; Hay, N. Molecular pathways: Reactive oxygen species homeostasis in cancer cells and implications for cancer therapy. *Clin. Cancer Res.* **2013**, *19*, 4309–4314. [[CrossRef](#)]
22. Martinez-Outschoorn, U.E.; Balliet, R.M.; Lin, Z.; Whitaker-Menezes, D.; Howell, A.; Sotgia, F.; Lisanti, M.P. Hereditary ovarian cancer and two-compartment tumor metabolism: Epithelial loss of BRCA1 induces hydrogen peroxide production, driving oxidative stress and NFκB activation in the tumor stroma. *Cell Cycle* **2012**, *11*, 4152–4166. [[CrossRef](#)]
23. Brigelius-Flohe, R.; Kipp, A. Glutathione peroxidases in different stages of carcinogenesis. *Biochim. Biophys. Acta (BBA)-Gen. Subj.* **2009**, *1790*, 1555–1568. [[CrossRef](#)] [[PubMed](#)]
24. Weinstein, R.; Savariar, E.N.; Felsen, C.N.; Tsien, R.Y. In vivo targeting of hydrogen peroxide by activatable cell-penetrating peptides. *J. Am. Chem. Soc.* **2014**, *136*, 874–877. [[CrossRef](#)]
25. Zhu, L.; Zhang, Y.; Xu, P.; Wen, W.; Li, X.; Xu, J. PtW/MoS₂ hybrid nanocomposite for electrochemical sensing of H₂O₂ released from living cells. *Biosens. Bioelectron.* **2016**, *80*, 601–606. [[CrossRef](#)] [[PubMed](#)]
26. Xi, J.; Xie, C.; Zhang, Y.; Wang, L.; Xiao, J.; Duan, X.; Ren, J.; Xiao, F.; Wang, S. Pd nanoparticles decorated N-doped graphene quantum dots@N-doped carbon hollow nanospheres with high electrochemical sensing performance in cancer detection. *ACS Appl. Mater. Interfaces* **2016**, *8*, 22563–22573. [[CrossRef](#)] [[PubMed](#)]
27. Yu, C.; Wang, L.; Li, W.; Zhu, C.; Bao, N.; Gu, H. Detection of cellular H₂O₂ in living cells based on horseradish peroxidase at the interface of Au nanoparticles decorated graphene oxide. *Sens. Actuators B Chem.* **2015**, *211*, 17–24. [[CrossRef](#)]
28. Razmi, H.; Mohammad-Rezaei, R.; Heidari, H. Self-assembled Prussian blue nanoparticles based electrochemical sensor for high sensitive determination of H₂O₂ in acidic media. *Electroanalysis* **2009**, *21*, 2355–2362. [[CrossRef](#)]
29. Liu, Y.; Wang, D.; Xu, L.; Hou, H.; You, T. A novel and simple route to prepare a Pt nanoparticle-loaded carbon nanofiber electrode for hydrogen peroxide sensing. *Biosens. Bioelectron.* **2011**, *26*, 4585–4590. [[CrossRef](#)]
30. Liu, C.-J.; Yu, S.-L.; Liu, Y.-P.; Dai, X.-J.; Wu, Y.; Li, R.-J.; Tao, J.-C. Synthesis, cytotoxic activity evaluation and HQSAR study of novel isosteviol derivatives as potential anticancer agents. *Eur. J. Med. Chem.* **2016**, *115*, 26–40. [[CrossRef](#)]
31. Cardoso, A.R.; Moreira, F.T.; Fernandes, R.; Sales, M.G.F. Novel and simple electrochemical biosensor monitoring attomolar levels of miRNA-155 in breast cancer. *Biosens. Bioelectron.* **2016**, *80*, 621–630. [[CrossRef](#)] [[PubMed](#)]
32. Yahalom, G.; Weiss, D.; Novikov, I.; Bevers, T.B.; Radvanyi, L.G.; Liu, M.; Piura, B.; Iacobelli, S.; Sandri, M.T.; Cassano, E. An antibody-based blood test utilizing a panel of biomarkers as a new method for improved breast cancer diagnosis. *Biomark. Cancer* **2013**, *5*, 71–80. [[CrossRef](#)] [[PubMed](#)]
33. Yang, C.; Denno, M.E.; Pyakurel, P.; Venton, B.J. Recent trends in carbon nanomaterial-based electrochemical sensors for biomolecules: A review. *Anal. Chim. Acta* **2015**, *887*, 17–37. [[CrossRef](#)]
34. Wang, Z.; Dai, Z. Carbon nanomaterial-based electrochemical biosensors: An overview. *Nanoscale* **2015**, *7*, 6420–6431. [[CrossRef](#)] [[PubMed](#)]
35. Vashist, S.K.; Luong, J.H. Recent advances in electrochemical biosensing schemes using graphene and graphene-based nanocomposites. *Carbon* **2015**, *84*, 519–550. [[CrossRef](#)]
36. Lawal, A.T. Synthesis and utilisation of graphene for fabrication of electrochemical sensors. *Talanta* **2015**, *131*, 424–443. [[CrossRef](#)] [[PubMed](#)]
37. Kuila, T.; Bose, S.; Khanra, P.; Mishra, A.K.; Kim, N.H.; Lee, J.H. Recent advances in graphene-based biosensors. *Biosens. Bioelectron.* **2011**, *26*, 4637–4648. [[CrossRef](#)]
38. Liu, Y.; Dong, X.; Chen, P. Biological and chemical sensors based on graphene materials. *Chem. Soc. Rev.* **2012**, *41*, 2283–2307. [[CrossRef](#)]

39. Wu, S.; He, Q.; Tan, C.; Wang, Y.; Zhang, H. Graphene-based electrochemical sensors. *Small* **2013**, *9*, 1160–1172. [[CrossRef](#)]
40. Ping, J.; Wang, Y.; Fan, K.; Wu, J.; Ying, Y. Direct electrochemical reduction of graphene oxide on ionic liquid doped screen-printed electrode and its electrochemical biosensing application. *Biosens. Bioelectron.* **2011**, *28*, 204–209. [[CrossRef](#)] [[PubMed](#)]
41. Zhang, R.; Chen, W. Recent advances in graphene-based nanomaterials for fabricating electrochemical hydrogen peroxide sensors. *Biosens. Bioelectron.* **2017**, *89*, 249–268. [[CrossRef](#)]
42. Pohanka, M.; Skládal, P. Electrochemical biosensors—Principles and applications. *J. Appl. Biomed.* **2008**, *6*, 57–64. [[CrossRef](#)]
43. Vigneshvar, S.; Sudhakumari, C.; Senthilkumaran, B.; Prakash, H. Recent advances in biosensor technology for potential applications—An overview. *Front. Bioeng. Biotechnol.* **2016**, *4*, 11. [[CrossRef](#)]
44. Lazcka, O.; del Campo, F.J.; Munoz, F.X. Pathogen detection: A perspective of traditional methods and biosensors. *Biosens. Bioelectron.* **2007**, *22*, 1205–1217. [[CrossRef](#)] [[PubMed](#)]
45. He, F. Development of Capillary-Driven Microfluidic Biosensors for Food Safety and Quality Assurance. Ph.D. Thesis, University of Massachusetts Amherst, Amherst, MA, USA, 2014.
46. Zhu, C.; Yang, G.; Li, H.; Du, D.; Lin, Y. Electrochemical sensors and biosensors based on nanomaterials and nanostructures. *Anal. Chem.* **2015**, *87*, 230–249. [[CrossRef](#)]
47. Pundir, C.S.; Deswal, R.; Narwal, V. Quantitative analysis of hydrogen peroxide with special emphasis on biosensors. *Bioprocess Biosyst. Eng.* **2018**, *41*, 313–329. [[CrossRef](#)]
48. Yunus, S.; Jonas, A.M.; Lakard, B. Potentiometric biosensors. In *Encyclopedia of Biophysics*; Roberts, G.C.K., Ed.; Springer: Berlin/Heidelberg, Germany, 2013.
49. Parrilla, M.; Cánovas, R.; Andrade, F.J. Enhanced potentiometric detection of hydrogen peroxide using a platinum electrode coated with nafion. *Electroanalysis* **2017**, *29*, 223–230. [[CrossRef](#)]
50. Zheng, X.; Guo, Z. Potentiometric determination of hydrogen peroxide at MnO₂-doped carbon paste electrode. *Talanta* **2000**, *50*, 1157–1162. [[CrossRef](#)]
51. Zhao, J.; Yan, Y.; Zhu, L.; Li, X.; Li, G. An amperometric biosensor for the detection of hydrogen peroxide released from human breast cancer cells. *Biosens. Bioelectron.* **2013**, *41*, 815–819. [[CrossRef](#)]
52. Li, J.; Tan, S.N.; Ge, H. Silica sol-gel immobilized amperometric biosensor for hydrogen peroxide. *Anal. Chim. Acta* **1996**, *335*, 137–145. [[CrossRef](#)]
53. Wang, B.; Dong, S. Sol-gel-derived amperometric biosensor for hydrogen peroxide based on methylene green incorporated in Nafion film. *Talanta* **2000**, *51*, 565–572. [[CrossRef](#)]
54. Tripathi, V.S.; Kandimalla, V.B.; Ju, H. Amperometric biosensor for hydrogen peroxide based on ferrocene-bovine serum albumin and multiwall carbon nanotube modified ormosil composite. *Biosens. Bioelectron.* **2006**, *21*, 1529–1535. [[CrossRef](#)]
55. Yu, J.; Ju, H. Amperometric biosensor for hydrogen peroxide based on hemoglobin entrapped in titania sol-gel film. *Anal. Chim. Acta* **2003**, *486*, 209–216. [[CrossRef](#)]
56. Povedano, E.; Montiel, V.R.-V.; Gamella, M.; Serafín, V.; Pedrero, M.; Moranova, L.; Bartosik, M.; Montoya, J.J.; Yáñez-Sedeño, P.; Campuzano, S. A novel zinc finger protein-based amperometric biosensor for miRNA determination. *Anal. Bioanal. Chem.* **2019**, *412*, 5031–5041. [[CrossRef](#)] [[PubMed](#)]
57. Li, Y.; Huan, K.; Deng, D.; Tang, L.; Wang, J.; Luo, L. Facile synthesis of ZnMn₂O₄@ rGO microspheres for ultrasensitive electrochemical detection of hydrogen peroxide from human breast cancer cells. *ACS Appl. Mater. Interfaces* **2019**, *12*, 3430–3437. [[CrossRef](#)] [[PubMed](#)]
58. Dong, W.; Ren, Y.; Bai, Z.; Yang, Y.; Chen, Q. Fabrication of hexahedral Au-Pd/graphene nanocomposites biosensor and its application in cancer cell H₂O₂ detection. *Bioelectrochemistry* **2019**, *128*, 274–282. [[CrossRef](#)] [[PubMed](#)]
59. Jiao, J.; Pan, M.; Liu, X.; Li, B.; Liu, J.; Chen, Q. A non-enzymatic sensor based on trimetallic nanoalloy with poly (diallyldimethylammonium chloride)-capped reduced graphene oxide for dynamic monitoring hydrogen peroxide production by cancerous cells. *Sensors* **2020**, *20*, 71. [[CrossRef](#)]
60. Shu, Y.; Zhang, L.; Cai, H.; Yang, Y.; Zeng, J.; Ma, D.; Gao, Q. Hierarchical mo₂c@ MoS₂ nanorods as electrochemical sensors for highly sensitive detection of hydrogen peroxide and cancer cells. *Sens. Actuators B Chem.* **2020**, 127863. [[CrossRef](#)]
61. Thiruppathi, M.; Lin, P.-Y.; Chou, Y.-T.; Ho, H.-Y.; Wu, L.-C.; Ho, J.-A.A. Simple aminophenol-based electrochemical probes for non-enzymatic, dual amperometric detection of NADH and hydrogen peroxide. *Talanta* **2019**, *200*, 450–457. [[CrossRef](#)]
62. Maji, S.K. Plasmon-enhanced electrochemical biosensing of hydrogen peroxide from cancer cells by gold nanorods. *ACS Appl. Nano Mater.* **2019**, *2*, 7162–7169. [[CrossRef](#)]
63. Du, H.; Zhang, X.; Liu, Z.; Qu, F. A supersensitive biosensor based on MoS₂ nanosheet arrays for the real-time detection of H₂O₂ secreted from living cells. *Chem. Commun.* **2019**, *55*, 9653–9656. [[CrossRef](#)] [[PubMed](#)]
64. Li, L.; Zhang, Y.; Zhang, L.; Ge, S.; Liu, H.; Ren, N.; Yan, M.; Yu, J. Based device for colorimetric and photoelectrochemical quantification of the flux of H₂O₂ releasing from MCF-7 cancer cells. *Anal. Chem.* **2016**, *88*, 5369–5377. [[CrossRef](#)]
65. Zhang, L.-N.; Deng, H.-H.; Lin, F.-L.; Xu, X.-W.; Weng, S.-H.; Liu, A.-L.; Lin, X.-H.; Xia, X.-H.; Chen, W. In situ growth of porous platinum nanoparticles on graphene oxide for colorimetric detection of cancer cells. *Anal. Chem.* **2014**, *86*, 2711–2718. [[CrossRef](#)]
66. Ge, S.; Liu, W.; Liu, H.; Liu, F.; Yu, J.; Yan, M.; Huang, J. Colorimetric detection of the flux of hydrogen peroxide released from living cells based on the high peroxidase-like catalytic performance of porous PtPd nanorods. *Biosens. Bioelectron.* **2015**, *71*, 456–462. [[CrossRef](#)] [[PubMed](#)]

67. Ye, X.; Shi, H.; He, X.; Wang, K.; He, D.; Yan, L.A.; Xu, F.; Lei, Y.; Tang, J.; Yu, Y. Iodide-responsive Cu–Au nanoparticle-based colorimetric platform for ultrasensitive detection of target cancer cells. *Anal. Chem.* **2015**, *87*, 7141–7147. [[CrossRef](#)] [[PubMed](#)]
68. Kim, J.-H.; Patra, C.R.; Arkalgud, J.R.; Boghossian, A.A.; Zhang, J.; Han, J.-H.; Reuel, N.F.; Ahn, J.-H.; Mukhopadhyay, D.; Strano, M.S. Single-molecule detection of H₂O₂ mediating angiogenic redox signaling on fluorescent single-walled carbon nanotube array. *ACS Nano* **2011**, *5*, 7848–7857. [[CrossRef](#)] [[PubMed](#)]
69. Maji, S.K.; Sreejith, S.; Mandal, A.K.; Ma, X.; Zhao, Y. Immobilizing gold nanoparticles in mesoporous silica covered reduced graphene oxide: A hybrid material for cancer cell detection through hydrogen peroxide sensing. *ACS Appl. Mater. Interfaces* **2014**, *6*, 13648–13656. [[CrossRef](#)] [[PubMed](#)]
70. Wang, Y.; Tang, L.; Li, Z.; Lin, Y.; Li, J. In situ simultaneous monitoring of ATP and GTP using a graphene oxide nanosheet-based sensing platform in living cells. *Nat. Protoc.* **2014**, *9*, 1944. [[CrossRef](#)]
71. McKibbin, P.L.; Kabori, A.; Taniguchi, Y.; Kool, E.T.; David, S.S. Surprising repair activities of nonpolar analogs of 8-oxoG expose features of recognition and catalysis by base excision repair glycosylases. *J. Am. Chem. Soc.* **2012**, *134*, 1653–1661. [[CrossRef](#)] [[PubMed](#)]
72. Li, L.; Lin, H.; Lei, C.; Nie, Z.; Huang, Y.; Yao, S. Label-free fluorescence assay for thrombin based on unmodified quantum dots. *Biosens. Bioelectron.* **2014**, *54*, 42–47. [[CrossRef](#)] [[PubMed](#)]
73. Ren, D.; Wong, N.T.; Handoko, A.D.; Huang, Y.; Yeo, B.S. Mechanistic insights into the enhanced activity and stability of agglomerated Cu nanocrystals for the electrochemical reduction of carbon dioxide to n-propanol. *J. Phys. Chem. Lett.* **2016**, *7*, 20–24. [[CrossRef](#)]
74. Zhou, Y.; Zhang, Y.; Lau, C.; Lu, J. Sequential determination of two proteins by temperature-triggered homogeneous chemiluminescent immunoassay. *Anal. Chem.* **2006**, *78*, 5920–5924. [[CrossRef](#)] [[PubMed](#)]
75. Liu, M.; Lin, Z.; Lin, J.-M. A review on applications of chemiluminescence detection in food analysis. *Anal. Chim. Acta* **2010**, *670*, 1–10. [[CrossRef](#)]
76. Kong, H.; Liu, D.; Zhang, S.; Zhang, X. Protein sensing and cell discrimination using a sensor array based on nanomaterial-assisted chemiluminescence. *Anal. Chem.* **2011**, *83*, 1867–1870. [[CrossRef](#)] [[PubMed](#)]
77. Ji, D.; Mohsen, M.G.; Harcourt, E.M.; Kool, E.T. ATP-Releasing Nucleotides: Linking DNA Synthesis to Luciferase Signaling. *Angew. Chem. Int. Ed.* **2016**, *55*, 2087–2091. [[CrossRef](#)]
78. Liu, B.-F.; Ozaki, M.; Hisamoto, H.; Luo, Q.; Utsumi, Y.; Hattori, T.; Terabe, S. Microfluidic chip toward cellular ATP and ATP-conjugated metabolic analysis with bioluminescence detection. *Anal. Chem.* **2005**, *77*, 573–578. [[CrossRef](#)] [[PubMed](#)]
79. Ju, J.; Chen, W. In situ growth of surfactant-free gold nanoparticles on nitrogen-doped graphene quantum dots for electrochemical detection of hydrogen peroxide in biological environments. *Anal. Chem.* **2015**, *87*, 1903–1910. [[CrossRef](#)] [[PubMed](#)]
80. Bai, J.; Jiang, X. A facile one-pot synthesis of copper sulfide-decorated reduced graphene oxide composites for enhanced detecting of H₂O₂ in biological environments. *Anal. Chem.* **2013**, *85*, 8095–8101. [[CrossRef](#)]
81. Lu, Y.; Liu, Y.; Zhang, S.; Wang, S.; Zhang, S.; Zhang, X. Aptamer-Based Plasmonic Sensor Array for Discrimination of Proteins and Cells with the Naked Eye. *Anal. Chem.* **2013**, *85*, 6571–6574. [[CrossRef](#)]
82. Gong, Y.; Chen, X.; Lu, Y.; Yang, W. Self-assembled dipeptide–gold nanoparticle hybrid spheres for highly sensitive amperometric hydrogen peroxide biosensors. *Biosens. Bioelectron.* **2015**, *66*, 392–398. [[CrossRef](#)] [[PubMed](#)]
83. Wang, Y.; Gu, H. Core-Shell-Type Magnetic Mesoporous Silica Nanocomposites for Bioimaging and Therapeutic Agent Delivery. *Adv. Mater.* **2015**, *27*, 576–585. [[CrossRef](#)]
84. Yang, J.; Shen, D.; Zhou, L.; Li, W.; Li, X.; Yao, C.; Wang, R.; El-Toni, A.M.; Zhang, F.; Zhao, D. Spatially confined fabrication of core–shell gold nanocages@mesoporous silica for near-infrared controlled photothermal drug release. *Chem. Mater.* **2013**, *25*, 3030–3037. [[CrossRef](#)]
85. Lee, D.; Khaja, S.D.; Velasquez-Castano, J.C.; Dasari, M.; Sun, C.; A Petros, J.; Taylor, W.R.; Murthy, N. In vivo imaging of hydrogen peroxide with chemiluminescent nanoparticles. *Nat. Mater.* **2007**, *6*, 765–769. [[CrossRef](#)] [[PubMed](#)]
86. Arnous, A.; Petrakis, C.; Makris, D.P.; Kefalas, P. A peroxyoxalate chemiluminescence-based assay for the evaluation of hydrogen peroxide scavenging activity employing 9,10-diphenylanthracene as the fluorophore. *J. Pharmacol. Toxicol. Methods* **2002**, *48*, 171–177. [[CrossRef](#)]
87. Koike, R.; Kato, Y.; Motoyoshiya, J.; Nishii, Y.; Aoyama, H. Unprecedented chemiluminescence behaviour during peroxyoxalate chemiluminescence of oxalates with fluorescent or electron-donating aryloxy groups. *Luminescence* **2006**, *21*, 164–173. [[CrossRef](#)]
88. Stevani, C.V.; Silva, S.M.; Baader, W.J. Studies on the Mechanism of the Excitation Step in Peroxyoxalate Chemiluminescence. *Eur. J. Org. Chem.* **2000**, *2000*, 4037–4046. [[CrossRef](#)]
89. Matsumoto, M. Advanced chemistry of dioxetane-based chemiluminescent substrates originating from bioluminescence. *J. Photochem. Photobiol. C* **2004**, *5*, 27–53. [[CrossRef](#)]
90. Lee, D.; Dasari, M.; Erigala, V.; Murthy, N.; Yu, J.; Dickson, R. Detection of hydrogen peroxide with chemiluminescent micelles. *Int. J. Nanomed.* **2008**, *3*, 471–476. [[CrossRef](#)]
91. Weissleder, R.; Pittet, M.J. Imaging in the era of molecular oncology. *Nature* **2008**, *452*, 580–589. [[CrossRef](#)]
92. Zhang, K.; Kaufman, R.J. From endoplasmic-reticulum stress to the inflammatory response. *Nature* **2008**, *454*, 455–462. [[CrossRef](#)] [[PubMed](#)]
93. Peer, D.; Karp, J.M.; Hong, S.; Farokhzad, O.C.; Margalit, R.; Langer, R. Nanocarriers as an emerging platform for cancer therapy. *Nat. Nanotechnol.* **2007**, *2*, 751–760. [[CrossRef](#)] [[PubMed](#)]

94. Nan, Y.; Zhao, W.; Li, N.; Liang, Z.; Xu, X. Chemiluminescence-triggered fluorophore release: Approach for in vivo fluorescence imaging of hydrogen peroxide. *Sens. Actuators B Chem.* **2019**, *281*, 296–302. [[CrossRef](#)]
95. Lee, Y.-D.; Lim, C.-K.; Singh, A.; Koh, J.; Kim, J.; Kwon, I.C.; Kim, S. Dye/Peroxalate Aggregated Nanoparticles with Enhanced and Tunable Chemiluminescence for Biomedical Imaging of Hydrogen Peroxide. *ACS Nano* **2012**, *6*, 6759–6766. [[CrossRef](#)] [[PubMed](#)]
96. Lee, E.S.; Deepagan, V.G.; Gil You, D.; Jeon, J.; Yi, G.-R.; Lee, J.Y.; Lee, D.S.; Suh, Y.D.; Park, J.H. Nanoparticles based on quantum dots and a luminol derivative: Implications for in vivo imaging of hydrogen peroxide by chemiluminescence resonance energy transfer. *Chem. Commun.* **2016**, *52*, 4132–4135. [[CrossRef](#)] [[PubMed](#)]
97. Geng, J.; Li, K.; Qin, W.; Tang, B.Z.; Liu, B. Red-Emissive Chemiluminescent Nanoparticles with Aggregation-Induced Emission Characteristics for In Vivo Hydrogen Peroxide Imaging. *Part. Part. Syst. Charact.* **2014**, *31*, 1238–1243. [[CrossRef](#)]
98. Jia, Y.; Sun, S.; Cui, X.; Wang, X.; Yang, L. Enzyme-like catalysis of polyoxometalates for chemiluminescence: Application in ultrasensitive detection of H₂O₂ and blood glucose. *Talanta* **2019**, *205*, 120139. [[CrossRef](#)] [[PubMed](#)]
99. Klassen, N.V.; Marchington, D.; McGowan, H.C. H₂O₂ Determination by the I₃⁻ Method and by KMnO₄ Titration. *Anal. Chem.* **1994**, *66*, 2921–2925. [[CrossRef](#)]
100. Kieber, R.J.; Helz, G.R. Two-method verification of hydrogen peroxide determinations in natural waters. *Anal. Chem.* **1986**, *58*, 2312–2315. [[CrossRef](#)]
101. Putt, K.S.; Pugh, R.B. A High-throughput microtiter plate based method for the determination of peracetic acid and hydrogen peroxide. *PLoS ONE* **2013**, *8*, e79218. [[CrossRef](#)] [[PubMed](#)]
102. Zaribafan, A.; Haghbeen, K.; Fazli, M.; Akhondali, A. Spectrophotometric method for hydrogen peroxide determination through oxidation of organic dyes. *Environ. Stud. Persian Gulf* **2014**, *1*, 93–101.
103. Matsubara, C.; Kudo, K.; Kawashita, T.; Takamura, K. Spectrophotometric determination of hydrogen peroxide with titanium 2-((5-bromopyridyl)azo)-5-(N-propyl-N-sulfopropylamino)phenol reagent and its application to the determination of serum glucose using glucose oxidase. *Anal. Chem.* **1985**, *57*, 1107–1109. [[CrossRef](#)]
104. Clapp, P.A.; Evans, D.F.; Sheriff, T.S. Spectrophotometric determination of hydrogen peroxide after extraction with ethyl acetate. *Anal. Chim. Acta* **1989**, *218*, 331–334. [[CrossRef](#)]
105. Mukhopadhyay, D.; Dasgupta, P.; Roy, D.S.; Palchoudhuri, S.; Chatterjee, I.; Ali, S.; Dastidar, S.G. A Sensitive In vitro Spectrophotometric Hydrogen Peroxide Scavenging Assay using 1,10-Phenanthroline. *Free Radic. Antioxid.* **2016**, *6*, 124–132. [[CrossRef](#)]
106. Elnemma, E.M. Spectrophotometric Determination of Hydrogen Peroxide by a Hydroquinone-Aniline System Catalyzed by Molybdate. *Bull. Korean Chem. Soc.* **2004**, *25*, 127–129.
107. Zhang, L.-S.; Wong, G.T. Spectrophotometric determination of H₂O₂ in marine waters with leuco crystal violet. *Talanta* **1994**, *41*, 2137–2145. [[CrossRef](#)]
108. Huang, Y.; Cai, R.; Mao, L.; LIU, Z.; HUANG, H. Spectrophotometric determination of hydrogen peroxide using β-CD-Hemin as a mimetic enzyme of peroxidase. *Anal. Sci.* **1999**, *15*, 889–894. [[CrossRef](#)]
109. Zhang, Q.; Fu, S.; Li, H.; Liu, Y. A novel method for the determination of hydrogen peroxide in bleaching effluents by spectroscopy. *BioResources* **2013**, *8*, 3699–3705. [[CrossRef](#)]
110. Eisenberg, G. Industrial and engineering chemistry. *Ind. Eng. Chem. Anal. Ed.* **1943**, *15*, 327–328. [[CrossRef](#)]
111. Graf, E.; Penniston, J.T. Method for determination of hydrogen peroxide, with its application illustrated by glucose assay. *Clin. Chem.* **1980**, *26*, 658–660. [[CrossRef](#)]
112. Pick, E.; Keisari, Y. A simple colorimetric method for the measurement of H₂O₂ produced by cells in culture. *J. Immunol. Methods* **1980**, *38*, 161–170. [[CrossRef](#)]
113. Fernando, C.D.; Soysa, P. Optimized enzymatic colorimetric assay for determination of hydrogen peroxide (H₂O₂) scavenging activity of plant extracts. *MethodsX* **2015**, *2*, 283–291. [[CrossRef](#)] [[PubMed](#)]
114. Su, G.; Wei, Y.; Guo, M. Direct Colorimetric Detection of Hydrogen Peroxide Using 4-Nitrophenyl Boronic Acid or Its Pinacol Ester. *Am. J. Anal. Chem.* **2011**, *2*, 879–884. [[CrossRef](#)]
115. Nitinaivinij, K.; Parnklang, T.; Thammacharoen, C.; Ekgasit, S.; Wongravee, K. Colorimetric determination of hydrogen peroxide by morphological decomposition of silver nanoprisms coupled with chromaticity analysis. *Anal. Methods* **2014**, *6*, 9816–9824. [[CrossRef](#)]
116. Takahashi, A.; Hashimoto, K.; Kumazawa, S.; Nakayama, T. Determination of Hydrogen Peroxide by High-Performance Liquid Chromatography with a Cation-Exchange Resin Gel Column and Electrochemical Detector. *Anal. Sci.* **1999**, *15*, 481–483. [[CrossRef](#)]
117. Wada, M.; Inoue, K.; Ihara, A.; Kishikawa, N.; Nakashima, K.; Kuroda, N. Determination of organic peroxides by liquid chromatography with on-line post-column ultraviolet irradiation and peroxyoxalate chemiluminescence detection. *J. Chromatogr. A* **2003**, *987*, 189–195. [[CrossRef](#)]
118. Nepomnyashchikh, Y.V.; Borkina, G.G.; Karavaeva, A.V.; Perkel', A.L. Photometric and Gas-Chromatographic Determination of Hydrogen Peroxide and Peroxybutanoic Acid in Oxidized Butanoic Acid. *J. Anal. Chem.* **2005**, *60*, 1024–1028. [[CrossRef](#)]
119. Magara, K.; Ikeda, T.; Sugimoto, T.; Hosoya, S. Quantitative Analysis of Hydrogen Peroxide by High Performance Liquid Chromatography. *Jpn. TAPPI J.* **2007**, *61*, 1481–1493. [[CrossRef](#)]
120. Tarno, H.; Qi, H.; Endoh, R.; Kobayashi, M.; Goto, H.; Futai, K. Types of frass produced by the ambrosia beetle *Platypus quercivorus* during gallery construction, and host suitability of five tree species for the beetle. *J. For. Res.* **2011**, *16*, 68–75. [[CrossRef](#)]

121. Wielandt, H. On the eigenvalues of $A + B$ and AB . *J. Res. Natl. Bur. Stand. Sect. B Math. Sci.* **1973**, *77B*, 61. [[CrossRef](#)]
122. Xu, K.; Tang, B.; Huang, H.; Yang, G.; Chen, Z.; Li, P.; An, L. Strong red fluorescent probes suitable for detecting hydrogen peroxide generated by mice peritoneal macrophages. *Chem. Commun.* **2005**, *48*, 5974–5976. [[CrossRef](#)]
123. Paździoch-Czochra, M.; Wideńska, A. Spectrofluorimetric determination of hydrogen peroxide scavenging activity. *Anal. Chim. Acta* **2002**, *452*, 177–184. [[CrossRef](#)]
124. Miller, E.W.; Albers, A.E.; Pralle, A.; Isacoff, E.Y.; Chang, C.J. Boronate-Based Fluorescent Probes for Imaging Cellular Hydrogen Peroxide. *J. Am. Chem. Soc.* **2005**, *127*, 16652–16659. [[CrossRef](#)]
125. Qian, P.; Qin, Y.; Lyu, Y.; Li, Y.; Wang, L.; Wang, S.; Liu, Y. A hierarchical cobalt/carbon nanotube hybrid nanocomplex-based ratiometric fluorescent nanosensor for ultrasensitive detection of hydrogen peroxide and glucose in human serum. *Anal. Bioanal. Chem.* **2019**, *411*, 1517–1524. [[CrossRef](#)] [[PubMed](#)]
126. Onoda, M.; Uchiyama, T.; Mawatari, K.-I.; Kaneko, K.; Nakagomi, K. Simple and Rapid Determination of Hydrogen Peroxide Using Phosphine-based Fluorescent Reagents with Sodium Tungstate Dihydrate. *Anal. Sci.* **2006**, *22*, 815–817. [[CrossRef](#)] [[PubMed](#)]
127. Lyublinskaya, O.; Antunes, F. Measuring intracellular concentration of hydrogen peroxide with the use of genetically encoded H_2O_2 biosensor HyPer. *Redox Biol.* **2019**, *24*, 101200. [[CrossRef](#)]
128. Belousov, V.V.; Fradkov, A.F.; Lukyanov, K.; Staroverov, D.; Shakhbazov, K.S.; Terskikh, A.V.; Lukyanov, S. Genetically encoded fluorescent indicator for intracellular hydrogen peroxide. *Nat. Methods* **2006**, *3*, 281–286. [[CrossRef](#)]
129. Zheng, M.; Åslund, F.; Storz, G. Activation of the OxyR Transcription Factor by Reversible Disulfide Bond Formation. *Science* **1998**, *279*, 1718–1722. [[CrossRef](#)]
130. Markvicheva, K.N.; Bilan, D.; Mishina, N.; Gorokhovatsky, A.Y.; Vinokurov, L.M.; Lukyanov, S.; Belousov, V.V. A genetically encoded sensor for H_2O_2 with expanded dynamic range. *Bioorganic Med. Chem.* **2011**, *19*, 1079–1084. [[CrossRef](#)]
131. Bilan, D.S.; Pase, L.; Joosen, L.; Gorokhovatsky, A.Y.; Ermakova, Y.G.; Gadella, T.W.J.; Grabher, C.; Schultz, C.; Lukyanov, S.; Belousov, V.V. HyPer-3: A Genetically Encoded H_2O_2 Probe with Improved Performance for Ratiometric and Fluorescence Lifetime Imaging. *ACS Chem. Biol.* **2013**, *8*, 535–542. [[CrossRef](#)]
132. Pak, V.V.; Ezerina, D.; Lyublinskaya, O.; Pedre, B.; Tyurin-Kuzmin, P.A.; Mishina, N.M.; Thauvin, M.; Young, D.; Wahni, K.; Gache, S.A.M.; et al. Ultrasensitive Genetically Encoded Indicator for Hydrogen Peroxide Identifies Roles for the Oxidant in Cell Migration and Mitochondrial Function. *Cell Metab.* **2020**, *31*, 642–653.e6. [[CrossRef](#)] [[PubMed](#)]
133. Ermakova, Y.; Bilan, D.; Matlashov, M.; Mishina, N.; Markvicheva, K.N.; Subach, O.M.; Subach, F.V.; Bogeski, I.; Hoth, M.; Enikolopov, G.; et al. Red fluorescent genetically encoded indicator for intracellular hydrogen peroxide. *Nat. Commun.* **2014**, *5*, 5222. [[CrossRef](#)]
134. Choi, H.-J.; Kim, S.-J.; Mukhopadhyay, P.; Cho, S.; Woo, J.-R.; Storz, G.; Ryu, S.-E. Structural Basis of the Redox Switch in the OxyR Transcription Factor. *Cell* **2001**, *105*, 103–113. [[CrossRef](#)]
135. Xu, J.; Zhang, Y.; Yu, H.; Gao, X.; Shao, S. Mitochondria-Targeted Fluorescent Probe for Imaging Hydrogen Peroxide in Living Cells. *Anal. Chem.* **2015**, *88*, 1455–1461. [[CrossRef](#)] [[PubMed](#)]
136. Xiao, H.; Li, P.; Hu, X.; Shi, X.; Zhang, W.; Tang, B. Simultaneous fluorescence imaging of hydrogen peroxide in mitochondria and endoplasmic reticulum during apoptosis. *Chem. Sci.* **2016**, *7*, 6153–6159. [[CrossRef](#)] [[PubMed](#)]
137. Shen, R.; Liu, P.; Zhang, Y.; Yu, Z.; Chen, X.; Zhou, L.; Nie, B.; Żaczek, A.; Chen, J.; Liu, J. Sensitive Detection of Single-Cell Secreted H_2O_2 by Integrating a Microfluidic Droplet Sensor and Au Nanoclusters. *Anal. Chem.* **2018**, *90*, 4478–4484. [[CrossRef](#)] [[PubMed](#)]
138. Chen, Y.; Ye, J.; Lv, G.; Liu, W.; Jiang, H.; Liu, X.; Wang, X. Hydrogen Peroxide and Hypochlorite Responsive Fluorescent Nanoprobes for Sensitive Cancer Cell Imaging. *Biosensors* **2022**, *12*, 111. [[CrossRef](#)]
139. Hu, L.; Yuan, Y.; Zhang, L.; Zhao, J.; Majeed, S.; Xu, G. Copper nanoclusters as peroxidase mimetics and their applications to H_2O_2 and glucose detection. *Anal. Chim. Acta* **2013**, *762*, 83–86. [[CrossRef](#)]
140. Liu, H.; Gu, C.; Xiong, W.; Zhang, M. A sensitive hydrogen peroxide biosensor using ultra-small $CuInS_2$ nanocrystals as peroxidase mimics. *Sens. Actuators B Chem.* **2015**, *209*, 670–676. [[CrossRef](#)]
141. Su, L.; Qin, W.; Zhang, H.; Rahman, Z.U.; Ren, C.; Ma, S.; Chen, X. The peroxidase/catalase-like activities of MFe_2O_4 ($M = Mg, Ni, Cu$) MNPs and their application in colorimetric biosensing of glucose. *Biosens. Bioelectron.* **2015**, *63*, 384–391. [[CrossRef](#)]
142. Regalado, C.; García-Almendárez, B.E.; Duarte-Vázquez, M.A. Biotechnological applications of peroxidases. *Phytochem. Rev.* **2004**, *3*, 243–256. [[CrossRef](#)]
143. Hamid, M. Potential applications of peroxidases. *Food Chem.* **2009**, *115*, 1177–1186. [[CrossRef](#)]
144. Chekin, F.; Gorton, L.; Tapsoba, I. Direct and mediated electrochemistry of peroxidase and its electrocatalysis on a variety of screen-printed carbon electrodes: Amperometric hydrogen peroxide and phenols biosensor. *Anal. Bioanal. Chem.* **2014**, *407*, 439–446. [[CrossRef](#)]
145. Yang, H.; Liu, B.; Ding, Y.; Li, L.; Ouyang, X. Fabrication of cuprous oxide nanoparticles-graphene nanocomposite for determination of acetaminophen. *J. Electroanal. Chem.* **2015**, *757*, 88–93. [[CrossRef](#)]
146. Chulkova, I.; Derina, K.; Taishibekova, Y. The modified electrode for the determination of cholesterol. In Proceedings of the Chemistry and Chemical Technology in the XXI Century: Materials of the XVI International Scientific-Practical Conference of Students and Young Scientists Dedicated to the 115th Anniversary of Professor L.P. Kuleva, Tomsk, Russia, 25–29 May 2015; pp. 195–197.

147. Jelikić-Stankov, M.D.; Djurdjevic, P.; Stankov, D. Determination of uric acid in human serum by an enzymatic method using N-methyl-N-(4-aminophenyl)-3-methoxyaniline reagent. *J. Serb. Chem. Soc.* **2003**, *68*, 691–698. [[CrossRef](#)]
148. Zhou, B.; Wang, J.; Guo, Z.; Tan, H.; Zhu, X. A simple colorimetric method for determination of hydrogen peroxide in plant tissues. *Plant Growth Regul.* **2006**, *49*, 113–118. [[CrossRef](#)]
149. Chinnadayala, S.R.; Kakoti, A.; Santhosh, M.; Goswami, P. A novel amperometric alcohol biosensor developed in a 3rd generation bioelectrode platform using peroxidase coupled ferrocene activated alcohol oxidase as biorecognition system. *Biosens. Bioelectron.* **2014**, *55*, 120–126. [[CrossRef](#)]
150. Yu, F.; Huang, Y.; Cole, A.J.; Yang, V.C. The artificial peroxidase activity of magnetic iron oxide nanoparticles and its application to glucose detection. *Biomaterials* **2009**, *30*, 4716–4722. [[CrossRef](#)]
151. Mu, J.; Zhang, L.; Zhao, M.; Wang, Y. Co₃O₄ nanoparticles as an efficient catalase mimic: Properties, mechanism and its electrocatalytic sensing application for hydrogen peroxide. *J. Mol. Catal. A Chem.* **2013**, *378*, 30–37. [[CrossRef](#)]
152. Yoon, J.; Lee, T.; Bapurao G., B.; Jo, J.; Oh, B.-K.; Choi, J.-W. Electrochemical H₂O₂ biosensor composed of myoglobin on MoS₂ nanoparticle-graphene oxide hybrid structure. *Biosens. Bioelectron.* **2017**, *93*, 14–20. [[CrossRef](#)]
153. Wen, Z.; Ci, S.; Li, J. Pt Nanoparticles Inserting in Carbon Nanotube Arrays: Nanocomposites for Glucose Biosensors. *J. Phys. Chem. C* **2009**, *113*, 13482–13487. [[CrossRef](#)]
154. Pingarrón, J.M.; Yáñez-Sedeño, P.; González-Cortés, A. Gold nanoparticle-based electrochemical biosensors. *Electrochim. Acta* **2008**, *53*, 5848–5866. [[CrossRef](#)]
155. Zhou, M.; Zhai, Y.M.; Dong, S.J. Electrochemical sensing and biosensing platform based on chemically reduced graphene oxide. *Anal. Chem.* **2009**, *81*, 5603–5613. [[CrossRef](#)]
156. Xu, X.; Jiang, S.; Hu, Z.; Liu, S. Nitrogen-doped carbon nanotubes: High electrocatalytic activity toward the oxidation of hydrogen peroxide and its application for biosensing. *ACS Nano* **2010**, *4*, 4292–4298. [[CrossRef](#)]
157. Luo, Y.; Liu, H.; Rui, Q.; Tian, Y. Detection of Extracellular H₂O₂ Released from Human Liver Cancer Cells Based on TiO₂ Nanoneedles with Enhanced Electron Transfer of Cytochrome c. *Anal. Chem.* **2009**, *81*, 3035–3041. [[CrossRef](#)] [[PubMed](#)]
158. Shao, Y.; Wang, J.; Wu, H.; Liu, J.; Aksay, I.A.; Lin, Y. Graphene based electrochemical sensors and biosensors: A review. *Electroanal. Int. J. Devoted Fundam. Pract. Asp. Electroanal.* **2010**, *22*, 1027–1036. [[CrossRef](#)]
159. Kim, G.; Lee, Y.-E.K.; Xu, H.; Philbert, M.A.; Kopelman, R. Nanoencapsulation method for high selectivity sensing of hydrogen peroxide inside live cells. *Anal. Chem.* **2010**, *82*, 2165–2169. [[CrossRef](#)] [[PubMed](#)]
160. Sun, X.; Guo, S.; Liu, Y.; Sun, S. Dumbbell-like PtPd–Fe₃O₄ nanoparticles for enhanced electrochemical detection of H₂O₂. *Nano Lett.* **2012**, *12*, 4859–4863. [[CrossRef](#)] [[PubMed](#)]
161. Wang, T.; Zhu, H.; Zhuo, J.; Zhu, Z.; Papakonstantinou, P.; Lubarsky, G.; Lin, J.; Li, M. Biosensor Based on Ultrasmall MoS₂ Nanoparticles for Electrochemical Detection of H₂O₂ Released by Cells at the Nanomolar Level. *Anal. Chem.* **2013**, *85*, 10289–10295. [[CrossRef](#)] [[PubMed](#)]
162. Dou, B.; Yang, J.; Yuan, R.; Xiang, Y. Trimetallic Hybrid Nanoflower-Decorated MoS₂ Nanosheet Sensor for Direct in Situ Monitoring of H₂O₂ Secreted from Live Cancer Cells. *Anal. Chem.* **2018**, *90*, 5945–5950. [[CrossRef](#)] [[PubMed](#)]
163. Chang, H.-C.; Ho, J.-A.A. Gold nanocluster-assisted fluorescent detection for hydrogen peroxide and cholesterol based on the inner filter effect of gold nanoparticles. *Anal. Chem.* **2015**, *87*, 10362–10367. [[CrossRef](#)] [[PubMed](#)]
164. Cui, H.; Wang, W.; Duan, C.-F.; Dong, Y.-P.; Guo, J.-Z. Synthesis, characterization, and electrochemiluminescence of luminol-reduced gold nanoparticles and their application in a hydrogen peroxide sensor. *Chem.–A Eur. J.* **2007**, *13*, 6975–6984. [[CrossRef](#)] [[PubMed](#)]
165. Liu, Q.; Yang, Y.; Lv, X.; Ding, Y.; Zhang, Y.; Jing, J.; Xu, C. One-step synthesis of uniform nanoparticles of porphyrin functionalized ceria with promising peroxidase mimetics for H₂O₂ and glucose colorimetric detection. *Sens. Actuators B Chem.* **2017**, *240*, 726–734. [[CrossRef](#)]
166. Xiong, X.; You, C.; Cao, X.; Pang, L.; Kong, R.; Sun, X. Ni₂P nanosheets array as a novel electrochemical catalyst electrode for non-enzymatic H₂O₂ sensing. *Electrochim. Acta* **2017**, *253*, 517–521. [[CrossRef](#)]
167. Chen, L.; Wang, N.; Wang, X.; Ai, S. Protein-directed in situ synthesis of platinum nanoparticles with superior peroxidase-like activity, and their use for photometric determination of hydrogen peroxide. *Mikrochim. Acta* **2013**, *180*, 1517–1522. [[CrossRef](#)]
168. Ma, B.; Kong, C.; Hu, X.; Liu, K.; Huang, Q.; Lv, J.; Lu, W.; Zhang, X.; Yang, Z.; Yang, S. A sensitive electrochemical nonenzymatic biosensor for the detection of H₂O₂ released from living cells based on ultrathin concave Ag nanosheets. *Biosens. Bioelectron.* **2018**, *106*, 29–36. [[CrossRef](#)]
169. Asif, M.; Liu, H.; Aziz, A.; Wang, H.; Wang, Z.; Ajmal, M.; Xiao, F.; Liu, H. Core-shell iron oxide-layered double hydroxide: High electrochemical sensing performance of H₂O₂ biomarker in live cancer cells with plasma therapeutics. *Biosens. Bioelectron.* **2017**, *97*, 352–359. [[CrossRef](#)]
170. Li, Z.; Xin, Y.; Wu, W.; Fu, B.; Zhang, Z. Topotactic Conversion of Copper(I) Phosphide Nanowires for Sensitive Electrochemical Detection of H₂O₂ Release from Living Cells. *Anal. Chem.* **2016**, *88*, 7724–7729. [[CrossRef](#)]
171. Su, S.; Han, X.; Lu, Z.; Liu, W.; Zhu, D.; Chao, J.; Fan, C.; Wang, L.; Song, S.; Weng, L.; et al. Facile Synthesis of a MoS₂–Prussian Blue Nanocube Nanohybrid-Based Electrochemical Sensing Platform for Hydrogen Peroxide and Carcinoembryonic Antigen Detection. *ACS Appl. Mater. Interfaces* **2017**, *9*, 12773–12781. [[CrossRef](#)] [[PubMed](#)]
172. Yuan, L.; Lin, W.; Xie, Y.; Chen, B.; Zhu, S. Single fluorescent probe responds to H₂O₂, NO, and H₂O₂/NO with three different sets of fluorescence signals. *J. Am. Chem. Soc.* **2012**, *134*, 1305–1315. [[CrossRef](#)] [[PubMed](#)]

173. Boero, C.; Casulli, M.A.; Olivo, J.; Foglia, L.; Orso, E.; Mazza, M.; Carrara, S.; De Micheli, G. Design, development, and validation of an in-situ biosensor array for metabolite monitoring of cell cultures. *Biosens. Bioelectron.* **2014**, *61*, 251–259. [[CrossRef](#)]
174. Shi, B.-X.; Wang, Y.; Zhang, K.; Lam, T.-L.; Chan, H.L.-W. Monitoring of dopamine release in single cell using ultrasensitive ITO microsensors modified with carbon nanotubes. *Biosens. Bioelectron.* **2011**, *26*, 2917–2921. [[CrossRef](#)] [[PubMed](#)]
175. Li, D.-W.; Qin, L.-X.; Li, Y.; Nia, R.P.; Long, Y.-T.; Chen, H.-Y. CdSe/ZnS quantum dot–Cytochrome c bioconjugates for selective intracellular O₂-Sensing. *Chem. Commun.* **2011**, *47*, 8539–8541. [[CrossRef](#)] [[PubMed](#)]
176. Han, M.; Liu, S.; Bao, J.; Dai, Z. Pd nanoparticle assemblies—As the substitute of HRP, in their biosensing applications for H₂O₂ and glucose. *Biosens. Bioelectron.* **2012**, *31*, 151–156. [[CrossRef](#)]
177. Wang, Y.; Hasebe, Y. Carbon felt-based bioelectrocatalytic flow-through detectors: Highly sensitive amperometric determination of H₂O₂ based on a direct electrochemistry of covalently modified horseradish peroxidase using cyanuric chloride as a linking agent. *Sens. Actuators B Chem.* **2011**, *155*, 722–729. [[CrossRef](#)]
178. Wang, Z.; Yang, Y.; Leng, K.; Li, J.; Zheng, F.; Shen, G.; Yu, R. A Sequence-Selective Electrochemical DNA Biosensor Based on HRP-Labeled Probe for Colorectal Cancer DNA Detection. *Anal. Lett.* **2008**, *41*, 24–35. [[CrossRef](#)]
179. Crulhas, B.P.; Ramos, N.P.; Castro, G.R.; Pedrosa, V.A. Detection of hydrogen peroxide releasing from prostate cancer cell using a biosensor. *J. Solid State Electrochem.* **2016**, *20*, 2427–2433. [[CrossRef](#)]
180. Zhou, J.; Liao, C.; Zhang, L.; Wang, Q.; Tian, Y. Molecular Hydrogel-Stabilized Enzyme with Facilitated Electron Transfer for Determination of H₂O₂ Released from Live Cells. *Anal. Chem.* **2014**, *86*, 4395–4401. [[CrossRef](#)]
181. Goenka, S.; Sant, V.; Sant, S. Graphene-based nanomaterials for drug delivery and tissue engineering. *J. Control. Release* **2014**, *173*, 75–88. [[CrossRef](#)]
182. Pumera, M.; Ambrosi, A.; Bonanni, A.; Chng, E.L.K.; Poh, H.L. Graphene for electrochemical sensing and biosensing. *TrAC Trends Anal. Chem.* **2010**, *29*, 954–965. [[CrossRef](#)]
183. Gao, H.; Duan, H. 2D and 3D graphene materials: Preparation and bioelectrochemical applications. *Biosens. Bioelectron.* **2015**, *65*, 404–419. [[CrossRef](#)] [[PubMed](#)]
184. Favero, G.; Fusco, G.; Mazzei, F.; Tasca, F.; Antiochia, R. Electrochemical Characterization of Graphene and MWCNT Screen-Printed Electrodes Modified with AuNPs for Laccase Biosensor Development. *Nanomaterials* **2015**, *5*, 1995–2006. [[CrossRef](#)] [[PubMed](#)]
185. Song, Y.; Luo, Y.; Zhu, C.; Li, H.; Du, D.; Lin, Y. Recent advances in electrochemical biosensors based on graphene two-dimensional nanomaterials. *Biosens. Bioelectron.* **2016**, *76*, 195–212. [[CrossRef](#)] [[PubMed](#)]
186. Chen, Y.; Tan, C.; Zhang, H.; Wang, L. Two-dimensional graphene analogues for biomedical applications. *Chem. Soc. Rev.* **2015**, *44*, 2681–2701. [[CrossRef](#)]
187. Tan, S.M.; Sofer, Z.; Pumera, M. Biomarkers Detection on Hydrogenated Graphene Surfaces: Towards Applications of Graphane in Biosensing. *Electroanalysis* **2013**, *25*, 703–705. [[CrossRef](#)]
188. Yang, G.; Zhu, C.; Du, D.; Zhu, J.; Lin, Y. Graphene-like two-dimensional layered nanomaterials: Applications in biosensors and nanomedicine. *Nanoscale* **2015**, *7*, 14217–14231. [[CrossRef](#)] [[PubMed](#)]
189. Gupta, A.; Sakthivel, T.; Seal, S. Recent development in 2D materials beyond graphene. *Prog. Mater. Sci.* **2015**, *73*, 44–126. [[CrossRef](#)]
190. Lin, Y.; Connell, J.W. Advances in 2D boron nitride nanostructures: Nanosheets, nanoribbons, nanomeshes, and hybrids with graphene. *Nanoscale* **2012**, *4*, 6908–6939. [[CrossRef](#)] [[PubMed](#)]
191. Zhu, C.; Du, D.; Lin, Y. Graphene and graphene-like 2D materials for optical biosensing and bioimaging: A review. *2D Mater.* **2015**, *2*, 032004. [[CrossRef](#)]
192. McCreery, R.L. Advanced Carbon Electrode Materials for Molecular Electrochemistry. *Chem. Rev.* **2008**, *108*, 2646–2687. [[CrossRef](#)] [[PubMed](#)]
193. Takahashi, S.; Abiko, N.; Anzai, J.-I. Redox Response of Reduced Graphene Oxide-Modified Glassy Carbon Electrodes to Hydrogen Peroxide and Hydrazine. *Materials* **2013**, *6*, 1840–1850. [[CrossRef](#)] [[PubMed](#)]
194. Hamilton, C.E.; Lomeda, J.R.; Sun, Z.; Tour, J.M.; Barron, A.R. High-Yield Organic Dispersions of Unfunctionalized Graphene. *Nano Lett.* **2009**, *9*, 3460–3462. [[CrossRef](#)]
195. Lv, W.; Guo, M.; Liang, M.-H.; Jin, F.-M.; Cui, L.; Zhi, L.; Yang, Q.-H. Graphene-DNA hybrids: Self-assembly and electrochemical detection performance. *J. Mater. Chem.* **2010**, *20*, 6668–6673. [[CrossRef](#)]
196. Woo, S.; Kim, Y.-R.; Chung, T.D.; Piao, Y.; Kim, H. Synthesis of a graphene–carbon nanotube composite and its electrochemical sensing of hydrogen peroxide. *Electrochim. Acta* **2012**, *59*, 509–514. [[CrossRef](#)]
197. Wang, Y.; Shao, Y.; Matson, D.W.; Li, J.; Lin, Y. Nitrogen-Doped Graphene and Its Application in Electrochemical Biosensing. *ACS Nano* **2010**, *4*, 1790–1798. [[CrossRef](#)]
198. Li, M.; Wu, Z.-S.; Ren, W.; Cheng, H.-M.; Tang, N.; Wu, W.; Zhong, W.; Du, Y. The doping of reduced graphene oxide with nitrogen and its effect on the quenching of the material's photoluminescence. *Carbon* **2012**, *50*, 5286–5291. [[CrossRef](#)]
199. Yeh, M.-H.; Li, Y.-S.; Chen, G.-L.; Lin, L.-Y.; Li, T.-J.; Chuang, H.-M.; Hsieh, C.-Y.; Lo, S.-C.; Chiang, W.-H.; Ho, K.-C. Facile Synthesis of Boron-doped Graphene Nanosheets with Hierarchical Microstructure at Atmosphere Pressure for Metal-free Electrochemical Detection of Hydrogen Peroxide. *Electrochim. Acta* **2015**, *172*, 52–60. [[CrossRef](#)]

200. Yang, G.-H.; Zhou, Y.-H.; Wu, J.-J.; Cao, J.-T.; Li, L.-L.; Liu, H.-Y.; Zhu, J.-J. Microwave-assisted synthesis of nitrogen and boron co-doped graphene and its application for enhanced electrochemical detection of hydrogen peroxide. *RSC Adv.* **2013**, *3*, 22597–22604. [[CrossRef](#)]
201. Zor, E.; Saglam, M.E.; Akin, I.; Saf, A.O.; Bingol, H.; Ersoz, M. Green synthesis of reduced graphene oxide/nanopolypyrrole composite: Characterization and H₂O₂ determination in urine. *RSC Adv.* **2014**, *4*, 12457–12466. [[CrossRef](#)]
202. Luo, J.; Chen, Y.; Ma, Q.; Liu, R.; Liu, X. Layer-by-layer assembled ionic-liquid functionalized graphene–polyaniline nanocomposite with enhanced electrochemical sensing properties. *J. Mater. Chem. C* **2014**, *2*, 4818–4827. [[CrossRef](#)]
203. Wang, Q.; Li, M.; Szunerits, S.; Boukherroub, R. Environmentally Friendly Reduction of Graphene Oxide Using Tyrosine for Nonenzymatic Amperometric H₂O₂ Detection. *Electroanalysis* **2014**, *26*, 156–163. [[CrossRef](#)]
204. Nguyen, V.H.; Tran, T.H.; Shim, J.-J. Glassy carbon electrode modified with a graphene oxide/poly(o-phenylenediamine) composite for the chemical detection of hydrogen peroxide. *Mater. Sci. Eng. C* **2014**, *44*, 144–150. [[CrossRef](#)] [[PubMed](#)]
205. Huang, Y.; Li, S.F.Y. Electrocatalytic performance of silica nanoparticles on graphene oxide sheets for hydrogen peroxide sensing. *J. Electroanal. Chem.* **2013**, *690*, 8–12. [[CrossRef](#)]
206. Kong, F.-Y.; Li, W.-W.; Wang, J.-Y.; Fang, H.-L.; Fan, D.-H.; Wang, W. Direct electrolytic exfoliation of graphite with hemin and single-walled carbon nanotube: Creating functional hybrid nanomaterial for hydrogen peroxide detection. *Anal. Chim. Acta* **2015**, *884*, 37–43. [[CrossRef](#)] [[PubMed](#)]
207. Lei, W.; Wu, L.; Huang, W.; Hao, Q.; Zhang, Y.; Xia, X. Microwave-assisted synthesis of hemin–graphene/poly(3,4-ethylenedioxythiophene) nanocomposite for a biomimetic hydrogen peroxide biosensor. *J. Mater. Chem. B* **2014**, *2*, 4324–4330. [[CrossRef](#)]
208. Zhang, T.; Gu, Y.; Li, C.; Yan, X.; Lu, N.; Liu, H.; Zhang, Z.; Zhang, H. Fabrication of Novel Electrochemical Biosensor Based on Graphene Nanohybrid to Detect H₂O₂ Released from Living Cells with Ultrahigh Performance. *ACS Appl. Mater. Interfaces* **2017**, *9*, 37991–37999. [[CrossRef](#)]
209. Xi, F.; Zhao, D.; Wang, X.; Chen, P. Non-enzymatic detection of hydrogen peroxide using a functionalized three-dimensional graphene electrode. *Electrochem. Commun.* **2013**, *26*, 81–84. [[CrossRef](#)]
210. Zhang, J.; Zhao, M.; Yang, J.; Wu, G.; Wu, H.; Chen, C.; Liu, A. Metal-free rGO/GO hybrid microelectrode array for sensitive and in-situ hydrogen peroxide sensing. *Electrochim. Acta* **2019**, *326*, 134967. [[CrossRef](#)]
211. Tian, Y.; Wei, Z.; Zhang, K.; Peng, S.; Zhang, X.; Liu, W.; Chu, K. Three-dimensional phosphorus-doped graphene as an efficient metal-free electrocatalyst for electrochemical sensing. *Sens. Actuators B Chem.* **2017**, *241*, 584–591. [[CrossRef](#)]
212. Radhakrishnan, S.; Kim, S.J. An enzymatic biosensor for hydrogen peroxide based on one-pot preparation of CeO₂-reduced graphene oxide nanocomposite. *RSC Adv.* **2015**, *5*, 12937–12943. [[CrossRef](#)]
213. Wang, S.; Zhu, Y.; Yang, X.; Li, C. Photoelectrochemical detection of H₂O₂ based on flower-like CuInS₂-graphene hybrid. *Electroanalysis* **2014**, *26*, 573–580. [[CrossRef](#)]
214. Song, H.; Ni, Y.; Kokot, S. Investigations of an electrochemical platform based on the layered MoS₂-graphene and horseradish peroxidase nanocomposite for direct electrochemistry and electrocatalysis. *Biosens. Bioelectron.* **2014**, *56*, 137–143. [[CrossRef](#)]
215. Liu, Y.; Liu, X.; Guo, Z.; Hu, Z.; Xue, Z.; Lu, X. Horseradish peroxidase supported on porous graphene as a novel sensing platform for detection of hydrogen peroxide in living cells sensitively. *Biosens. Bioelectron.* **2017**, *87*, 101–107. [[CrossRef](#)]
216. Fan, Z.; Lin, Q.; Gong, P.; Liu, B.; Wang, J.; Yang, S. A new enzymatic immobilization carrier based on graphene capsule for hydrogen peroxide biosensors. *Electrochim. Acta* **2015**, *151*, 186–194. [[CrossRef](#)]
217. Wu, P.; Cai, Z.; Chen, J.; Zhang, H.; Cai, C. Electrochemical measurement of the flux of hydrogen peroxide releasing from RAW 264.7 macrophage cells based on enzyme-attapulgite clay nanohybrids. *Biosens. Bioelectron.* **2011**, *26*, 4012–4017. [[CrossRef](#)] [[PubMed](#)]
218. Wang, Y.; Zhang, H.; Yao, D.; Pu, J.; Zhang, Y.; Gao, X.; Sun, Y. Direct electrochemistry of hemoglobin on graphene/Fe₃O₄ nanocomposite-modified glass carbon electrode and its sensitive detection for hydrogen peroxide. *J. Solid State Electrochem.* **2013**, *17*, 881–887. [[CrossRef](#)]
219. Cheng, Y.; Feng, B.; Yang, X.; Yang, P.; Ding, Y.; Chen, Y.; Fei, J. Electrochemical biosensing platform based on carboxymethyl cellulose functionalized reduced graphene oxide and hemoglobin hybrid nanocomposite film. *Sens. Actuators B Chem.* **2013**, *182*, 288–293. [[CrossRef](#)]
220. Xie, L.; Xu, Y.; Cao, X. Hydrogen peroxide biosensor based on hemoglobin immobilized at graphene, flower-like zinc oxide, and gold nanoparticles nanocomposite modified glassy carbon electrode. *Colloids Surf. B Biointerfaces* **2013**, *107*, 245–250. [[CrossRef](#)] [[PubMed](#)]
221. Li, M.; Xu, S.; Tang, M.; Liu, L.; Gao, F.; Wang, Y. Direct electrochemistry of horseradish peroxidase on graphene-modified electrode for electrocatalytic reduction towards H₂O₂. *Electrochim. Acta* **2011**, *56*, 1144–1149. [[CrossRef](#)]
222. Zhang, L.; Han, G.; Liu, Y.; Tang, J.; Tang, W. Immobilizing haemoglobin on gold/graphene–chitosan nanocomposite as efficient hydrogen peroxide biosensor. *Sens. Actuators B Chem.* **2014**, *197*, 164–171. [[CrossRef](#)]
223. Liu, H.; Su, X.; Duan, C.; Dong, X.; Zhou, S.; Zhu, Z. Microwave-assisted hydrothermal synthesis of Au NPs–Graphene composites for H₂O₂ detection. *J. Electroanal. Chem.* **2014**, *731*, 36–42. [[CrossRef](#)]
224. Vilian, A.T.E.; Chen, S.-M. Simple approach for the immobilization of horseradish peroxidase on poly-l-histidine modified reduced graphene oxide for amperometric determination of dopamine and H₂O₂. *RSC Adv.* **2014**, *4*, 55867–55876. [[CrossRef](#)]

225. Xiong, W.; Qu, Q.; Liu, S. Self-assembly of ultra-small gold nanoparticles on an indium tin oxide electrode for the enzyme-free detection of hydrogen peroxide. *Mikrochim. Acta* **2014**, *181*, 983–989. [[CrossRef](#)]
226. Sheng, Q.; Wang, M.; Zheng, J. A novel hydrogen peroxide biosensor based on enzymatically induced deposition of polyaniline on the functionalized graphene–carbon nanotube hybrid materials. *Sens. Actuators B Chem.* **2011**, *160*, 1070–1077. [[CrossRef](#)]
227. Zhou, K.; Zhu, Y.; Yang, X.; Luo, J.; Li, C.; Luan, S. A novel hydrogen peroxide biosensor based on Au–graphene–HRP–chitosan biocomposites. *Electrochim. Acta* **2010**, *55*, 3055–3060. [[CrossRef](#)]
228. Wang, T.; Liu, J.; Ren, J.; Wang, J.; Wang, E. Mimetic biomembrane–AuNPs–graphene hybrid as matrix for enzyme immobilization and bioelectrocatalysis study. *Talanta* **2015**, *143*, 438–441. [[CrossRef](#)] [[PubMed](#)]
229. Nandini, S.; Manjunatha, R.; Shanmugam, S.; Melo, J.S.; Suresh, G.S. Electrochemical biosensor for the selective determination of hydrogen peroxide based on the co-deposition of palladium, horseradish peroxidase on functionalized-graphene modified graphite electrode as composite. *J. Electroanal. Chem.* **2013**, *689*, 233–242. [[CrossRef](#)]
230. Nalini, S.; Shanmugam, S.; Neelagund, S.E.; Melo, J.S.; Suresh, G.S.; Nandini, S. Amperometric hydrogen peroxide and cholesterol biosensors designed by using hierarchical curtailed silver flowers functionalized graphene and enzymes deposits. *J. Solid State Electrochem.* **2014**, *18*, 685–701. [[CrossRef](#)]
231. Huang, K.-J.; Niu, D.-J.; Liu, X.; Wu, Z.-W.; Fan, Y.; Chang, Y.-F.; Wu, Y.-Y. Direct electrochemistry of catalase at amine-functionalized graphene/gold nanoparticles composite film for hydrogen peroxide sensor. *Electrochim. Acta* **2011**, *56*, 2947–2953. [[CrossRef](#)]
232. Dinesh, B.; Mani, V.; Saraswathi, R.; Chen, S.-M. Direct electrochemistry of cytochrome c immobilized on a graphene oxide–carbon nanotube composite for picomolar detection of hydrogen peroxide. *RSC Adv.* **2014**, *4*, 28229–28237. [[CrossRef](#)]
233. Mani, V.; Dinesh, B.; Chen, S.-M.; Saraswathi, R. Direct electrochemistry of myoglobin at reduced graphene oxide-multiwalled carbon nanotubes-platinum nanoparticles nanocomposite and biosensing towards hydrogen peroxide and nitrite. *Biosens. Bioelectron.* **2014**, *53*, 420–427. [[CrossRef](#)]
234. Liu, F.; Xu, Q.; Huang, W.; Zhang, Z.; Xiang, G.; Zhang, C.; Liang, C.; Lian, H.; Peng, J. Green synthesis of porous graphene and its application for sensitive detection of hydrogen peroxide and 2,4-dichlorophenoxyacetic acid. *Electrochim. Acta* **2019**, *295*, 615–623. [[CrossRef](#)]
235. Ebrahimi, A.; Zhang, K.; Dong, C.; Subramanian, S.; Butler, D.; Bolotsky, A.; Goodnight, L.; Cheng, Y.; Robinson, J.A. FeS_x-graphene heterostructures: Nanofabrication-compatible catalysts for ultra-sensitive electrochemical detection of hydrogen peroxide. *Sens. Actuators B Chem.* **2019**, *285*, 631–638. [[CrossRef](#)]
236. Hu, Z.; Dai, Z.; Hu, X.; Yang, B.; Liu, Q.; Gao, C.; Zheng, X.; Yu, Y. A facile preparation of FePt-loaded few-layer MoS₂ nanosheets nanocomposites (F-MoS₂-FePt NCs) and their application for colorimetric detection of H₂O₂ in living cells. *J. Nanobiotechnol.* **2019**, *17*, 38. [[CrossRef](#)] [[PubMed](#)]
237. Dai, H.; Chen, Y.; Niu, X.; Pan, C.; Chen, H.; Chen, X. High-performance electrochemical biosensor for nonenzymatic H₂O₂ sensing based on Au@C-Co₃O₄ heterostructures. *Biosens. Bioelectron.* **2018**, *118*, 36–43. [[CrossRef](#)]
238. Liu, J.; Bo, X.; Yang, J.; Yin, D.; Guo, L. One-step synthesis of porphyrinic iron-based metal-organic framework/ordered mesoporous carbon for electrochemical detection of hydrogen peroxide in living cells. *Sens. Actuators B Chem.* **2017**, *248*, 207–213. [[CrossRef](#)]
239. Shu, Y.; Xu, J.; Chen, J.; Xu, Q.; Xiao, X.; Jin, D.; Pang, H.; Hu, X. Ultrasensitive electrochemical detection of H₂O₂ in living cells based on ultrathin MnO₂ nanosheets. *Sens. Actuators B Chem.* **2017**, *252*, 72–78. [[CrossRef](#)]
240. Ensafi, A.A.; Jafari-Asl, M.; Rezaei, B. A novel enzyme-free amperometric sensor for hydrogen peroxide based on Nafion/exfoliated graphene oxide–Co₃O₄ nanocomposite. *Talanta* **2013**, *103*, 322–329. [[CrossRef](#)]
241. Sarkar, A.; Ghosh, A.B.; Saha, N.; Bhadu, G.R.; Adhikary, B. Newly Designed Amperometric Biosensor for Hydrogen Peroxide and Glucose Based on Vanadium Sulfide Nanoparticles. *ACS Appl. Nano Mater.* **2018**, *1*, 1339–1347. [[CrossRef](#)]
242. Li, S.-J.; Du, J.-M.; Zhang, J.-P.; Zhang, M.-J.; Chen, J. A glassy carbon electrode modified with a film composed of cobalt oxide nanoparticles and graphene for electrochemical sensing of H₂O₂. *Mikrochim. Acta* **2014**, *181*, 631–638. [[CrossRef](#)]
243. Zheng, L.; Ye, D.; Xiong, L.; Xu, J.; Tao, K.; Zou, Z.; Huang, D.; Kang, X.; Yang, S.; Xia, J. Preparation of cobalt-tetraphenylporphyrin/reduced graphene oxide nanocomposite and its application on hydrogen peroxide biosensor. *Anal. Chim. Acta* **2013**, *768*, 69–75. [[CrossRef](#)]
244. Hosu, I.S.; Wang, Q.; Vasilescu, A.; Petcu, S.F.; Raditoiu, V.; Railian, S.; Zaitsev, V.; Turcheniuk, K.; Wang, Q.; Li, M.; et al. Cobalt phthalocyanine tetracarboxylic acid modified reduced graphene oxide: A sensitive matrix for the electrocatalytic detection of peroxynitrite and hydrogen peroxide. *RSC Adv.* **2015**, *5*, 1474–1484. [[CrossRef](#)]
245. Liu, X.; Zhu, H.; Yang, X. An amperometric hydrogen peroxide chemical sensor based on graphene-Fe₃O₄ multilayer films modified ITO electrode. *Talanta* **2011**, *87*, 243–248. [[CrossRef](#)] [[PubMed](#)]
246. Yang, S.; Li, G.; Wang, G.; Zhao, J.; Hu, M.; Qu, L. A novel nonenzymatic H₂O₂ sensor based on cobalt hexacyanoferrate nanoparticles and graphene composite modified electrode. *Sens. Actuators B Chem.* **2015**, *208*, 593–599. [[CrossRef](#)]
247. Kubendhiran, S.; Thirumalraj, B.; Chen, S.-M.; Karuppiah, C. Electrochemical co-preparation of cobalt sulfide/reduced graphene oxide composite for electrocatalytic activity and determination of H₂O₂ in biological samples. *J. Colloid Interface Sci.* **2018**, *509*, 153–162. [[CrossRef](#)]

248. Karimi, M.A.; Banifatemeh, F.; Hatefi-Mehrjardi, A.; Tavallali, H.; Eshaghia, Z.; Deilamy-Rad, G. A novel rapid synthesis of Fe₂O₃/graphene nanocomposite using ferrate (VI) and its application as a new kind of nanocomposite modified electrode as electrochemical sensor. *Mater. Res. Bull.* **2015**, *70*, 856–864. [[CrossRef](#)]
249. Li, Z.; Zheng, X.; Zheng, J. A non-enzymatic sensor based on Au@Ag nanoparticles with good stability for sensitive detection of H₂O₂. *New J. Chem.* **2016**, *40*, 2115–2120. [[CrossRef](#)]
250. Zhu, S.; Guo, J.; Dong, J.; Cui, Z.; Lu, T.; Zhu, C.; Zhang, D.; Ma, J. Sonochemical fabrication of Fe₃O₄ nanoparticles on reduced graphene oxide for biosensors. *Ultrason. Sonochem.* **2013**, *20*, 872–880. [[CrossRef](#)]
251. Zhang, P.; Huang, Y.; Lu, X.; Zhang, S.; Li, J.; Wei, G.; Su, Z. One-Step Synthesis of Large-Scale Graphene Film Doped with Gold Nanoparticles at Liquid–Air Interface for Electrochemistry and Raman Detection Applications. *Langmuir* **2014**, *30*, 8980–8989. [[CrossRef](#)] [[PubMed](#)]
252. Ye, Y.; Kong, T.; Yu, X.; Wu, Y.; Zhang, K.; Wang, X. Enhanced nonenzymatic hydrogen peroxide sensing with reduced graphene oxide/ferroferric oxide nanocomposites. *Talanta* **2012**, *89*, 417–421. [[CrossRef](#)]
253. Yang, X.; Wang, L.; Zhou, G.; Sui, N.; Gu, Y.; Wan, J. Electrochemical Detection of H₂O₂ Based on Fe₃O₄ Nanoparticles with Graphene Oxide and Polyamidoamine Dendrimer. *J. Clust. Sci.* **2014**, *26*, 789–798. [[CrossRef](#)]
254. Zhu, M.; Li, N.; Ye, J. Sensitive and Selective Sensing of Hydrogen Peroxide with Iron-Tetrasulphophthalocyanine-Graphene-Nafion Modified Screen-Printed Electrode. *Electroanalysis* **2012**, *24*, 1212–1219. [[CrossRef](#)]
255. Palanisamy, S.; Chen, S.-M.; Sarawathi, R. A novel nonenzymatic hydrogen peroxide sensor based on reduced graphene oxide/ZnO composite modified electrode. *Sens. Actuators B Chem.* **2012**, *166–167*, 372–377. [[CrossRef](#)]
256. Jiang, B.-B.; Wei, X.-W.; Wu, F.-H.; Wu, K.-L.; Chen, L.; Yuan, G.-Z.; Dong, C.; Ye, Y. A non-enzymatic hydrogen peroxide sensor based on a glassy carbon electrode modified with cuprous oxide and nitrogen-doped graphene in a nafion matrix. *Mikrochim. Acta* **2014**, *181*, 1463–1470. [[CrossRef](#)]
257. Xu, F.; Deng, M.; Li, G.; Chen, S.; Wang, L. Electrochemical behavior of cuprous oxide–reduced graphene oxide nanocomposites and their application in nonenzymatic hydrogen peroxide sensing. *Electrochim. Acta* **2013**, *88*, 59–65. [[CrossRef](#)]
258. Liu, M.; Liu, R.; Chen, W. Graphene wrapped Cu₂O nanocubes: Non-enzymatic electrochemical sensors for the detection of glucose and hydrogen peroxide with enhanced stability. *Biosens. Bioelectron.* **2013**, *45*, 206–212. [[CrossRef](#)] [[PubMed](#)]
259. Li, L.; Du, Z.; Liu, S.; Hao, Q.; Wang, Y.; Li, Q.; Wang, T. A novel nonenzymatic hydrogen peroxide sensor based on MnO₂/graphene oxide nanocomposite. *Talanta* **2010**, *82*, 1637–1641. [[CrossRef](#)] [[PubMed](#)]
260. Dong, S.; Xi, J.; Wu, Y.; Liu, H.; Fu, C.; Liu, H.; Xiao, F. High loading MnO₂ nanowires on graphene paper: Facile electrochemical synthesis and use as flexible electrode for tracking hydrogen peroxide secretion in live cells. *Anal. Chim. Acta* **2015**, *853*, 200–206. [[CrossRef](#)] [[PubMed](#)]
261. Feng, X.; Zhang, Y.; Song, J.; Chen, N.; Zhou, J.; Huang, Z.; Ma, Y.; Zhang, L.; Wang, L. MnO₂/graphene nanocomposites for nonenzymatic electrochemical detection of hydrogen peroxide. *Electroanalysis* **2015**, *27*, 353–359. [[CrossRef](#)]
262. Hassan, M.; Jiang, Y.; Bo, X.; Zhou, M. Sensitive nonenzymatic detection of hydrogen peroxide at nitrogen-doped graphene supported-CoFe nanoparticles. *Talanta* **2018**, *188*, 339–348. [[CrossRef](#)] [[PubMed](#)]
263. Lu, N.; Zheng, B.; Gu, Y.; Yan, X.; Zhang, T.; Liu, H.; Xu, H.; Xu, Z.; Li, X.; Zhang, Z. Fabrication of CoNPs-embedded porous carbon composites based on morphochemical imprinting strategy for detection of H₂O₂ released from living cells. *Electrochim. Acta* **2019**, *321*, 134717. [[CrossRef](#)]
264. Benvidi, A.; Nafar, M.T.; Jahanbani, S.; Tezerjani, M.D.; Rezaeinasab, M.; Dalirnasab, S. Developing an electrochemical sensor based on a carbon paste electrode modified with nano-composite of reduced graphene oxide and CuFe₂O₄ nanoparticles for determination of hydrogen peroxide. *Mater. Sci. Eng. C* **2017**, *75*, 1435–1447. [[CrossRef](#)] [[PubMed](#)]
265. Dang, W.; Sun, Y.; Jiao, H.; Xu, L.; Lin, M. AuNPs-NH₂/Cu-MOF modified glassy carbon electrode as enzyme-free electrochemical sensor detecting H₂O₂. *J. Electroanal. Chem.* **2020**, *856*, 113592. [[CrossRef](#)]
266. Wang, W.; Tang, H.; Wu, Y.; Zhang, Y.; Li, Z. Highly electrocatalytic biosensor based on Hemin@ AuNPs/reduced graphene oxide/chitosan nanohybrids for non-enzymatic ultrasensitive detection of hydrogen peroxide in living cells. *Biosens. Bioelectron.* **2019**, *132*, 217–223. [[CrossRef](#)]
267. Sun, Y.; Luo, M.; Meng, X.; Xiang, J.; Wang, L.; Ren, Q.; Guo, S. Graphene/Intermetallic PtPb Nanoplates Composites for Boosting Electrochemical Detection of H₂O₂ Released from Cells. *Anal. Chem.* **2017**, *89*, 3761–3767. [[CrossRef](#)] [[PubMed](#)]
268. Zhang, Y.; Liu, Y.; He, J.; Pang, P.; Gao, Y.; Hu, Q. Electrochemical behavior of graphene/Nafion/Azure I/Au nanoparticles composites modified glass carbon electrode and its application as nonenzymatic hydrogen peroxide sensor. *Electrochim. Acta* **2013**, *90*, 550–555. [[CrossRef](#)]
269. Wang, L.; Dong, Y.; Zhang, Y.; Zhang, Z.; Chi, K.; Yuan, H.; Zhao, A.; Ren, J.; Xiao, F.; Wang, S. PtAu alloy nanoflowers on 3D porous ionic liquid functionalized graphene-wrapped activated carbon fiber as a flexible microelectrode for near-cell detection of cancer. *NPG Asia Mater.* **2016**, *8*, e337. [[CrossRef](#)]
270. Yuan, B.; Xu, C.; Liu, L.; Shi, Y.; Li, S.; Zhang, R.; Zhang, D. Polyethylenimine-bridged graphene oxide–gold film on glassy carbon electrode and its electrocatalytic activity toward nitrite and hydrogen peroxide. *Sens. Actuators B* **2014**, *198*, 55–61. [[CrossRef](#)]
271. Lorestani, F.; Shahnavaz, Z.; Mn, P.; Alias, Y.; Manan, N.S.A. One-step hydrothermal green synthesis of silver nanoparticle-carbon nanotube reduced-graphene oxide composite and its application as hydrogen peroxide sensor. *Sens. Actuators B Chem.* **2015**, *208*, 389–398. [[CrossRef](#)]

272. Chang, H.-C.; Wang, X.; Shiu, K.-K.; Zhu, Y.; Wang, J.; Li, Q.; Chen, B.; Jiang, H. Layer-by-layer assembly of graphene, Au and poly (toluidine blue O) films sensor for evaluation of oxidative stress of tumor cells elicited by hydrogen peroxide. *Biosens. Bioelectron.* **2013**, *41*, 789–794. [[CrossRef](#)] [[PubMed](#)]
273. Bai, X.; Shiu, K.-K. Investigation of the optimal weight contents of reduced graphene oxide–gold nanoparticles composites and their application in electrochemical biosensors. *J. Electroanal. Chem.* **2014**, *720–721*, 84–91. [[CrossRef](#)]
274. Liu, R.; Li, S.; Zhang, G.; Dolbecq, A.; Mialane, P.; Keita, B. Polyoxometalate-Mediated Green Synthesis of Graphene and Metal Nanohybrids: High-Performance Electrocatalysts. *J. Clust. Sci.* **2014**, *25*, 711–740. [[CrossRef](#)]
275. Yu, B.; Feng, J.; Liu, S.; Zhang, T. Preparation of reduced graphene oxide decorated with high density Ag nanorods for non-enzymatic hydrogen peroxide detection. *RSC Adv.* **2013**, *3*, 14303–14307. [[CrossRef](#)]
276. Fang, Y.; Guo, S.; Zhu, C.; Zhai, Y.; Wang, E. Self-Assembly of Cationic Polyelectrolyte-Functionalized Graphene Nanosheets and Gold Nanoparticles: A Two-Dimensional Heterostructure for Hydrogen Peroxide Sensing. *Langmuir* **2010**, *26*, 11277–11282. [[CrossRef](#)] [[PubMed](#)]
277. Xu, F.; Sun, Y.; Zhang, Y.; Shi, Y.; Wen, Z.; Li, Z. Graphene–Pt nanocomposite for nonenzymatic detection of hydrogen peroxide with enhanced sensitivity. *Electrochem. Commun.* **2011**, *13*, 1131–1134. [[CrossRef](#)]
278. Gao, C.-H.; Zhu, X.-Z.; Zhang, L.; Zhou, D.-Y.; Wang, Z.-K.; Liao, L.-S. Comparative studies on the inorganic and organic p-type dopants in organic light-emitting diodes with enhanced hole injection. *Appl. Phys. Lett.* **2013**, *102*, 153301. [[CrossRef](#)]
279. Pang, P.; Yang, Z.; Xiao, S.; Xie, J.; Zhang, Y.; Gao, Y. Nonenzymatic amperometric determination of hydrogen peroxide by graphene and gold nanorods nanocomposite modified electrode. *J. Electroanal. Chem.* **2014**, *727*, 27–33. [[CrossRef](#)]
280. Li, X.-R.; Xu, M.-C.; Chen, H.-Y.; Xu, J.-J. Bimetallic Au@Pt@Au core–shell nanoparticles on graphene oxide nanosheets for high-performance H₂O₂ bi-directional sensing. *J. Mater. Chem. B* **2015**, *3*, 4355–4362. [[CrossRef](#)]
281. Yao, L.; Yan, Y.; Lee, J.-M. Synthesis of Porous Pd Nanostructure and Its Application in Enzyme-Free Sensor of Hydrogen Peroxide. *ACS Sustain. Chem. Eng.* **2017**, *5*, 1248–1252. [[CrossRef](#)]
282. Fu, L.; Lai, G.; Jia, B.; Yu, A. Preparation and Electrocatalytic Properties of Polydopamine Functionalized Reduced Graphene Oxide–Silver Nanocomposites. *Electrocatalysis* **2014**, *6*, 72–76. [[CrossRef](#)]
283. Liu, S.; Tian, J.; Wang, L.; Sun, X. Microwave-assisted rapid synthesis of Ag nanoparticles/graphene nanosheet composites and their application for hydrogen peroxide detection. *J. Nanopart. Res.* **2011**, *13*, 4539–4548. [[CrossRef](#)]
284. Shan, L.; Liu, H.; Wang, G. Preparation of tungsten-doped BiVO₄ and enhanced photocatalytic activity. *J. Nanopart. Res.* **2015**, *17*, 181. [[CrossRef](#)]
285. Liu, J.; Bo, X.; Zhao, Z.; Guo, L. Highly exposed Pt nanoparticles supported on porous graphene for electrochemical detection of hydrogen peroxide in living cells. *Biosens. Bioelectron.* **2015**, *74*, 71–77. [[CrossRef](#)]
286. Zhang, C.; Zhang, Y.; Miao, Z.; Ma, M.; Du, X.; Lin, J.; Han, B.; Takahashi, S.; Anzai, J.-I.; Chen, Q. Dual-function amperometric sensors based on poly (diallyldimethylammonium chloride)-functionalized reduced graphene oxide/manganese dioxide/gold nanoparticles nanocomposite. *Sens. Actuators B Chem.* **2016**, *222*, 663–673. [[CrossRef](#)]
287. Liu, S.; Wang, L.; Tian, J.; Luo, Y.; Zhang, X.; Sun, X. Aniline as a dispersing and stabilizing agent for reduced graphene oxide and its subsequent decoration with Ag nanoparticles for enzymeless hydrogen peroxide detection. *J. Colloid Interface Sci.* **2011**, *363*, 615–619. [[CrossRef](#)] [[PubMed](#)]
288. Zhu, J.; Kim, K.; Liu, Z.; Feng, H.; Hou, S. Electroless Deposition of Silver Nanoparticles on Graphene Oxide Surface and Its Applications for the Detection of Hydrogen Peroxide. *Electroanalysis* **2014**, *26*, 2513–2519. [[CrossRef](#)]
289. Zhang, P.; Zhang, X.; Zhang, S.; Lu, X.; Li, Q.; Su, Z.; Wei, G. One-pot green synthesis, characterizations, and biosensor application of self-assembled reduced graphene oxide–gold nanoparticle hybrid membranes. *J. Mater. Chem. B* **2013**, *1*, 6525–6531. [[CrossRef](#)]
290. Li, S.-J.; Shi, Y.-F.; Liu, L.; Song, L.-X.; Pang, H.; Du, J.-M. Electrostatic self-assembly for preparation of sulfonated graphene/gold nanoparticle hybrids and their application for hydrogen peroxide sensing. *Electrochim. Acta* **2012**, *85*, 628–635. [[CrossRef](#)]
291. Zhang, Y.; Wang, Z.; Ji, Y.; Liu, S. Synthesis of Ag nanoparticle–carbon nanotube–reduced graphene oxide hybrids for highly sensitive non-enzymatic hydrogen peroxide detection. *RSC Adv.* **2015**, *5*, 39037–39041. [[CrossRef](#)]
292. Nia, P.M.; Lorestani, F.; Meng, W.P.; Alias, Y. A novel non-enzymatic H₂O₂ sensor based on polypyrrole nanofibers–silver nanoparticles decorated reduced graphene oxide nano composites. *Appl. Surf. Sci.* **2015**, *332*, 648–656.
293. Lu, D.; Zhang, Y.; Lin, S.; Wang, L.; Wang, C. Synthesis of PtAu bimetallic nanoparticles on graphene–carbon nanotube hybrid nanomaterials for nonenzymatic hydrogen peroxide sensor. *Talanta* **2013**, *112*, 111–116. [[CrossRef](#)] [[PubMed](#)]
294. Liu, P.; Li, J.; Liu, X.; Li, M.; Lu, X. One-pot synthesis of highly dispersed PtAu nanoparticles–CTAB–graphene nanocomposites for nonenzyme hydrogen peroxide sensor. *J. Electroanal. Chem.* **2015**, *751*, 1–6. [[CrossRef](#)]
295. Cui, X.; Wu, S.; Li, Y.; Wan, G. Sensing hydrogen peroxide using a glassy carbon electrode modified with in-situ electrodeposited platinum–gold bimetallic nanoclusters on a graphene surface. *Mikrochim. Acta* **2014**, *182*, 265–272. [[CrossRef](#)]
296. Sun, Y.; He, K.; Zhang, Z.; Zhou, A.; Duan, H. Real-time electrochemical detection of hydrogen peroxide secretion in live cells by Pt nanoparticles decorated graphene–carbon nanotube hybrid paper electrode. *Biosens. Bioelectron.* **2015**, *68*, 358–364. [[CrossRef](#)]
297. Xu, C.; Zhang, L.; Liu, L.; Shi, Y.; Wang, H.; Wang, X.; Wang, F.; Yuan, B.; Zhang, D. A novel enzyme-free hydrogen peroxide sensor based on polyethylenimine-grafted graphene oxide–Pd particles modified electrode. *J. Electroanal. Chem.* **2014**, *731*, 67–71. [[CrossRef](#)]
298. Liu, H.; Chen, X.; Huang, L.; Wang, J.; Pan, H. Palladium Nanoparticles Embedded into Graphene Nanosheets: Preparation, Characterization, and Nonenzymatic Electrochemical Detection of H₂O₂. *Electroanalysis* **2014**, *26*, 556–564. [[CrossRef](#)]

299. Chen, X.-M.; Cai, Z.-X.; Huang, Z.-Y.; Oyama, M.; Jiang, Y.-Q.; Chen, X. Ultrafine palladium nanoparticles grown on graphene nanosheets for enhanced electrochemical sensing of hydrogen peroxide. *Electrochim. Acta* **2013**, *97*, 398–403. [[CrossRef](#)]
300. Sun, W.; Cai, X.; Wang, Z.; Zhao, H.; Lan, M. A novel modification method via in-situ reduction of AuAg bimetallic nanoparticles by polydopamine on carbon fiber microelectrode for H₂O₂ detection. *Microchem. J.* **2020**, *154*, 104595. [[CrossRef](#)]
301. Xie, Y.; Zhan, Y. Electrochemical capacitance of porous reduced graphene oxide/nickel foam. *J. Porous Mater.* **2015**, *22*, 403–412. [[CrossRef](#)]
302. Zhao, Y.; Hu, Y.; Hou, J.; Jia, Z.; Zhong, D.; Zhou, S.; Huo, D.; Yang, M.; Hou, C. Electrochemical biointerface based on electrodeposition AuNPs on 3D graphene aerogel: Direct electron transfer of Cytochrome c and hydrogen peroxide sensing. *J. Electroanal. Chem.* **2019**, *842*, 16–23. [[CrossRef](#)]
303. Fu, Y.; Huang, D.; Li, C.; Zou, L.; Ye, B. Graphene blended with SnO₂ and Pd-Pt nanocages for sensitive non-enzymatic electrochemical detection of H₂O₂ released from living cells. *Anal. Chim. Acta* **2018**, *1014*, 10–18. [[CrossRef](#)] [[PubMed](#)]
304. Lu, J.; Hu, Y.; Wang, P.; Liu, P.; Chen, Z.; Sun, D. Electrochemical biosensor based on gold nanoflowers-encapsulated magnetic metal-organic framework nanozymes for drug evaluation with in-situ monitoring of H₂O₂ released from H9C2 cardiac cells. *Sens. Actuators B Chem.* **2020**, *311*, 127909. [[CrossRef](#)]
305. Hu, J.; Wisetsuwannaphum, S.; Foord, J.S. Glutamate biosensors based on diamond and graphene platforms. *Faraday Discuss.* **2014**, *172*, 457–472. [[CrossRef](#)] [[PubMed](#)]
306. Chang, Q.; Tang, H. Optical determination of glucose and hydrogen peroxide using a nanocomposite prepared from glucose oxidase and magnetite nanoparticles immobilized on graphene oxide. *Mikrochim. Acta* **2014**, *181*, 527–534. [[CrossRef](#)]
307. Zhang, J.; Zhang, F.; Yang, H.; Huang, X.; Liu, H.; Zhang, J.; Guo, S. Graphene Oxide as a Matrix for Enzyme Immobilization. *Langmuir* **2010**, *26*, 6083–6085. [[CrossRef](#)]
308. Dresselhaus, M.; Dresselhaus, G.; Jorio, A. Unusual properties and structure of carbon nanotubes. *Annu. Rev. Mater. Res.* **2004**, *34*, 247–278. [[CrossRef](#)]
309. Primo, E.N.; Gutiérrez, F.; Rubianes, M.D.; Ferreyra, N.F.; Rodríguez, M.C.; Pedano, M.L.; Gasnier, A.; Gutierrez, A.; Eguílaz, M.; Dalmasso, P.; et al. Electrochemistry in one dimension: Applications of carbon nanotubes. *Electrochem. Carbon Electrodes* **2015**, 83–120. [[CrossRef](#)]
310. Yu, D.; Wang, P.; Zhao, Y.; Fan, A. Iodophenol blue-enhanced luminol chemiluminescence and its application to hydrogen peroxide and glucose detection. *Talanta* **2016**, *146*, 655–661. [[CrossRef](#)] [[PubMed](#)]
311. Georgakilas, V.; Perman, J.A.; Tucek, J.; Zboril, R. Broad Family of Carbon Nanoallotropes: Classification, Chemistry, and Applications of Fullerenes, Carbon Dots, Nanotubes, Graphene, Nanodiamonds, and Combined Superstructures. *Chem. Rev.* **2015**, *115*, 4744–4822. [[CrossRef](#)]
312. Yáñez-Sedeño, P.; González-Cortés, A.; Agüí, L.; Pingarrón, J.M. Uncommon carbon nanostructures for the preparation of electrochemical immunosensors. *Electroanalysis* **2016**, *28*, 1679–1691. [[CrossRef](#)]
313. Jacobs, C.B.; Peairs, M.J.; Venton, B.J. Review: Carbon nanotube based electrochemical sensors for biomolecules. *Anal. Chim. Acta* **2010**, *662*, 105–127. [[CrossRef](#)] [[PubMed](#)]
314. Yang, J.; Xu, Y.; Zhang, R.; Wang, Y.; He, P.; Fang, Y. Direct Electrochemistry and Electrocatalysis of the Hemoglobin Immobilized on Diazonium-Functionalized Aligned Carbon Nanotubes Electrode. *Electroanal. Int. J. Devoted Fundam. Pract. Asp. Electroanal.* **2009**, *21*, 1672–1677. [[CrossRef](#)]
315. Esplandiu, M.J.; Pacios, M.; Cyganek, L.; Bartroli, J.; Del Valle, M. Enhancing the electrochemical response of myoglobin with carbon nanotube electrodes. *Nanotechnology* **2009**, *20*, 355502. [[CrossRef](#)]
316. Zhang, H.; Ruan, J.; Liu, W.; Jiang, X.; Du, T.; Jiang, H.; Alberto, P.; Gottschalk, K.-E.; Wang, X. Monitoring dynamic release of intracellular hydrogen peroxide through a microelectrode based enzymatic biosensor. *Anal. Bioanal. Chem.* **2018**, *410*, 4509–4517. [[CrossRef](#)] [[PubMed](#)]
317. Wang, S.; Xie, F.; Liu, G. Direct electrochemistry and electrocatalysis of heme proteins on SWCNTs-CTAB modified electrodes. *Talanta* **2009**, *77*, 1343–1350. [[CrossRef](#)]
318. Chen, L.; Lu, G. Novel amperometric biosensor based on composite film assembled by polyelectrolyte-surfactant polymer, carbon nanotubes and hemoglobin. *Sens. Actuators B Chem.* **2007**, *121*, 423–429. [[CrossRef](#)]
319. Zong, S.; Cao, Y.; Ju, H. Amperometric biosensor for hydrogen peroxide based on myoglobin doped multiwalled carbon nanotube enhanced grafted collagen matrix. *Anal. Lett.* **2007**, *40*, 1556–1568. [[CrossRef](#)]
320. Nagaraju, D.; Pandey, R.K.; Lakshminarayanan, V. Electrocatalytic studies of Cytochrome c functionalized single walled carbon nanotubes on self-assembled monolayer of 4-ATP on gold. *J. Electroanal. Chem.* **2009**, *627*, 63–68. [[CrossRef](#)]
321. Chen, S.; Yuan, R.; Chai, Y.; Yin, B.; Xu, Y. Multilayer Assembly of Hemoglobin and Colloidal Gold Nanoparticles on Multiwall Carbon Nanotubes/Chitosan Composite for Detecting Hydrogen Peroxide. *Electroanal. Int. J. Devoted Fundam. Pract. Asp. Electroanal.* **2008**, *20*, 2141–2147. [[CrossRef](#)]
322. Ren, Q.-Q.; Wu, J.; Zhang, W.-C.; Wang, C.; Qin, X.; Liu, G.-C.; Li, Z.-X.; Yu, Y. Real-time in vitro detection of cellular H₂O₂ under camptothecin stress using horseradish peroxidase, ionic liquid, and carbon nanotube-modified carbon fiber ultramicroelectrode. *Sens. Actuators B Chem.* **2017**, *245*, 615–621. [[CrossRef](#)]
323. Pandey, R.R.; Guo, Y.; Gao, Y.; Chusuei, C.C. A Prussian blue ZnO carbon nanotube composite for chronoamperometrically assaying H₂O₂ in BT20 and 4T1 breast cancer cells. *Anal. Chem.* **2019**, *91*, 10573–10581. [[CrossRef](#)] [[PubMed](#)]

324. Bai, J.; Sun, C.; Jiang, X. Carbon dots-decorated multiwalled carbon nanotubes nanocomposites as a high-performance electrochemical sensor for detection of H₂O₂ in living cells. *Anal. Bioanal. Chem.* **2016**, *408*, 4705–4714. [[CrossRef](#)]
325. Sahraoui, Y.; Chaliaa, S.; Maaref, A.; Haddad, A.; Bessueille, F.; Jaffrezic-Renault, N. Synergistic effect of polyoxometalate and single walled carbon nanotubes on peroxidase-like mimics and highly sensitive electrochemical detection of hydrogen peroxide. *Electroanalysis* **2020**, *32*, 683–689. [[CrossRef](#)]
326. Liu, J.-X.; Ding, S.-N. Non-enzymatic amperometric determination of cellular hydrogen peroxide using dendrimer-encapsulated Pt nanoclusters/carbon nanotubes hybrid composites modified glassy carbon electrode. *Sens. Actuators B Chem.* **2017**, *251*, 200–207. [[CrossRef](#)]
327. Roushani, M.; Bakyas, K.; Dizajdizi, B.Z. Development of sensitive amperometric hydrogen peroxide sensor using a CuNPs/MB/MWCNT-C60-Cs-IL nanocomposite modified glassy carbon electrode. *Mater. Sci. Eng. C* **2016**, *64*, 54–60. [[CrossRef](#)] [[PubMed](#)]
328. Zhao, P.; Zhao, Y.; Jiang, L.; Chen, S.; Ji, Z.; Hou, C.; Huo, D.; Yang, M. 3D carbon nanotubes spaced graphene aerogel incorporated with prussian blue nanoparticles for real-time detection of H₂O₂ released from living cells. *J. Electrochem. Soc.* **2020**, *167*, 047511. [[CrossRef](#)]
329. Zhang, Y.; Xiao, J.; Sun, Y.; Wang, L.; Dong, X.; Ren, J.; He, W.; Xiao, F. Flexible nanohybrid microelectrode based on carbon fiber wrapped by gold nanoparticles decorated nitrogen doped carbon nanotube arrays: In situ electrochemical detection in live cancer cells. *Biosens. Bioelectron.* **2018**, *100*, 453–461. [[CrossRef](#)] [[PubMed](#)]
330. Guo, X.; Cao, Q.; Liu, Y.; He, T.; Liu, J.; Huang, S.; Tang, H.; Ma, M. Organic electrochemical transistor for in situ detection of H₂O₂ released from adherent cells and its application in evaluating the in vitro cytotoxicity of nanomaterial. *Anal. Chem.* **2019**, *92*, 908–915. [[CrossRef](#)]
331. Tavakkoli, H.; Akhond, M.; Ghorbankhani, G.A.; Absalan, G. Electrochemical sensing of hydrogen peroxide using a glassy carbon electrode modified with multiwalled carbon nanotubes and zein nanoparticle composites: Application to HepG2 cancer cell detection. *Mikrochim. Acta* **2020**, *187*, 105. [[CrossRef](#)]
332. Wayu, M.B.; Spidle, R.T.; Devkota, T.; Deb, A.K.; Delong, R.K.; Ghosh, K.C.; Wanekaya, A.K.; Chusuei, C.C. Morphology of hydrothermally synthesized ZnO nanoparticles tethered to carbon nanotubes affects electrocatalytic activity for H₂O₂ detection. *Electrochim. Acta* **2013**, *97*, 99–104. [[CrossRef](#)]
333. Goran, J.M.; Phan, E.N.H.; Favela, C.A.; Stevenson, K.J. H₂O₂ Detection at carbon nanotubes and nitrogen-doped carbon nanotubes: Oxidation, reduction, or disproportionation? *Anal. Chem.* **2015**, *87*, 5989–5996. [[CrossRef](#)] [[PubMed](#)]
334. Li, X.; Li, H.; Liu, T.; Hei, Y.; Hassan, M.; Zhang, S.; Lin, J.; Wang, T.; Bo, X.; Wang, H.-L.; et al. The biomass of ground cherry husks derived carbon nanoplates for electrochemical sensing. *Sens. Actuators B Chem.* **2018**, *255*, 3248–3256. [[CrossRef](#)]
335. Wu, Z.-L.; Li, C.-K.; Yu, J.-G.; Chen, X.-Q. MnO₂/reduced graphene oxide nanoribbons: Facile hydrothermal preparation and their application in amperometric detection of hydrogen peroxide. *Sens. Actuators B Chem.* **2017**, *239*, 544–552. [[CrossRef](#)]
336. Zhang, M.; Zheng, J.; Wang, J.; Xu, J.; Hayat, T.; Alharbi, N.S. Direct electrochemistry of cytochrome c immobilized on one dimensional Au nanoparticles functionalized magnetic N-doped carbon nanotubes and its application for the detection of H₂O₂. *Sens. Actuators B Chem.* **2019**, *282*, 85–95. [[CrossRef](#)]
337. Chen, S.; Yuan, R.; Chai, Y.; Hu, F. Electrochemical sensing of hydrogen peroxide using metal nanoparticles: A review. *Mikrochim. Acta* **2013**, *180*, 15–32. [[CrossRef](#)]
338. Chou, T.-C.; Wu, K.-Y.; Hsu, F.-X.; Lee, C.-K. Pt-MWCNT modified carbon electrode strip for rapid and quantitative detection of H₂O₂ in food. *J. Food Drug Anal.* **2018**, *26*, 662–669. [[CrossRef](#)]
339. Tabrizi, M.A.; Shamsipur, M.; Saber, R.; Sarkar, S. Flow injection amperometric sandwich-type aptasensor for the determination of human leukemic lymphoblast cancer cells using MWCNTs-Pd nano/PTCA/aptamer as labeled aptamer for the signal amplification. *Anal. Chim. Acta* **2017**, *985*, 61–68. [[CrossRef](#)]
340. Werner, E. Determination of cellular H₂O₂ production. *Sci. Signal.* **2003**, *2003*, PL3. [[CrossRef](#)]
341. Ma, Z.; Jiang, M.; Zhu, Q.; Luo, Y.; Chen, G.; Pan, M.; Xie, T.; Huang, X.; Chen, D. A porous hollow fiber sensor for detection of cellular hydrogen peroxide release based on cell-in-lumen configuration. *Sens. Actuators B Chem.* **2020**, *321*, 128516. [[CrossRef](#)]
342. Zhao, Y.; Huo, D.; Bao, J.; Yang, M.; Chen, M.; Hou, J.; Fa, H.; Hou, C. Biosensor based on 3D graphene-supported Fe₃O₄ quantum dots as biomimetic enzyme for in situ detection of H₂O₂ released from living cells. *Sens. Actuators B Chem.* **2017**, *244*, 1037–1044. [[CrossRef](#)]
343. Xi, J.; Zhang, Y.; Wang, Q.; Xiao, J.; Chi, K.; Duan, X.; Chen, J.; Tang, C.; Sun, Y.; Xiao, F.; et al. Multi-element doping design of high-efficient carbocatalyst for electrochemical sensing of cancer cells. *Sens. Actuators B Chem.* **2018**, *273*, 108–117. [[CrossRef](#)]
344. Zhao, A.; She, J.; Manoj, D.; Wang, T.; Sun, Y.; Zhang, Y.; Xiao, F. Functionalized graphene fiber modified by dual nanoenzyme: Towards high-performance flexible nanohybrid microelectrode for electrochemical sensing in live cancer cells. *Sens. Actuators B Chem.* **2020**, *310*, 127861. [[CrossRef](#)]
345. Yang, Y.; Ohnouteck, L.; Ajmal, S.; Zheng, X.; Feng, Y.; Li, K.; Wang, T.; Deng, Y.; Liu, Y.; Xu, D.; et al. “Hot edges” in an inverse opal structure enable efficient CO₂ electrochemical reduction and sensitive in situ Raman characterization. *J. Mater. Chem. A* **2019**, *7*, 11836–11846. [[CrossRef](#)]
346. Sinha, A.; Dhanjai; Zhao, H.; Huang, Y.; Lu, X.; Chen, J.; Jain, R. MXene: An emerging material for sensing and biosensing. *TrAC Trends Anal. Chem.* **2018**, *105*, 424–435. [[CrossRef](#)]

347. Chen, J.; Tong, P.; Huang, L.; Yu, Z.; Tang, D. Ti₃C₂ MXene nanosheet-based capacitance immunoassay with tyramine-enzyme repeats to detect prostate-specific antigen on interdigitated micro-comb electrode. *Electrochim. Acta* **2019**, *319*, 375–381. [[CrossRef](#)]
348. Chen, X.; Sun, X.; Xu, W.; Pan, G.; Zhou, D.; Zhu, J.; Wang, H.; Bai, X.; Dong, B.; Song, H. Ratiometric photoluminescence sensing based on Ti₃C₂MXene quantum dots as an intracellular pH sensor. *Nanoscale* **2018**, *10*, 1111–1118. [[CrossRef](#)]
349. Lin, H.; Chen, Y.; Shi, J. Insights into 2D MXenes for versatile biomedical applications: Current advances and challenges ahead. *Adv. Sci.* **2018**, *5*, 1800518. [[CrossRef](#)]
350. Dai, C.; Lin, H.; Xu, G.; Liu, Z.; Wu, R.; Chen, Y. Biocompatible 2D titanium carbide (MXenes) composite nanosheets for pH-responsive MRI-guided tumor hyperthermia. *Chem. Mater.* **2017**, *29*, 8637–8652. [[CrossRef](#)]
351. Liu, J.; Jiang, X.; Zhang, R.; Zhang, Y.; Wu, L.; Lu, W.; Li, J.; Li, Y.; Zhang, H. MXene-Enabled Electrochemical Microfluidic Biosensor: Applications toward Multicomponent Continuous Monitoring in Whole Blood. *Adv. Funct. Mater.* **2019**, *29*, 1807326. [[CrossRef](#)]
352. Guan, Q.; Ma, J.; Yang, W.; Zhang, R.; Zhang, X.; Dong, X.; Fan, Y.; Cai, L.; Cao, Y.; Zhang, Y.; et al. Highly fluorescent Ti₃C₂ MXene quantum dots for macrophage labeling and Cu²⁺ ion sensing. *Nanoscale* **2019**, *11*, 14123–14133. [[CrossRef](#)]